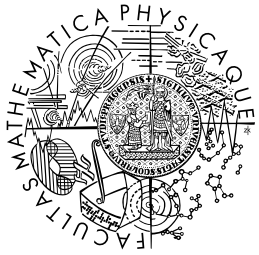

FACULTY
OF MATHEMATICS
AND PHYSICS
Charles University

DOCTORAL THESIS

Adéla Melcrová

Model membranes studied by advanced fluorescence techniques and molecular dynamics simulations

J. Heyrovský Institute of Physical Chemistry
Czech Academy of Sciences

Supervisor of the doctoral thesis:	prof. Martin Hof, Ph.D., DSc.
Consultants of the doctoral thesis:	Mgr. Piotr Jurkiewicz, Ph.D.
	Lukasz Cwiklik, Ph.D., DSc.
Study programme:	Physics
Study branch:	Biophysics, Chemical and Macromolecular Physics

Prague 2019

I declare that I carried out this doctoral thesis independently, and only with the cited sources, literature and other professional sources.

I understand that my work relates to the rights and obligations under the Act No. 121/2000 Sb., the Copyright Act, as amended, in particular the fact that the Charles University has the right to conclude a license agreement on the use of this work as a school work pursuant to Section 60 subsection 1 of the Copyright Act.

In Prague 21.1.2019 signature of the author

Most of all I thank to my beloved husband Josef. Without his immense support, belief in my scientific qualities, and help with the care of our children, the work on this thesis would last much longer. I thank to him and my children as well as my extended family and friends for bringing joy and happiness into my life so I can easily focus on the scientific work I also love.

I thank to my supervisor Martin and my consultants Piotr and Lukasz for introducing me to the scientific environment, for their patience, and for their friendly attitude.

Title: Model membranes studied by advanced fluorescence techniques and molecular dynamics simulations

Author: Adéla Melcrová

Institute: J. Heyrovský Institute of Physical Chemistry of the Czech Academy of Sciences

Supervisor: prof. Martin Hof, Ph.D., DSc., J. Heyrovský Institute of Physical Chemistry of the Czech Academy of Sciences

Consultants: Mgr. Piotr Jurkiewicz, Ph.D., J. Heyrovský Institute of Physical Chemistry of the Czech Academy of Sciences
Lukasz Cwiklik, Ph.D., DSc., J. Heyrovský Institute of Physical Chemistry of the Czech Academy of Sciences

Abstract:

In this thesis, we start with the description of the biophysical properties of the plasma membrane models upon signaling processess. Calcium signaling is characterized by a rapid increase of its cytosolic concentration. We identify calcium binding sites and characterize the binding in the plasma membrane models of increasing complexity from pure phospholipid bilayers, through cholesterol and peptide rich lipid membranes, to membranes extracted from HEK293 cells. We use Time-Dependent Fluorescent Shift method, which provides direct information on hydration and mobility in defined regions of a lipid bilayer, accompanied with molecular dynamic (MD) simulations, which give molecular details of the studied interactions.
The initial step of signaling mediated by PAG protein is its double palmitoylation. We investigate changes of the biophysical properties of both the lipid membrane and the peptide itself upon the incorporation of the palmitoyls. Employing all atom MD simulations, we study inter- and intramolecular interactions as well as changes in membrane hydration, thickness, or lipid ordering.
The second part of the thesis, realized in a direct collaboration with a pharmacological company, is focused on the tear film (TF) of the human eye and related pharmacological issues. We use extensive coarse grain MD simulations to mimic big patches of the TF and investigate the molecular mechanism of the TF stabilization upon addition of surfactant molecules, which are being developed for the treatment of dry eye disease.

Keywords: calcium signaling, protein palmitoylations, plasma membrane models, tear film, fluorescence spectroscopy, molecular dynamic simulations

Contents

Introduction

Formation of a membrane separating the inner volume from the surroundings was probably a crutial step for the formation of the first cell [Russell et al., 1993, Deamer, 2017]. During the evolution, cellular membranes adopted a wide variety of functions. Membranes are external boundaries of cells, they regulate molecular traffic in and out of the cell, they contain receptors for extracellular communication and transmit the external stimulli into intracellular signaling [Nelson and Cox, 2005]. In eukaryotic cells, membranes divide the intracellular space into compartments, hence, segragate crucial cellular processes into specialized organelles: metabolism, transport of nutrients and ions, storing and transmission of genetic information, and replication of nucleic acids [Nelson and Cox, 2005, Deamer, 2017].

One of the main roles of the outer membrane of an eukaryotic cell, the plasma membrane, is the recognition of the external stimulli to the cell and transduction of the signal into intracellular signaling cascades. Endocrine signaling is the most common way of signaling in between cells, during which an organism releases a signal molecule to the blood stream of an animal or to the sap of a plant. A less general type of such events is the paracrine signalization, during which the signal molecules diffuse by some local mediator to the surrounding cells. This type of signalization is mostly used in the regulation of local inflammation at the place of infection, or in the cell proliferation during wound healing. The third type of signalization is the communication between neurons. The signal is transduced in between the neural cells in neural synapses by the release of a neurotransmitter. The release of the neurotransmitter is triggered by the fast increase of Ca^{2+} concentration in the synapse. Finally, the forth way of the intercellular communication is a direct contact through the signal molecules in the plasma membranes of the involved cells. Direct interaction between the signaling molecule and the receptor molecule is the most efficient way of signaling, and it acts on the shortest distance. This type of communication does not require a release of any molecule [Alberts et al., 2002].

Receiving a signal from the outside triggers signaling cascades in the cell, which can activate a whole range of possible signaling pathways leading to cell survival, division, differenciation or programmed death [Alberts et al., 2002, Pani and Singh, 2009]. One of the simplest signaling agents are Ca^{2+} ions. Ca^{2+} manages a host of vital cell functions including regulation of cell growth or cell differentiation [Pani and Singh, 2009, Orrenius et al., 2003], Ca^{2+} also has the central role in the regulation of the cell death as it can activate distinct parts of the cell death programme [Orrenius et al., 2003]. The physiological functions of cells are tightly regulated by changes of cytosolic Ca^{2+} concentration. Rapid changes can be achieved by the influx of Ca^{2+} via transmembrane channels, or release of Ca^{2+} from the internal stores [Pani and Singh, 2009, Orrenius et al., 2003]. Key proteins involved in Ca^{2+} signaling are localized in plasma membranes, hence, we describe the interactions of Ca^{2+} ions with models of the plasma membrane with increasing complexity going from the pure phospholipid membranes to the extracts from the human HEK293 cells.

Posttranslational modifications of proteins are another example of the in-

tracellular signals. We study the activation of Phosphoprotein associated with glycosphingolipid-enriched microdomains (PAG), or alternativelly called Csk-binding protein [Svec, 2008]. PAG natively rests in the plasma membrane in its passive form and is activated by incorporation of the two specific palmitoylations on its cysteine residues. Modification by palmitoyl chains targets PAG to lipid domains [Svec, 2008] which is followed by the recruitment of Csk, a major suppresor of Src-family kinases, and the linkage of the lipid domain to the cytoskeleton [Svec, 2008, Hrdinka and Horejsi, 2014]. Our focus lays on the changes in membrane biophysics upon incorporation of these palmitoyls.

Similar structures to phospholipid bilayers, phospholipid monolayers, are present at the surface of the lungs (lung surfactant) and the eyes (tear film). Being directly exposed to the environment, the human eye needs to be protected from various external risk factors such as changes of the air temperature and humidity, air pollutions, or infectious organisms and viruses [Cwiklik, 2016]. In the last part of this thesis, we focus on the modeling of the tear film of the human eye and the related pharmacological issues.

1. Biological membranes and their models for biophysical studies

Biological membranes can be with some modifications described by Singer-Nicolson fluid mosaic membrane model [Singer and Nicolson, 1972]. This model can be imagined like a sea of constantly moving lipids with integral and membrane-spanning proteins [Singer and Nicolson, 1972, Mouritsen, 2011]. The lateral and rotational freedom of the molecular components in the membrane, originally predicted in Singer-Nicolson model, is however not unrestricted. Lipids and proteins might not be distributed randomly but rather in lateral domains [Singer and Nicolson, 1972, Vereb et al., 2003]. We still do not know the sizes of such domains, but since 2003 the view point has changed and now we rather think of nanoscale [Cebecauer et al., 2018]. Such compartmentalization occurs to be as important for the effective signal transduction as is the membrane fluidity [Vereb et al., 2003]. The fluidity of the membrane allows for lateral movement for membrane proteins and lipids and, hence, their direct interaction during signalization events. It allows for distribution of membrane lipids and proteins by diffusion after their incorporation in the membranes to other places within the cell. It also allows for membrane fusion and ensures uniform distribution of membrane molecules in the cell division [Alberts et al., 2002]. Considering the non-random distribution of the membrane components and its major role in cellular signaling, the fluidity also permits for continuous, dynamic restructuring of the molecular clusters within the membrane according to the needs of the cell [Vereb et al., 2003].

The complexity of biological membranes is high consisting of mainly lipids and proteins. The main classes of lipids in eukaryotic cells are phospholipids, sphingolipids and sterols, however, each type of membrane has characteristic lipids and proteins with varying of their relative proportions [Alberts et al., 2002, Nelson and Cox, 2005].

Study of biological membranes in vivo is often challenging as living cells are

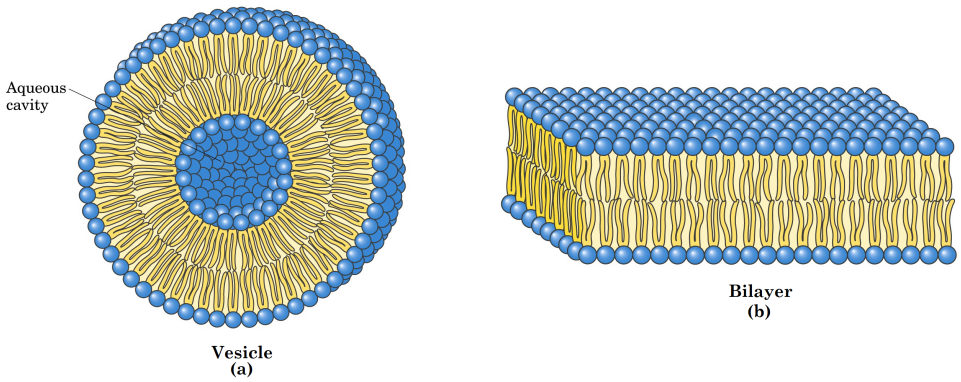

Figure 1.1: Membrane models. a) Vesicle, and b) Lipid bilayer. Taken from [Nelson and Cox, 2005].

dynamic entities with metabolism, self-repairing systems and both active and passive transport through the membranes and within the cell [Alberts et al., 2002, Nelson and Cox, 2005]. Hence, to get insight into individual processes in the membranes we need to study their simplified models. One of the most simplified models of a biological membrane is a lipid bilayer. Such model can be step by step enriched by new components including different kinds of lipids, proteins, or glycolipids and glycoproteins. Lipid bilayers can be experimentally prepared in a form of vesicles of various sizes (from <100 nm to >1000 nm in diameter), either unilamellar or multilamellar, being the simplest models of closed cell membranes [Mouritsen, 2011]. For the spectroscopic studies we use large unilamellar vesicles (LUVs, Figure 1.1a) with the size of 150 nm in diameter. The size of the vesicles is so large that for the studied ions and their binding the membrane appears to be locally flat. Hence we can directly relate the results obtained in the experiments with molecular dynamic (MD) simulation models where we use flat bilayers (Figure 1.1b) with the same composition as in the experiments. In such artificial system we can study the concrete interactions in between ions, lipids, proteins or other entities present in our model. An intermediate step towards real cellular membranes is usage of cellular extracts for the vesicles preparation. This way, we can maintain the complexity of the real biological membrane and still avoid the interactions with the cell environment.

1.1 Bilayer models of the inner leaflet of the plasma membrane

The main phospholipid components of the plasma membrane are phosphatidylcholine (PC), phosphatidylethanolamine (PE), phosphatidylserine (PS), phosphatidylinositol (PI) and its phosphorylated forms and phosphatidic acid (PA). Other highly represented lipids are sphingomyelin (SM) and cholesterol [Alberts et al., 2002, Nelson and Cox, 2005]. The distribution of lipids between the inner and outer leaflet of the plasma membrane is highly assymetric. Choline-containing lipids (PC, SM) are typically found more in the outer (extracellular) leaflet, whereas the PS, PE, PA and PI with its phosphorylated forms are more common in the inner (cytoplasmic) leaflet [Alberts et al., 2002, Nelson and Cox, 2005]. Note that the lipids in the inner leaflet are usually negatively charged (PI, PS), and they often have a smaller headgroup (PE, PA) inducing a negative curvature of the membrane.

The structure and flexibility of the lipid membrane depends on many factors, among which the strongest are the lipid headgroup and acyl tail composition, and temperature. The acyl tails influence the fluidity of the lipid membrane especially strongly as the melting temperature of the liquid ordered phase has a characteristic dependence on the length and the degree of saturation of the tails. The fatty acyl chains composition in the plasma mebrane is ideal to keep the membrane in fluid phases, while two fluid phases, liquid-ordered and liquid-disordered, with different physical characteristics, can coexist within a single membrane [Feigenson, 2006, 2007]. It is thus crucial to choose the proper fatty acyl chain composition to correctly model the native fluid membrane. In mammal cells, the majority of phospholipids in the plasma membrane have 16 or 18 carbons

long acyl chains, with one of the two acyl tails usually unsaturated [Cotman et al., 1969, Han and Gross, Richard, 1994]. Present are also lipids combining one acyl chain with the length of 16 or 18 carbons and the other consisting of 20 or 22 carbons, the latter one usually with a higher degree of unsaturation [Cotman et al., 1969, Han and Gross, Richard, 1994]. In the model membrane studies, we choose the representative lipids with saturated palmitic acid (16:0) and unsaturated oleic acid (18:1).

In mammal cells the fluidity of the membranes is also buffered by the presence of cholesterol [Vereb et al., 2003, Mouritsen, 2011, van Meer et al., 2008]. Cholesterol is one of the key components of the plasma membrane. It is prominent there although barely deteclable in membranes of mitochondria or endoplasmic reticulum [Nelson and Cox, 2005, van Meer et al., 2008].

In this thesis we employ mimics of the inner leaflet of the plasma membrane, where cellular signaling triggered by Ca^{2+} ions or PAG protein palmitoylation take place. We use a lipid bilayer consisting of only PC molecules, namely 1,2-dioleoyl-sn-glycero-3-phosphocholine (DOPC) with both unsaturated chains and 1-palmitoyl-2-oleoyl-sn-glycero-3-phosphocholine (POPC) with one unsaturated acyl tail as the simplest model allowing us to concentrate on details of ionic or palmitoylation influence on different parts of phospholipid molecules. The addition of phosphatidylserine (PS) or phosphatidylglycerol (PG) in concentration of 20 mol% gives the physiologically relevant negative charge to the model. We again use 1,2-dioleoyl- and 1-palmitoyl-2-oleoyl-sn-glycero-3-phosphoserine (DOPS and POPS) molecules in a case of PS, and only once unsaturated 1-palmitoyl-2-oleoyl-sn-glycero-3-phosphoglycerol (POPG) in a case of PG.

To increase the complexity of the model and to get closer to the real plasma membrane of a living cell we add cholesterol and transmembrane peptides to our model. Since, the plasma membrane can contain up to 30 mol% of cholesterol, hence we add 10, 20, and 30 mol% of cholesterol to obtain trends of its influence in this range. The proteins are present in the plasma membrane in the non-negligible amount of about 50% of mass [Alberts et al., 2002, Nelson and Cox, 2005]. However, since the weight fraction counts whole proteins, i.e., also their cytoplasmic parts, we estimate the physiological amount of the transmembrane domains to be lower, approximately 3 mol%.

1.2 Model of the tear film of the human eye

The human eye is covered by several distinct layers which together form the so-called tear film (TF). There is an aqueous layer in a direct contact with the eye cornal epithelium, on top of which is the layer of lipids, the so-called tear film lipid layer (TFLL).

The TF topology is depicted in Figure 1.2 and described in [McCulley and Shine, 1997, Olson et al., 2003, Foulks, 2007, Cwiklik, 2016, Willcox et al., 2017]. The surface of cornea is covered by a layer of mucin, between 2.5 to 5 μm thick. This layer is anchored to corneal epithelium and is composed predominantly of sugar-rich glycosylated proteins produced by epithelial cells. Such a structure makes the surface of the epithelial cells wettable and, hence, assists in water re-spreading after each blink of the eye.

On top of the mucin layer, there is a 4 μm thick aqueous layer. Except of

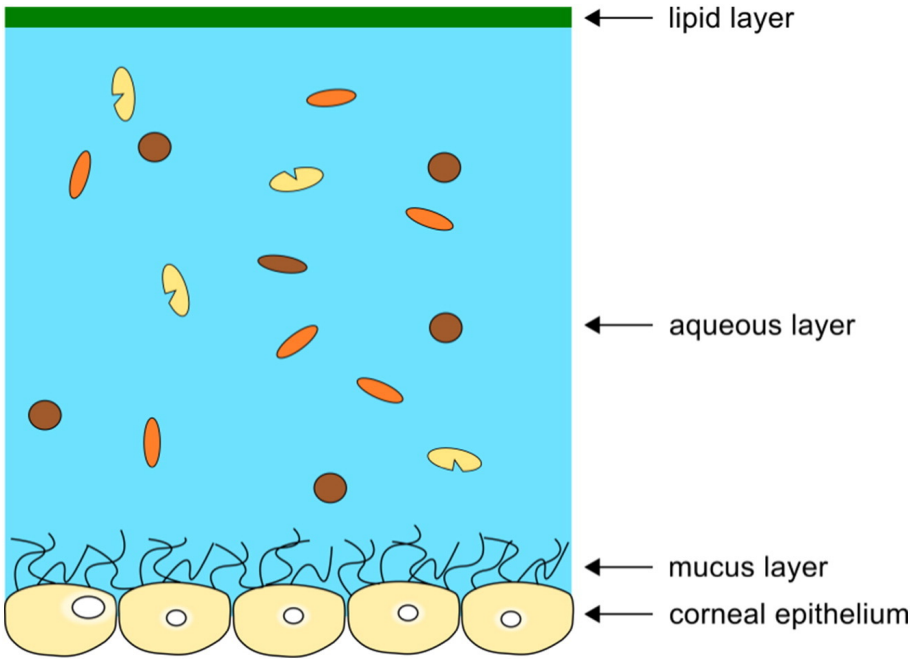

Figure 1.2: Scheme of the tear film (TF) structure. Corneal epithelium cells are covered by a mucin layer which makes the surface of the epithelial cells wettable. Mucus layer is covered by a thick aqueous layer with many water soluble and insoluble molecules and ions. The most outer layer is made of lipids, the tear film lipid layer (TFLL). Figure taken from [Cwiklik, 2016].

water it contains numerous water soluble and also insoluble components such as electrolytes, proteins, peptides and small molecule metabolites. The main function of the aqueous layer is to provide an optically smooth surface for light refraction. It also lubricates the eye surface during blinks and eye movements, prevents eye surface dehydration, protects against pathogens and pollutants from air, and provides nutrition to corneal cells.

TFLL is the most outer layer of the TF. It is a relatively thin, 0.015 to 0.160 μm, layer of lipids [Cwiklik, 2016], which prevents loss of the aqueous layer through overspill and evaporation [Willcox et al., 2017], it reduces surface tension to approximately two-thirds of that of water stabilizing the TF at the cornea surface [Cwiklik, 2016], and has an antimicrobial activity against both Gram-positive and Gram-negative bacteria [Mudgil, 2014].

The lipids in TFLL are organized in a multi-layered fashion (see Figure 1.3) [McCulley and Shine, 1997, Olson et al., 2003, Foulks, 2007, Cwiklik, 2016, Willcox et al., 2017]. The interface between the aqueous layer and the lipid layer is formed by a thin sub-layer of polar amphihilic lipids. These lipids make a monolayer topped with a bulky layer of non-polar hydrophobic lipids. The thickness of the polar monolayer is estimated to be 2-9 nm [Butovich, 2009], whereas the non-polar phase is 33-40 nm thick [Cwiklik, 2016].

We investigate the role of the lipid layer on the stability of the TF, especially related to the dry eye disease (DED). DED is associated with the loss of anti-evaporative properties of the lipid layer. We use MD simulations to observe molecular-level interactions between lipid film components and possible drugs for DED treatment. The stability and spreading of the TF are heavily influenced

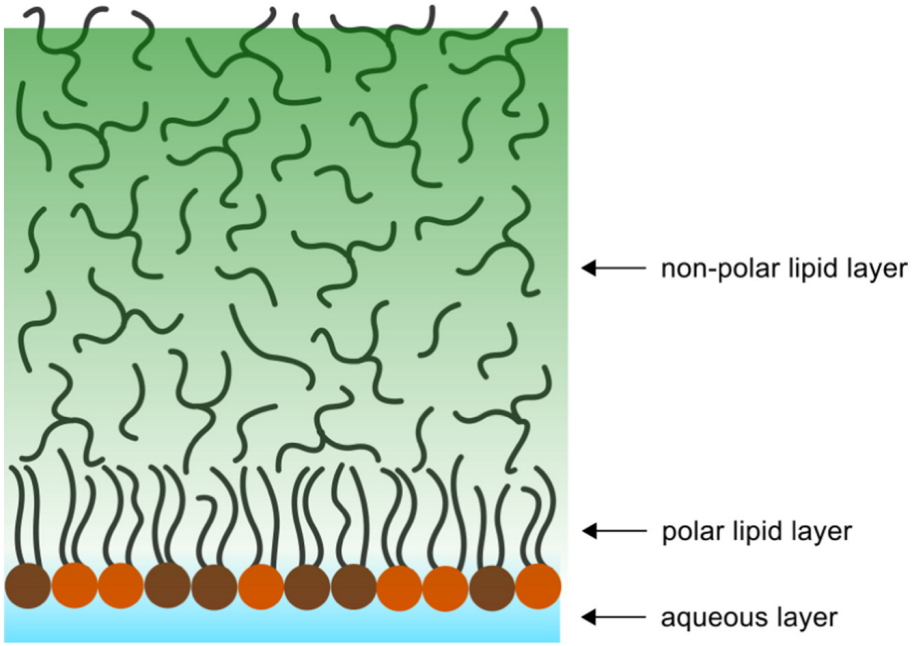

Figure 1.3: Scheme of the tear film lipid layer (TFLL) structure. TFLL consists of a monolayer of polar lipids topped by a thicker non-polar lipid layer. The non-polar phase is exposed to the gas phase. Figure taken from [Cwiklik, 2016].

by the molecular lipid composition. The lipid composition of TFLL is however also varying with gender, age and eye blinking patterns [Brown et al., 2016, Butovich, 2009]. Overall, the non-polar lipids consist of 30-45 mol% cholesterol esters with long acyl chains (C22:1-C34:1), and ∼30-50 mol% wax esters with mostly 18:1 fatty acyl chains mixed with C18-C30 alcohol chains. The lipid layer contains also 4 mol% of (O-acyl)-ω-hydroxy fatty acids. The biggest part of the polar lipids are phospholipids, mainly glycerophospholipids, lysophospholipids, and sphingomyelins. The majority of phospholipids are phosphatydilcholines (PC, >60 mol%), followed by phosphatidylethanolamines (PE, ∼15 mol%) [Cwiklik, 2016].

In our computational modeling, we approximate the polar monolayer of TFLL consists from 1-palmitoyl-2-oleoyl-phosphatidylcholine (POPC), 1-palmitoyl-2-oleoyl-phosphatidylethanolamine (POPE), N-palmitoyl-d-erythrosphingosine (PPCE), and N-palmitoyl-d-erythrosphingosylphosphorylcholine (PPCS) in molar ratios derived from the lipidomic studies [Rantamäki et al., 2011]. The simplified model of the non-polar layer is built as an equimolar mixture of glycerine trioleate (TO) and cholesteryl oleate (CO). The representative configuration of the computational model of the TFLL used in our MD simulations is depicted at Figure 1.4. A thick layer of water, representing the aqueous phase of the TF, is covered by a monolayer of polar lipids from both bottom and top. From the other side, these monolayers are surrounded by the layer of non-polar lipids exposed to the gas phase, representing the TFLL-air interface.

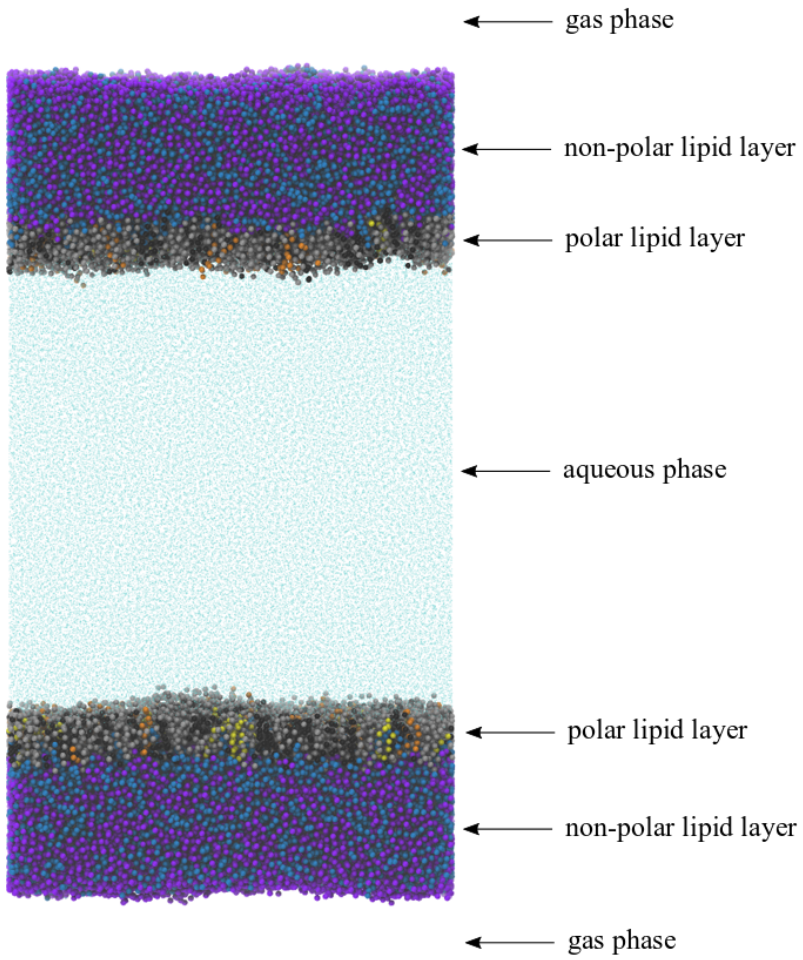

Figure 1.4: Representative snapshot of the tear film model using MARTINI force field [Marrink et al., 2007]. Water molecules (cyan) are in the middle of the simulation box. Monolayer of polar lipids is formed at the water-lipids interface. The polar lipids layer consists of POPC (grey), POPE (black), PPCE (orange), and PPCS (yellow). The non-polar lipid layer is an equimolar mixture of CO (blue) and TO (violet). The non-polar subphase of the TFLL is exposed to the gas phase.

2. Advanced fluorescence techniques

To investigate the biophysical properties of biological membranes we use the phenomena of fluorescence. Fluorescence, as a form of luminiscence, is the emission of light from an electronic excited state. Such states are typically reached by photoexcitation. The excited molecules relax in the order of $10^{-12} - 10^{-10}$s to the first electronic excited state. After some residual time a photon is spontaneously emitted, the molecule looses the energy and returns to one of the vibrational states of the electronic ground state. The individual residual times vary since the process of photon emission is stochastic. The energy of the emitted photon is always lower than the energy needed for the excitation because of the fast relaxation processes in the excited states, which happen before the emission [Lakowicz, 1999].

Fluorescence lifetime of a fluorophore is the time between the absorption and emission events. During that time the fluorophore interacts with its environment which influences its emission. The fluorescence lifetime is characteristic for each molecule and reflects its average time spent in the excited state before returning to the ground state. Typical fluorescence lifetimes are in the orders of $10^{-8} - 10^{-9}$ s [Lakowicz, 1999].

The lifetime, τ, is determined by the rate constants of radiative, Γ, and non-radiative, k_{nr}, processes, both depopulating the excited state:

$$\tau = \frac{1}{\Gamma + k_{nr}} \tag{2.1}$$

The fluorescence lifetime can be obtained from time resolved measurements of fluorescence intensity decays by fitting the data with the function:

$$I(t) = I(0) \sum_i \alpha_i exp\left(\frac{-t}{\tau_i}\right) \tag{2.2}$$

where $I(t)$ is the fluorescence intensity dependence in time t, $I(0)$ the fluorescence intensity in time $t = 0$, and α_i are preexponential factors [Lakowicz, 1999].

The decays are obtained after exposition of the sample to a laser pulse shorter than the decay time of the fluorophore. The decays can be recorded statistically by the time correlated single photon counting (TCSPC) procedure. The experimental setup for this procedure uses such a laser intensity which excites ideally only one fluorophore at a time. The software waits until the emmited photon reaches the detector and records the time the fluorophore spent in the excited state. Such emmision times are recorded for thousands of photons providing enough statistics for the reconstruction of the fluorescence decay curve.

2.1 Time dependent fluorescent shift

Time dependent fluorescent shift (TDFS) method is based on the modulation of the fluorescence intensity decays of a fluorophore by the relaxation of the

surrounding molecules.

Upon electronic excitation the electric dipole moment of the fluorophore changes rapidly (10^{-15} s). The fluorophore's solvation shell responds to this change by the reorientation of the polar molecules in the surroundings. As the solvation shell relaxes, the energy of the fluorophore's excited state lowers shifting the emmited wavenumber, $\nu(t)$, to lower energies (Figure 2.1).

The total amount of the shift, $\Delta\nu = \nu(0) - \nu(\infty)$, is directly proportional to the polarity of the solvation shell [Horng et al., 1995, Jurkiewicz et al., 2005]. The kinetics of the relaxation process is characterized by the correlation function, $C(t)$, also called the spectral response function,

$$C(t) = \frac{\nu(t) - \nu(\infty)}{\nu(0) - \nu(\infty)} \tag{2.3}$$

A simple measure of the TDFS kinetics can be obtained from C(t) by fitting it to one or more exponential functions, or by its numerical integration over time,

$$\tau_r = \int_0^\infty C(t)dt \tag{2.4}$$

In a viscous medium, the solvent molecules reorient only slowly, hence, the time of their relaxation is longer. Integrated relaxation time τ_r is closely proportional to the viscosity of the solvent surrounding the fluorophore [Arzhantsev et al., 2003, Ingram et al., 2003, Ito et al., 2004, Jurkiewicz et al., 2005]. This parameter, defined in equation 2.4, gives only an approximate measure of the solvation kinetics. A more precise fitting of the correlation function $C(t)$ gives more accurate evaluation of the relaxation time τ_r. The $C(t)$ function reflects the process of the solvent relaxation, which is not monoexponential, especially in such an anisotropic media as phospholipid bilayers, where the fitting model for $C(t)$ should generally contain multiple exponential components [Jurkiewicz et al., 2005].

The $C(t)$ function can be determined by the spectral reconstruction from the set of emission decays recorded at different emission wavelengths spanning the full range of possible emission wavelengths of the fluorophore, and the corresponding steady-state emission spectrum $S(\lambda)$. The decays are fitted by a sum of exponential functions to obtain a parametric form of the intesity decay $D(\lambda, t)$ at each wavelength. The time resolved emission spectra, $S(\lambda, t)$, i.e., emission spectra at any time after excitation, can be then reconstructed,

$$S(\lambda, t) = \frac{D(\lambda, t)S(\lambda)}{\int_0^\infty D(\lambda, t)dt} \tag{2.5}$$

The time resolved emission spectra are then transformed into the wavenumber domain and fitted by a log-normal line shape function approximating the broad assymetric electronic emission bands. We obtain a time-dependent position of the spectrum, $\nu(t)$, which is then used to obtain parameter τ_r according to equations 2.3 and 2.4.

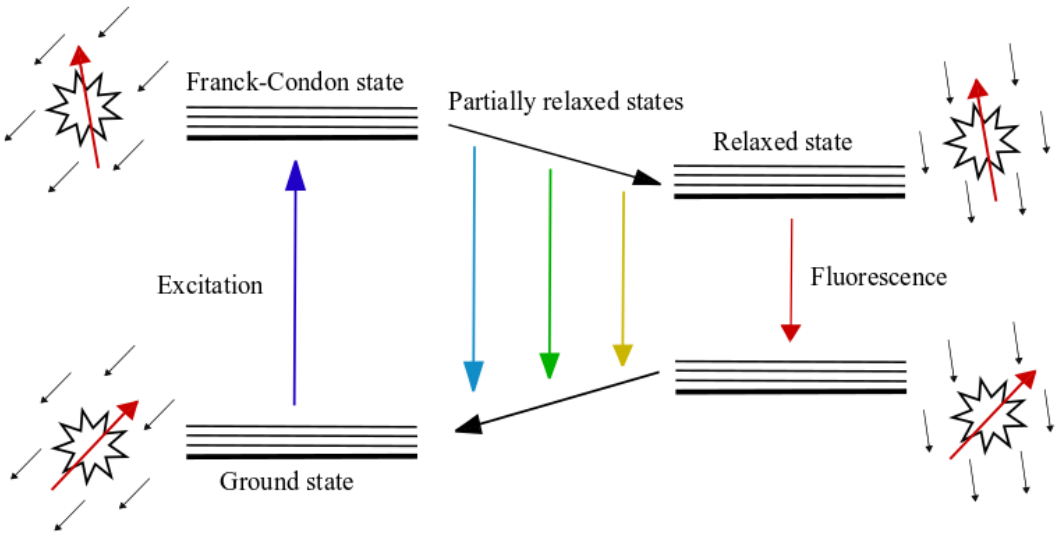

Figure 2.1: Schematic representation of solvent relaxation process. In the ground state the solvent molecules are oriented according to the electric dipole moment of the fluorophore. They cannot immediatelly react on the fast reorientation of the fluorophore's electric dipole moment upon it's excitation (Franck-Condon state). Solvent relaxation processes then follow lowering the energy of the excited state (Partially relaxed states, and Relaxed state). Fluorescence occurs throughout this process, hence, we observe a gradual shift in the energy of the emitted wavelengths. After the deexcitation of the fluorophore, its electric dipole moment changes again followed by the solvent relaxation to the ground state.

TDFS method probes the dynamics of the surrounding of a fluorophore. For the membrane studies various probes with the defined location of their fluorophores within the phospholipid bilayer are available (Figure 2.2) [Jurkiewicz et al., 2005]. In this thesis, we probe the ionic effects in the membrane models of the inner leaflet of the plasma membrane. Ions are expected to influence mainly the outer parts of the membrane and can penetrate down to the carbonyl level. Suitable probes for such studies are Laurdan and Dtmac, located at sn-1 carbonyls and phosphate groups, respectively, of both 1,2-dioleoylphosholipids and 1-palmitoyl-2-oleoylphospholipids [Jurkiewicz et al., 2005]. In such an environment, the parameters obtained from TDFS measurements with these dyes, $\Delta\nu$ and τ_r, reflect the polarity and mobility of the hydrated lipids. In many cases, the polarity directly representa the hydration level in the probed region of the membrane. However, interpreting the ionic effects on membranes from such experiments is complicated by the presence of the ion itself, which can also directly influence the local polarity around the fluorophore.

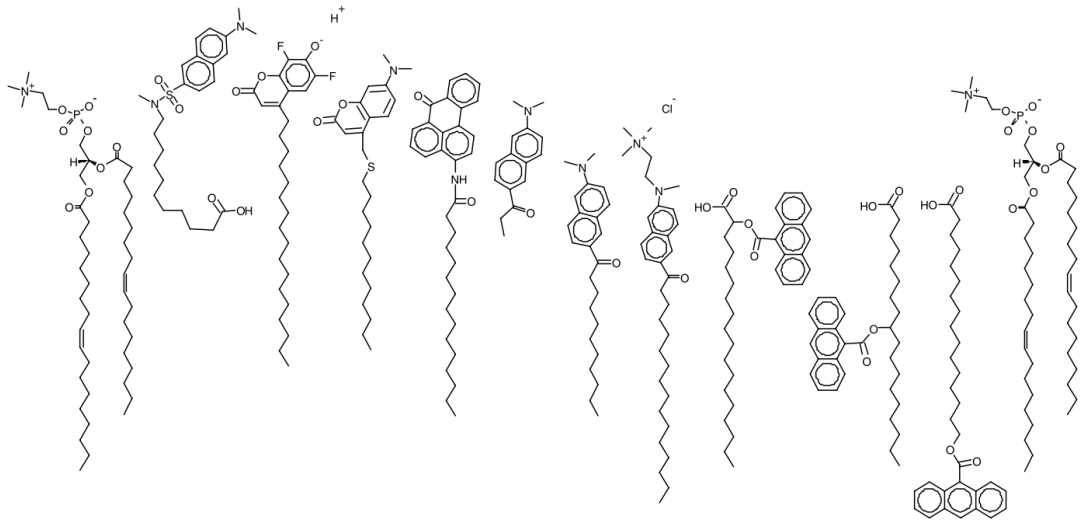

Figure 2.2: Position of the fluorescent probes relative to the dioleoylphosphatidyl choline (DOPC) molecule. From the left: DOPC,
11-((5-dimethylaminonaphthalene-1-sulfonyl)amino)undecanoic acid (Dauda),
6,8-difluoro-4-heptadecyl-7-hydroxycoumarin (C17DiFU),
4-[(n-dodecylthio)methyl]-7-(N,N-dimethylamino)-coumarin (DTMAC),
N-palmitoyl-3-aminobenzanthrone (ABA-C15),
6-propionyl-2-dimethylaminonaphthalene (Prodan),
6-lauroyl-2-dimethylaminonaphthalene (Laurdan),
6-hexadecanoyl-2-(((2-(trimethylammonium)ethyl)methyl)-
amino)naphthalenechloride (Patman),
2-(9-anthroyloxy)stearic acid (2-AS),
9-(9-anthroyloxy)stearic acid (9-AS),
(16-(9-anthroyloxy)palmitoic acid (16-AP)
DOPC.
Figure taken from [Jurkiewicz et al., 2005].

3. Classical molecular dynamics simulations

We employ the fluorescent techniques to get the experimental evidence of the studied phenomena. However, the interpretation of the results is often not definite as the experiments provide only mediated results. We observe changes in response of a fluorescent probe and we try to determine what is the reason for this change. Employing molecular dynamic (MD) simulations gives us the molecular level view on the studied system and thus helps with the interpretation of the experimental results. MD simulations are free from a possible influence of a fluorescent probe on the studied system. They are on the other hand burdened by errors arising from the usage of available force fields.

Within this thesis we concentrate on behavior of biological membranes, interactions between membrane components as well as interactions of lipids and proteins with water molecules and ions. For these purposes we can neglect quantum effects and calculate the progression of the system of interest using classical Newton's equations of motion.

In classical MD simulations the system of interest is propagated step by step by solving Newton's equations of motion in discrete timesteps. The basic approximation used for classical MD is Born-Oppenheimer approximation. Each particle, usually representing an individual atom, is described by the position of its nucleus and its velocity. The nuclei move in an averaged field of electrons and the nuclear movement is separated from the motion of electrons [Allen and Tildesley, 1987]. The result of an MD simulation is a trajectory, i. e., positions and velocities of atoms in time, which we can use to obtain structural and dynamical properties of the simulated system.

3.1 Empirical force fields

The interactions between particles, used as the forces applied on each particle in Newton's equations of motion, are described as an approximate interaction potential, a force field.

Historically, empirical force fields was derived so that their properties fitted well on various experimental results. This approach is often combined with quantum mechanical calculations to improve the accuracy of the modern force fields [Foloppe and MacKerell, 2000, Mackerell et al., 2004]. Empirical force fields are computationally efficient allowing us to simulate large systems as liquids or biomolecules ($\sim$nm or $\sim$ μm in size) on long timescales ($\sim$ μs or even $\sim$ ms). They however require an assumption of a model, and they are only approximate. Moreover, the parameters can be affected by the expetimental errors arising from the partial fitting of the model to the experimental results. Up to date, it is however not possible to calculate exact potential from the first-principle methods directly during the simulations for such big systems as biomolecules or biomembranes. Methods based on direct calculation of many-body potential during the simulation run are for example Car-Parinello [Car and Parrinello, 1985, Tuckerman, 1996] MD or *ab initio* MD [Sprik et al., 1996, Bockstedte et al., 1997]. They

are computationally highly demanding and hence the simulation is limited in the system size, simulation time, and statistics. Hence, only empirical force fields are used within this thesis.

The interaction potential, U, is composed of the terms each describing a different model interaction:

$$\begin{aligned} U = & \sum_{bonds} K_b(b - b_0)^2 + \sum_{angles} K_\Theta(\Theta - \Theta_0)^2 + \\ & \sum_{dihedrals} K_\Phi[1 + cos(n\Phi - \delta)] + \\ & \sum_{nonbonded} 4\epsilon_{ij} \left[\left(\frac{R_{min_{ij}}}{r_{ij}} \right)^{12} - \left(\frac{R_{min_{ij}}}{r_{ij}} \right)^{6} \right] + \left(\frac{q_i q_j}{\epsilon r_{ij}} \right). \end{aligned} \tag{3.1}$$

The individual terms in the Equation 3.1 correspond to the potentials representing chemical bonds, valence angle, dihedral angle and to non-covalent interactions, respectively. The first term in the Equation 3.1 describes the covalent forces that tightly bind the atoms together within the molecule and thus form chemical bonds [Israelachvili, 2011]. The bond potential can be in the first approximation described as a harmonic oscillator. K_b stands for the stiffness of a chemical bond, b_0 is the equlibrium distance between the atoms connected with the bond of the length b. The harmonic potential represents the chemical bond accurately only near the equilibrium length of a chemical bond where the potential is not anharmonic. Anharmonicity has to be introduced to correctly represent nonequidistant energy levels or possibility of bond dissociation.

The second term in the Equation 3.1 analogically describes the potential of valence angles. K_Θ is a harmonic force constant, Θ and Θ_0 are the instantaneous and equilibrium angles, respectively.

Torsion (dihedral) angle potential (the third term in Equation 3.1) accounts for rotational torsion potential around a bond axis. K_Φ stands for the dihedral force constant (the energy barrier to rotation), n is the number of energetic minima, Φ is a torsion angle, and δ is an angular offset, or a phase shift. The energetic minima and maxima depend on the architecture of the given molecule, e. g. the rotation of $C - C$ bond in an isolated molecule of ethan, $CH_3 - CH_3$, has 3 minima corresponding to hydrogen atoms at the two carbons pointing to the same direction. More complicated systems often require a set of such terms with different symmetry numbers and force constants.

The last terms in the Equation 3.1 describe nonbonded interactions in the system. Nonbonded interactions can be divided into long-ranged (electrostatic) and short-ranged (dispersion) forces. The largest contribution to the long-ranged forces arises from the electrostatic interactions in between charges, dipoles and also higher multipoles.

Considering electrostatic interactions we also have to account for polarization effects. An ion or a polar molecule induces dipole moment in the surrounding atoms and molecules. The common form of the empirical force fields (Equation 3.1) account only for the polarization of nuclei, however, the polarization of electrons is neglected. This part of polarization, the electronic polarization, arises from the displacement of its negatively charged electron cloud relative to the positively charged nucleus upon the interaction with the external electric field [Israelachvili, 2011]. Compared to electrostatics, polarization forces are always

attractive but are in general in shorter range than electrostatic forces which can be both attractive and repulsive.

The shortest-range forces are van der Waals interactions describing the London dispersion forcesrising from the interaction of induced dipoles. Such forces are induced as a result of uneven distributions of electrons of an atom. The electrons thus create an instantaneous dipole which can induce a dipole in a neighboring atom, causing a force [Israelachvili, 2011]. Similarly to the polarization they are only attractive.

The nonbonded interactions in the Equation 3.1 are described by the Lennard-Jones potential and a Coulomb interaction term for charge-charge electrostatics. The Lennard-Jones potential in the square brackets consists of a long-distance attractive interaction proportional to $(1/r)^6$ and a short-distance repulsive interaction proportional to $(1/r)^{12}$. The attraction part of this potential describes the action of van der Waals interactions, the repulsive forces arise from the overlap of the elctron clouds at very small interatomic distances [Israelachvili, 2011].

3.2 Atomistic, united-atom, and coarse grained models of biological membranes

Empirical force fields for biomolecules can be sorted to three main groups, which differ in the level of description – atomistic (each atom is represented as a separate particle), united-atom (hydrogen atoms included into their functional groups), and coarse grained (usually whole functional groups represented as a particle). We used a representative popular force field for each such category, and highlighted their respective level of detail on a common phospholipid molecule in Figure 3.1 on an example of a POPC molecule. Popular atomistic force fields for lipids description are Slipids [Jämbeck and Lyubartsev, 2012b,a], CHARMM [Tieleman et al., 2006] or Lipid14 [Dickson et al., 2014]. Each atom in these models is represented by a single particle achieving an atomistic level of description. Berger lipids [Berger et al., 1997] is a united-atom model, in which the hydrogen atoms are not described explicitly. Parameters accounting for their presence are included in the parameters describing the nearest non-hydrogen atom. Such a simplification of the molecular description enhances the computational speed and efficiency of the united-atom models compared to the atomistic models at the cost of losing the accurate positions and interactions of the hydrogen atoms.

In the research field of biological membranes, atomistic and united-atom models have provided new insights into the conformational dynamics of membrane constituents as well as protein-ligand, protein-protein, and protein-lipid interactions [Friedman et al., 2018]. For large systems, in which we are rather interested in the mesoscopic and large-scale behaviour, the use of coarse grained models is often justified [Marrink and Tieleman, 2013]. A popular example of such a model is MARTINI [Marrink et al., 2004], in which 2-5 heavy atoms are represented as a single particle. Generally, the usage of coarse grained methods gives us fewer interaction sites and thus less computational burden. Additionally, the kinetics in such models are faster thanks to the smoother energy landscapes which arise from the reduced dimensionality of the system [Friedman et al., 2018, Hakobyan and Heuer, 2013]. This effect is observed in the work comparing the performance

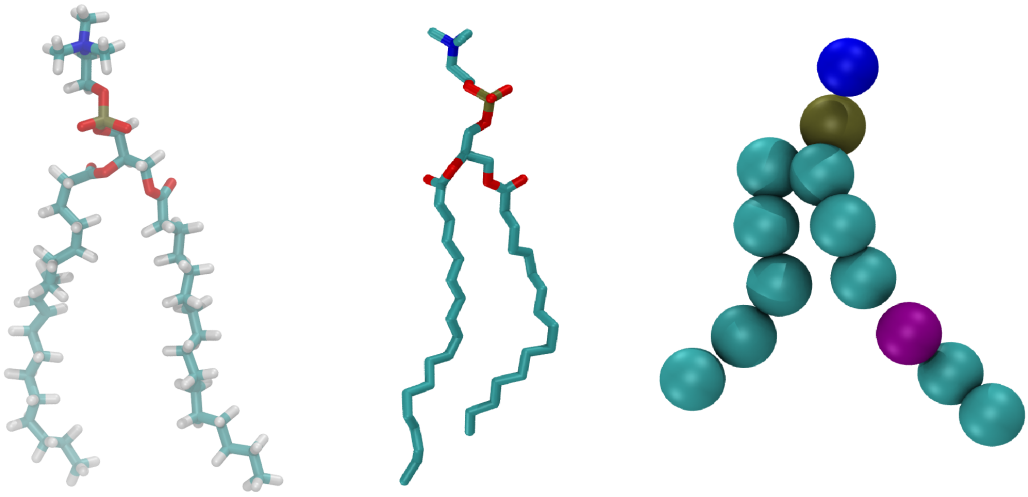

Figure 3.1: Representation of POPC molecule by all-atom Slipids (left), united-atom Berger (middle), and coarse-grained MARTINI (right) force field. In Slipids and Berger, carbon atoms are depicted in light blue, oxygen in red, phosphorus in golden, nitrogen in dark blue. Hydrogens presented in Slipids are colored white. MARTINI beads involve group of few atoms. The colors correspond to heavy atoms inside of the bead analogically to Slipids and Berger. The purple bead represents the carbons around the double bond in the oleoyl chain.

and accuracy of a united-atom (Berger) and a coarse grained (MARTINI) force field were compared at the example of lipid demixing in ternary lipid mixtures [Hakobyan and Heuer, 2013]. In the coarse grained model full lipid demixing was reached already after 1 μs of the simulation, whereas for the united-atom approach a simulation time of 9 μs is too short to reach this state. The structural behavior and the phase separation process are similar, although minor differences can be observed. The coarse grained models thus can be used to observe structural features and overall behavior of macromolecules. The apparent drawback of the coarse grained models is their lower resolution compared to the atomistic or united-atom models. We can combine the advantages of both approaches by back-mapping the coarse grained model to an atomistic representation [Wassenaar et al., 2014], or by employing hybrid multiscale simulations in which parts of the system are represented on a coarse grained level while other parts have atomistic resolution [Genheden and Essex, 2015, Kar and Feig, 2017, Kuhn et al., 2015].

3.3 Effective inclusion of polarization effects in ions via Electronic continuum correction

For an accurate description of ion-membrane interactions the model of the ions is equally important as the model of the lipid molecules. In our studies, we use ion models with the electronic continuum correction (ECC) [Kohagen et al., 2014, 2016]. ECC accounts for polarization effects within nonpolarizable simula-

tions via rescaling ionic charges by a factor of 0.75 [Leontyev and Stuchebrukhov, 2011]. ECC leads to significant improvements in the description of ions, particularly multivalent ions like calcium cations [Kohagen et al., 2014]. The correction prevents an excessive ion clustering present in simulations with full-charge ions, which overestimate the strength of ion-ion interactions with respect to ion-water interactions [Kohagen et al., 2014]. So far the ECC parameters for calcium, sodium, lithium, and chloride ions [Kohagen et al., 2014, 2016] were developed. Recently, ECC has been also applied to headgroups of POPC [Melcr et al., 2018] improving the description of ion-lipid interactions even further. The combination of ECC-POPC and ECC-ions was able to correctly reproduce the experimental results such as X-ray scattering form factors, and headgroup order parameters gained from nuclear magnetic resonance measurements.

3.4 Force fields and models employed in this work

Within the presented thesis, several models were employed to study the effects of ions on membranes, inter- and intramolecular interactions in models consisting of phospholipids, cholesterol, and peptides, impact of palmitoylation of a protein on membranes, or structure of the healthy and polar lipid deficient tear film (TF) mimicking the dry eye disease (DED) condition as well as the influence of topical drugs used for DED treatment on the TF.

At the first part of the research presented in this thesis we describe lipids using united-atom Berger force field ([Berger et al., 1997]; chapters 4.1 and 4.3, and corresponding papers [Melcrova et al., 2016, 2019b]). This force field was proved to well reproduce many relevant structural parameters of biological membranes such as area per lipid, lipid headgroup orientation, lipid order parameters, density profiles, membrane thickness, lipid and water diffusion, or electrostatic potential and dipole moment [Berger et al., 1997, Siu et al., 2008]. For the correct water dynamics close to the membrane surface Berger force field is paired with SPC water model [Chen and Smith, 2007, Siu et al., 2008]. Berger force field parameters were recently used for example for description of an asymmetric plasma membrane [Vácha et al., 2009], interaction of bilayers with ions [Böckmann and Grubmüller, 2004a, Jurkiewicz et al., 2012], effect of lipid acyl chain saturation on membrane biophysics [Martinez-Seara et al., 2008, 2009], cholesterol effects on lipid membranes [Ferreira et al., 2013], or formation and rupture of an aquaeous pore over the membrane [Hub and Awasthi, 2017]. Berger lipids have the advantage of a smaller computational demand compared to all atom models, however they suffer from some inaccuracies; Berger lipids overestimate the membrane ordering effect of cholesterol for cholesterol concentrations above 30 mol% [Ferreira et al., 2013]; the acyl chains of phospholipids interact too strongly with peptides in this model [Tieleman et al., 2006] resulting in membrane condensation; lipid headgroups interact too strongly with the ions [Catte et al., 2016]; or free energy barrier for pore formation by antimicrobial peptides is strongly modulated [Bennett et al., 2016].

In 2016, an open source project at the platform nmrlipids.blogspot.fi released a publication comparing different all-atom and united-atom force fields in terms

of their accuracy in the description of ions-lipid interactions [Catte et al., 2016]. It was shown that Berger lipids overestimate the penetration depth of the ions to the membrane. As we are interested in knowledge about detailed interactions between ions and lipids we shifted with our later studies (chapters 4.2 and 4.6, and papers [Melcrova et al., 2017, 2019a]) to all-atom Slipids force field. The Slipids force field was shown to well describe the features of bilayers consisting of phospholipids, sphingolipids and cholesterol [Jämbeck and Lyubartsev, 2012a, 2013]. Compared to the Berger, the Slipids force field improves the overestimated interaction of the phospholipid headgroups with the adsorbed ions as the structural features of the PC headgroups and that of the adsorbed ions are in a better agreement with experiments especially with the ECC-ions (Supporting information of [Catte et al., 2016]). The Slipids force field was recently used for example to describe modeling of transmembrane potential [Melcr et al., 2016], binding of ions to curved membranes [Magarkar et al., 2017], or mechanism of binding of a soluble protein to the phospholipid membrane [Enkavi et al., 2017].

In the TF structure project we aim at observing the remodeling of a healthy and a dry eye TF after a blink of an eye, as well as the embedding of drug molecules to the TF. A realistic model of the TF of the human eye requires a simulation of a patches of the TF at lateral sizes between 25 x 25 nm^2 and 34 x 34 nm^2, making it a suitable for a coarse grained model description. Usage of all-atom or united-atom force fields would be highly computationally demanding as we simulate 6-25 thousand lipids and 360-1400 thousand water molecules for times of $\sim \mu$s. Moreover, large-scale structure of such molecular assemblies can be captured with a simplified, less detailed, coarse grained models like MARTINI [Marrink et al., 2004, 2007]. In MARTINI, typically a four-to-one mapping is used, i.e. on average four atoms are represented by a single interaction center, a MARTINI bead. The rule applies to all types of molecules including water, for which one MARTINI bead represents four water molecules. The beads are then considered as interaction sites interacting according to forces described in 3.1. Coarse graining allows for not only simulations of bigger molecular assemblies but also for longer timescales as the time step can be prolonged from 2 fs typical for all-atom simulations up to 30-50 fs in MARTINI runs. For instance, current computational resources make it possible to perform simulations of membrane patches typically consisting from 128 phospholipids and embeded in ∼5000 water molecules at the time scales of hundreds of nanoseconds or microsecond using all-atom or united-atom description. In contrast, using the coarse grained MARTINI force field enables us to calculate micro- or even miliseconds long trajectories for thousands of lipids, i.e., millions of MARTINI beads [Marrink and Tieleman, 2013]. MARTINI force field was developed with the aim for a broad range of applications without the need of reparametrization of the model each time. The MARTINI model can be used to model a wide range of biological events requiring action of large complexes such as modelling of the whole lipid vesicles [Marrink and Mark, 2003b, Risselada and Marrink, 2009a,b, Risselada et al., 2008, Leung et al., 2012], lipid flip-flop and lipid desorption [Bennett et al., 2009, Ogushi et al., 2012], deformation of asymmetric membranes [Esteban-Martín et al., 2009, Yoo and Cui, 2009, Yesylevskyy and Demchenko, 2012, Maftouni et al., 2013], membrane permeation of drugs and amphiphiles [Pickholz and Giupponi, 2010, Notman et al., 2007], lipid phase behavior including modelling of spontaneous

formation of liquid-ordered and liquid-disordered domains in bilayers [Risselada and Marrink, 2008], predicting binding modes of proteins to membranes and adaptation of membranes around proteins [Klingelhoefer et al., 2009, Balali-Mood et al., 2009, Lumb and Sansom, 2013, Qin et al., 2013, Tjörnhammar and Edholm, 2013], self-assembly of proteins [Periole et al., 2007, Frederix et al., 2011, Sørensen et al., 2011] or lipoprotein particles [Shih et al., 2007, Catte et al., 2008, Murtola et al., 2011, Vuorela et al., 2010], and membrane fusion [Marrink and Mark, 2003a, 2004, Kasson and Pande, 2007, Kasson et al., 2006].

4. Signaling events studied in model membranes

In this chapter we summarize the results from the investigation of two distinct signaling triggers in the plasma membrane, namely Ca^{2+} ions and palmitoylations of a transmembrane protein.

Calcium signaling events are characterized by a fast influx of Ca^{2+} into the cell interior via calcium channels [Berridge et al., 2003]. We describe the interactions of such cations with plasma membrane models with increasing complexity going from pure phospholipid bilayers to membrane extracts from human HEK293 cells. In Chapter 4.1 and paper [Melcrova et al., 2016], we focus on identification of the local binding sites of Ca^{2+} ions in phospholipid bilayers, and on the global changes in the biophysical properties of the membrane upon Ca^{2+} binding. We increase the complexity of the plasma membrane model by adding cholesterol observing its influence on calcium ions interaction with the membranes in Chapter 4.3 and paper [Melcrova et al., 2019b]. Our results from cholesterol-containing model membranes were also compared with the membranes isolated from HEK293 cells. We further enriched the plasma membrane model with the trasmembrane peptides to better mimic the real protein-rich plasma membrane. With such a model, we have investigated the impact of the transmembrane peptides presence on the affinity of the membrane for calcium as well as the biophysical properties of the lipid bilayer itself (Chapter 4.5).

In mammalian cells the most abundant metal cation is however not Ca^{2+}, but the monovalent cations Na^+ and K^+ with resting concentrations of 100-150 mM in extracellular and cytosolic compartments, respectively. Global changes in the distribution of these cations during the cell homeostasis trigger changes in the cell volume, osmotic balance regulation, and electrostatic potential [Sten-Knudsen, 2002, Jentsch, 2016]. Although divalent Ca^{2+} ions are present in much lower concentrations (1-2 mM) than monovalent cations, they adsorb more efficiently to both zwitterionic and negatively charged membranes [Binder and Zschörnig, 2002, Porasso et al., 2009, Catte et al., 2016, Melcr et al., 2018]. We discuss different behavior of the adsorption of Na^+ and Ca^{2+} cations to zwitterionic membranes in Chapter 4.2 and paper [Melcrova et al., 2017], and we also investigate the effects a variety of monovalent cations, Cs^+, K^+, Na^+ and Li^+ on negatively charged membrane models and membranes of HEK293 cells in Chapter 4.4 and paper [Melcrova et al., 2019b].

Another way of intracellular signal transduction is the activation of proteins in the plasma membrane. One such activation mechanism can happen through palmitoylation of certain recognized protein residues. This is also the activation mechanism of the phosphoprotein associated with glycosphingolipid-enriched microdomains in the plasma membrane (PAG), which natively exists in the plasma membrane, and has a major role in the initiation step of many signaling pathways. It is an adaptor protein recruiting the cytoplasmic tyrosine kinase Csk, the major negative regulator of Src-family kinases, to place of signaling and modificates cytoskeleton [Hrdinka and Horejsi, 2014]. PAG can be switched between an active and passive form by two palmitoylations on its cytoplasmic membrane–proximal

cysteine residues [Brdicka et al., 2000, Svec, 2008, Hrdinka and Horejsi, 2014]. The biological function of the protein can be read elsewhere [Svec, 2008, Hrdinka and Horejsi, 2014]. In this work, we focus on the structural consequences of the two palmitoylations on the surrounding lipid bilayer. The results are summarized in Chapter 4.6 and paper [Melcrova et al., 2019a].

4.1 The complex nature of calcium cation interactions with phospholipid bilayers

Resting intracellular concentration of Ca^{2+} is only 1-2 mM. The calcium-triggered signalling events are, however, connected with rapid spikes of Ca^{2+} concentration caused by an influx of the Ca^{2+} into the cytosol via calcium channels [Berridge et al., 2003]. Ca^{2+} concentration can be locally and temporally up to 100-fold higher during such events. Global changes induced by the presence of Ca^{2+} ions at higher concentrations near cellular membranes are highly physiologically relevant as well as the identity of the local binding sites. This section focuses on identification and characterization of Ca^{2+} binding sites within the plasma membrane (published in paper [Melcrova et al., 2016]).

We use PC/PS (80/20, mol/mol) bilayers to model the inner leaflet of the plasma membrane. In such membranes, three possible binding sites can be distinguished: carboxyl groups of PS, phosphate groups of PC and PS, and carbonyl groups of PC and PS. To date, the studies on the binding sites of Ca^{2+} ions were incomplete and often inconsistent [Herbette et al., 1984, Huster et al., 2000, Binder and Zschörnig, 2002, Böckmann and Grubmüller, 2004b, Pedersen et al., 2006, Rodríguez et al., 2007, Uhríková et al., 2008, Porasso et al., 2009, Martín-Molina et al., 2012, Tsai et al., 2012]. In this work, we have probed Ca^{2+}-membrane interactions by a combination of spectroscopic methods and MD simulations to gain a complex molecular-level picture on Ca^{2+} binding to lipid bilayers. In the MD part of this study we use an ionic force-field which implicitly accounts for polarization effects (ECC ions). This improvement overcomes limitations of previously used force-fields where ion-lipid binding interactions were overshoot [Kohagen et al., 2014]. The experimental techniques include Time-dependent fluorescence shift (TDFS), Dynamic light scattering (DLS) and zeta potential measurements of large unilamellar vesicles (LUV) and Vibrational sum frequency spectroscopy (VSFS) performed on Langmuir monolayers.

DLS and zeta potential measurement of DOPC and DOPC/DOPS (80/20, mol/mol) vesicles reveal the macroscopic changes induced by Ca^{2+} ions (Figure 4.1). In previous studies it has been shown that calcium can lead to aggregation or fusion of negatively charged lipid vesicles [Wilschut et al., 1981, Nir et al., 1983]. For most of the DOPC samples unimodal distributions of liposome hydrodynamic diameters centered near 150 nm were obtained (Figure 4.1A). Vesicle aggregation with large aggregates of size $\sim$5 μm was only induced at 1 M $CaCl_2$. Reversible polydispersity was observed in DOPC/DOPS vesicles (Figure 4.1B). They aggregate in 5 to 30 mM $CaCl_2$ concentration range with largest detectable particles of size $>$5 μm, and become monodisperse again at 50 to 1000 mM $CaCl_2$. The reversible nature of this process and no indications of any persistent growth of the liposomes suggest that Ca^{2+} ions are able to bridge the lipid bilayers of

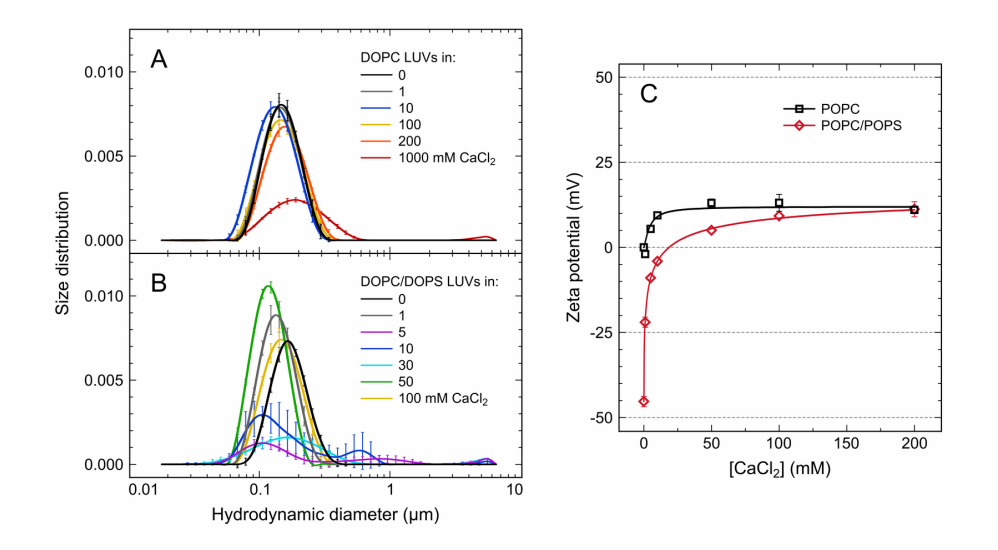

Figure 4.1: Dynamic light scattering (A,B) and zeta potential (C) measurements of large unilamellar vesicles (LUVs) composed of wither DOPC and DOPC/DOPS (80/20, mol/mol) for DLS measurements, or POPC and POPC/POPS (80/20, mol/mol) for zeta potential measurements. The LUVs were dispersed in 0.1 mM EDTA, or in $CaCl_2$ solutions of concetrations 1-1000 mM. Measured at 283 K. Standard deviations are depicted. Zeta potential data were fitted with Langmuir-Freundlich adsorption model [Sips, 1950]. Figure taken from [Melcrova et al., 2016].

neighboring vesicles, and that this process is reversible.

Zeta potential measurements (Figure 4.1C) then clearly show adsorption of Ca^{2+} ions on both POPC and POPC/POPS (80/20, mol/mol) vesicles. For instance, 200 mM $CaCl_2$ is sufficient to overcharge originally negatively charged POPC/POPS vesicles by adsorption of Ca^{2+} ions. The observed polydisperse character of DOPC/DOPS vesicles at intermediate $CaCl_2$ concentrations is thus the consequence of the bridging of neighboring vesicles by the ions, whereas at higher $CaCl_2$ concentrations this effect is overcome by the electrostatic repulsion of the subsequently positively charged vesicles.

Laurdan and Dtmac probes were used for TDFS measurements of calcium-induced changes at the carbonyl and phosphate levels of PC and PC/PS (80/20, mol/mol) membranes (see Figure 4.2A). The integrated relaxation time, τ, of Laurdan shows an overal slowdown of the lipid mobility at the carbonyl level of the phospholipids induced by the increasing concentation of $CaCl_2$ (Figure 4.2B). Three regions with a different slope of the τ response can be distinguished. First, there is a fast decrease in the lipid mobility at 0-5 mM $CaCl_2$ concentrations, followed by a plateau between 5-50 mM $CaCl_2$, and another decrease of the lipid mobility (i.e., increase of τ value). The initial increase corresponds to the binding of Ca^{2+} ions into the bilayer deeply into the carbonyl region. The seeming saturation of this process at 5-50 mM $CaCl_2$ concentrations can be explained by bridging of the opposing vesicles by Ca^{2+} ions as proved by DLS and zeta potential measurements. The further increase of $CaCl_2$ concentration provides additional binding of the ions, consequent electrostatic repulsion of the overcharged vesicles and further rigidification of the bilayer.

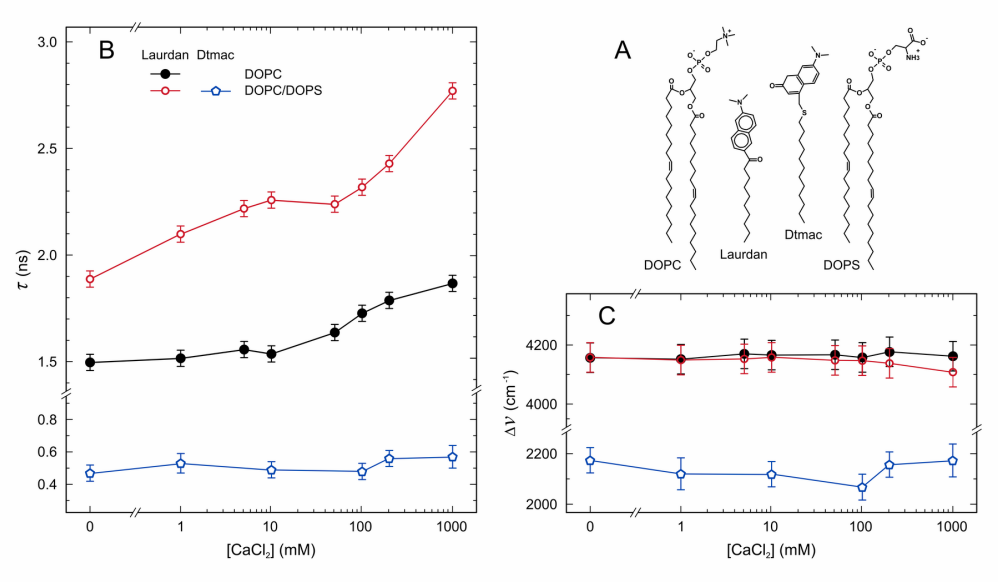

Figure 4.2: Time dependent fluorescence shift (TDFS) of Laurdan and Dtmac probes. A) Location of the probes with respect to DOPC and DOPS phospholipids in membranes. B) Integrated relaxation time, τ, and C) total spectral shift, $\Delta\nu$, measured at large unilamellar vesicles (LUVs) composed of DOPC or DOPC/DOPS (80/20, mol/mol) with 1 mol% of the probe. The LUVs were dispersed in 0.1 mM EDTA, or in $CaCl_2$ solutions of concetrations 1-1000 mM. Measured at 283 K. Standard deviations are depicted. Figure taken from [Melcrova et al., 2016].

Dtmac probe, located at the phosphate level of the phospholipids, does not show such dramatic effect of the increasing $CaCl_2$ concentration. Being exposed to the bulk water, Dtmac probes not only the relaxation of the phospholipid headgroups but also the fast relaxation of the bulk water itself buffering the effects induced by Ca^{2+}. Apparent changes were observed only for the negatively charged DOPC/DOPS vesicles dispersed in 1 M $CaCl_2$ solution (Figure 4.2B).

The total spectral shift, $\Delta\nu$, shows only slight dehydration at the carbonyl level (probed by Laurdan) at 200 mM and 1 M $CaCl_2$ in DOPC/DOPS system (Figure 4.2C). Note that $\Delta\nu$ reflects the polarity of the local environment rather than hydration. The presence of the ion itself changes the local polarity around the fluorescence probe and thus contributes to the relaxation process increasing $\Delta\nu$. Thus, the presence of Ca^{2+} ions can compensate for the dehydration effect possibly shown by a decrease of $\Delta\nu$. A slight dehydration of the phosphate level (probed by Dtmac) is observed for 0-100 mM $CaCl_2$ solutions. The decreasing trend of $\Delta\nu$ is reversed for 200 mM and 1 M concentrations, which can be again a consequence of the ion presence in the vicinity of the Dtmac probe.

We complemented our experimental findings by MD simulations of POPC and POPC/POPS (80/20, mol/mol) bilayers. Note that TDFS measurements of POPC and POPC/POPS vesicles show the same trends of τ and $\Delta\nu$ as those obtained at LUVs composed of doubly unsaturated DOPC and DOPS. The rigidifying effect of Ca^{2+} ions is demonstrated as a gradual decrease of the area per lipid (APL) in both POPC and POPC/POPS membranes upon the addition of 100-600 mM $CaCl_2$ to the system (Figure 4.3A,B). Up to 600 mM $CaCl_2$, all Ca^{2+}

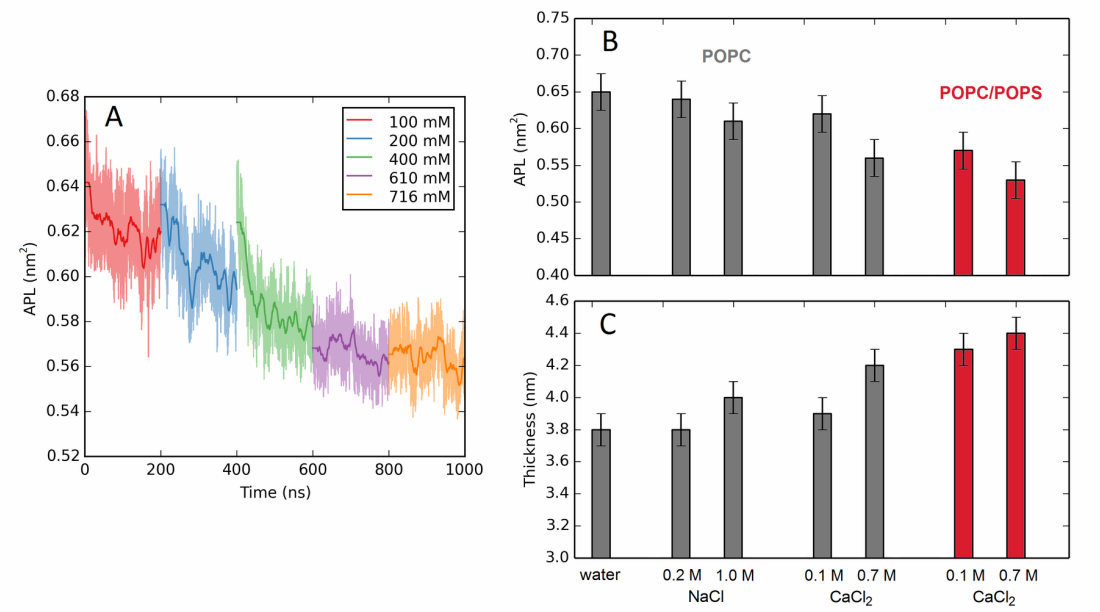

Figure 4.3: Area per lipid (A, B) and thickness (C) of the bilayers. (A) Area per lipid of the POPC bilayer during five MD simulations, each 200 ns long, with the increasing $CaCl_2$ concentration. Legend shows the bulk $CaCl_2$ concentrations at the beginning of the respective simulation run. Average area per lipid (B) and bilayer thickness (C) of POPC and POPC/POPS bilayers (80/20 mol/mol) in pure water and in 0.1 and 0.7 mM $CaCl_2$ solutions. Data for 0.15 NaCl and KCl are taken from additional 200 ns-long simulations calculated for comparison with $CaCl_2$. Error bars for APL are based on block analysis. The bilayer thickness is calculated from the density profiles as the phosphate–phosphate distance. The error bars represent the inaccuracy of the estimation of the peak positions. Figure taken from [Melcrova et al., 2016].

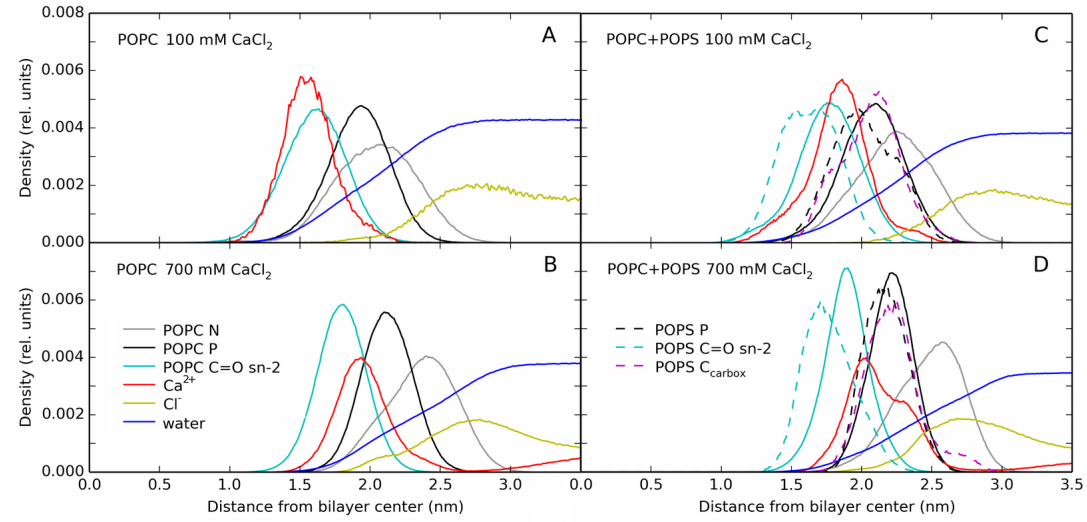

Figure 4.4: Density profiles calculated along the bilayer cross-section for nitrogen (N), phosphorous (P) and sn-2 carbonyl oxygen (C=O) atoms of POPC and POPS, carboxylate groups (C_{carbox}) of POPS, calcium (Ca^{2+}) and chloride (Cl^-) ions, and water molecules. Averages of the density profiles from both bilayer leaflets are depicted. Figure taken from [Melcrova et al., 2016].

Lipid bilayer	[$CaCl_2$]	Ca^{2+} coordination numbers		
		PO_4	C=O	COO^-
POPC	100 mM	3.0 ± 0.5	2.5 ± 0.5	—
	700 mM	2.6 ± 0.5	2.1 ± 0.5	—
POPC/POPS	100 mM	2.0 ± 0.5	1.8 ± 0.5	3.0 ± 0.5
(80/20, mol/mol)	700 mM	2.2 ± 0.5	1.3 ± 0.5	1.5 ± 0.5

Table 4.1: Average numbers of the considered groups in the first coordination shell of an absorbed Ca^{2+} ion. Standard deviations are given. Table taken from [Melcrova et al., 2016].

ions were adsorbed to the bilayers resulting in the effective 0 mM $CaCl_2$ concentration in the bulk water. No desorption events of the ions were observed during the whole 200 ns long simulations. Further increase of the bulk $CaCl_2$ to nominal concentration of 700 mM did not promote any additional changes in APL. A dynamic equilibrium between bulk and membrane-bound Ca^{2+} ions was reached, with the effective bulk concentration of 180 mM, i.e. comparable to the experimentally explored samples. Reduction of APL is likely caused by co-binding of a single Ca^{2+} ion between a few neighboring lipids. The lateral membrane compression is accompanied by the increase of bilayer thickness (Figure 4.3C).

The thickening effect can be also seen as a shift of all the nitrogen, phosphorous, and carbonyl peaks in the density profiles along the membrane normal in Figure 4.4. The density profiles show the different regimes of calcium binding at low (Figure 4.4A,C) and high (Figure 4.4B,D) nominal $CaCl_2$ concentrations. At low concentration, Ca^{2+} ions penetrate deep into the POPC bilayers, close to the carbonyl level (Figure 4.4A), the Ca^{2+} location is however shifted towards the water phase after reaching the bilayer saturation with ions (Figure 4.4B). In the mixed POPC/POPS bilayers the ions are located in between carbonyls and phosphates in both studied concentrations (Figure 4.4C,D). The mean distance of Ca^{2+} ions from the bilayer center increases only due to the membrane thickening.

The dehydration effect probed by TDFS measurements was also investigated by the MD simulations. We calculated the numbers of water molecules in the first solvation shell of the carbonyl oxygens and phosphate phosphors. In calcium saturated system (0.7 M $CaCl_2$ solution), the number of water molecules in the phosphate region is about 30% lower than in the 0.1 M $CaCl_2$ solution in both POPC and POPC/POPS systems. The dehydration of the carbonyl region is almost 40% and 20% for POPC and POPC/POPS systems, respectively.

To evaluate the binding of Ca^{2+} ions to individual atomic groups of phospholipids we calculated the average number of Ca^{2+} ions in the first coordination shell of the several functional groups (Table 4.1). These numbers are schematically visualized by the thickness of the red lines at Figure 4.5. In the POPC bilayers, the coordination numbers show a slight preference for PO_4 in comparison to C=O even at low $CaCl_2$ concentration, where the ions are located deeper in the membrane, close to the carbonyls (Figure 4.5A). Ca^{2+} ions shift towards the water phase (Figure 4.5B) with the increased $CaCl_2$ concentration preserving the ratio of 20% more ions bound to PO_4 than to C=O.

In a mixed POPC/POPS system, the negatively charged carboxylate group of POPS increases the complexity of the calcium binding. In the low concentration

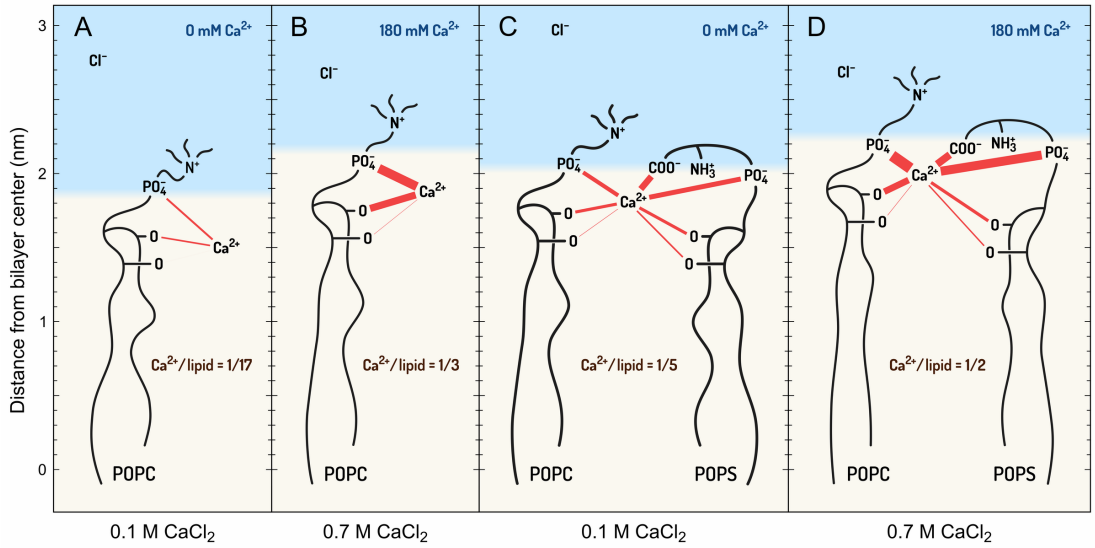

Figure 4.5: Scheme of calcium ions binding to POPC (A, B) and POPC/POPS (C, D) bilayers at low (A, C) and high (B, D) $CaCl_2$ concentrations. Nominal bulk $CaCl_2$ concentrations were 100 and 700 mM, resulted in 0 and 180 mM in the bulk water after equilibration of the binding process. The thickness of the red lines reflects the average number of Ca^{2+} ions in the first coordination shell of a given group. Final bulk Ca^{2+} concentrations are given in blue. Ratios of bound Ca^{2+} ions per phospholipid for each system are depicted in brown. Figure taken from [Melcrova et al., 2016].

regime, Ca^{2+} ions bind predominantly to COO^- followed by PO_4 and C=O. At high $CaCl_2$ concentration, the binding to PO_4 is strenghtened (Figure 4.5D). Interestingly, almost all the binding at carbonyl level occurs only to the carbonyls of the palmitoyl (sn-2) chains of both POPC and POPS. Oleoyl (sn-1) carbonyls are somewhat unattractive for the ions.

Ca^{2+} ions can be bound simultaneously to all the considered cation-binding groups (i.e., COO^- and PO_4 or C=O groups) of the same molecule. They are also concurrently bound to more than one lipid molecule, typically 2-3, at a time. The calculated binding capacity of the membrane for Ca^{2+} ions is 1 ion per 3 lipids for POPC and 1 ion per 2 lipids for mixed POPC/POPS membranes. Recent developements of the lipid force-fields however showed that these results are likely overestimated even with the usage of ECC ions [Catte et al., 2016, Melcr et al., 2018]. Moreover, the increased probability of Ca^{2+} ions close to the carbonyl region is likely an artefact of the Berger force-field used in our study [Catte et al., 2016]. Either way, any of these simulation models can be used to interpret our experimental finding from TDFS measurements, where the effects of ions in the carbonyl region is evidenced. Hence, only the precise balance of the Ca^{2+} binding sites and the binding capacity of the membrane remain unclear.

The overestimated depth of the Ca^{2+} ions placement in the membrane can be the cause of the small discrepancy in the comparison between TDFS, MD simulation results and the VSFS experiments [Melcrova et al., 2016]. VSFS experiments were used to investigate binding to carboxylate, phosphate and carbonyl groups in Langmuir monolayers. The carboxylates and phosphates are largely affected by the Ca^{2+} binding. The shifts in the corresponding VSFS spectral peaks indicate

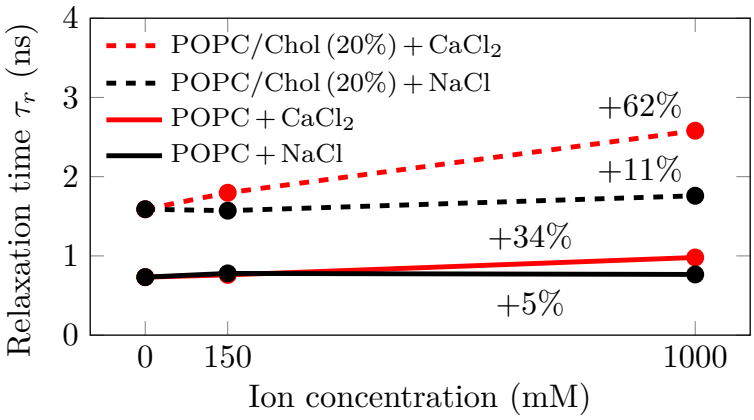

Figure 4.6: Integrated relaxation time, τ, from TDFS measurements. Measured at LUVs composed of POPC or POPC/20mol%chol (80/20, mol/mol) with 1 mol% of the probe. The LUVs were dispersed in EDTA, 0.1 mM, or in NaCl or $CaCl_2$ solutions of concetrations 150 and 1000 mM. Measured at 310 K. The percentage values show the relative increase of τ upon the addition of 1M salt. Error of a single measurement is ∼0.05 ns. We estimate the total error for the relative increase to be ∼10 percentage points. Figure taken from [Melcrova et al., 2017].

direct contact of Ca^{2+}. The changes induced in the carbonyl region are visible but smaller. Hence, the carbonyls are probably directly less occupied by the Ca^{2+} ions than calculated by the MD simulations. Their mobility and dynamics is however indeed affected as evidenced by both TDFS and VSFS measurements.

4.2 Two cations, two mechanisms: interactions of sodium and calcium with zwitterionic lipid membranes

Under the physiological condition, both extracellular and cytosolic compartments of cells are contain various salts. Hence, we investigate the impact of other biologically relevant ions on biophysical properties of cellular membranes. The most common monovalent cation at the extracellular space is Na^+ (at concentrations of 100-150 mM). In this section, we describe the different behavior of monovalent Na^+ and divalent Ca^{2+} when acting on zwitterionic plasma membrane models. The results of this study were published in [Melcrova et al., 2017].

We have studied the mechanism of Ca^{2+} and Na^+ interaction with the membrane surface using TDFS technique and MD simulations. Fluorescence experiments were measured at LUVs composed of either POPC or POPC/20mol%chol (80/20, mol/mol) at different salt concentrations with 1 mol% of Laurdan probe. We performed the measurements at 310 K (Figure 4.6), and also 288 K and 298 K obtaining similar trends for all the temperatures. Decreasing the temperature or adding cholesterol increases the relaxation time, τ (red lines in Figure 4.6) making the membrane more rigid. The addition of Na^+ ions, however, does not have any significant effect on either POPC ($\Delta\tau_r$ = 5%) or POPC/20mol%chol

($\Delta\tau_r$ = 11%) membranes (black lines in Figure 4.6). The observed increase in the relaxation time is within the error estimate. The Na^+ ions thus do not penetrate to the membranes and do not affect the relaxation of Laurdan resting at the carbonyl level of the phospholipids. The rigidification induced by Ca^{2+} ions arises from the bridging of neighboring lipid molecules and consequent lateral membrane compression as discussed in Chapter 4.1. Cholesterol presence enhances the Ca^{2+} influence on the studied membranes, $\Delta\tau_r$ = 34% and 62% for POPC and POPC/20mol%chol membranes, respectively (red lines in Figure 4.6). Consistently, MD simulations reveal the increased adsorption of Ca^{2+} ions to the cholesterol containing membranes [Melcrova et al., 2017]. These additional ions cause further bridging of the lipids and consequently lower the lipid mobility around Laurdan.

The binding of Ca^{2+} and Na^+ to lipid membranes is of a remarkably different nature as was consistently shown in both experiments and simulations. Na^+ ions interact only weakly with the membrane surface and their binding sites are thus of a rather transient character. The Na^+ ions do not compete for the binding and the number of bound ions is determined only by the number of the available binding sites, i.e. PC headgroups. In contrast, the Ca^{2+} ions exhibit a competitive behavior. Their binding energy is much higher making the Ca^{2+} binding nearly irreversible. Under these conditions the membrane surface is completely covered by Ca^{2+} ions. In our systems, the cholesterol acts as a spacer in between the phospholipids, and increases the membrane surface available for the ions. Cholesterol presence thus increases the Ca^{2+} ions adsorption even that it does not interact with the ions in any ways. Detailed study of the cholesterol impact on model membranes and its influence on Ca^{2+} binding capacity is described in detail in Chapter 4.3.

4.3 Simultaneous compression of lipid membranes by calcium and cholesterol

Cholesterol as a major membrane constituent of the eukaryotic organisms should not be excluded from the model of the plasma membrane. Cholesterol is known to compress the lipid bilayer as it induces lateral pressure. Moreover, it increases membrane stability and reduces its permeability for small solutes including salt ions [Rawicz et al., 2008]. On the molecular level, cholesterol is located in the hydrophobic region of the bilayer with the tendency to minimize the non-favorable contacts between its methyl groups and the double bonds of the acyl chains of unsaturated lipids as well as direct interactions with other cholesterol moieties [Chiu et al., 2002]. We investigate the interaction of calcium ions with the cholesterol-containing membranes and compare the data with the plasma membrane fragments extracted from HEK293 cells. Such approach gives us the possibility to directly evaluate the biological relevance of the observed interactions. Results of this study were submited for publication as [Melcrova et al., 2019b].

Figure 4.7 summarizes the results of our fluorescence experiments. The results of the TDFS measurements are in agreement with our previous studies about binding of Ca^{2+} to lipid membranes (Chapters 4.1 and 4.2, [Melcrova et al., 2016, 2017]). The relaxation time, τ, of Laurdan increases with the addition of $CaCl_2$

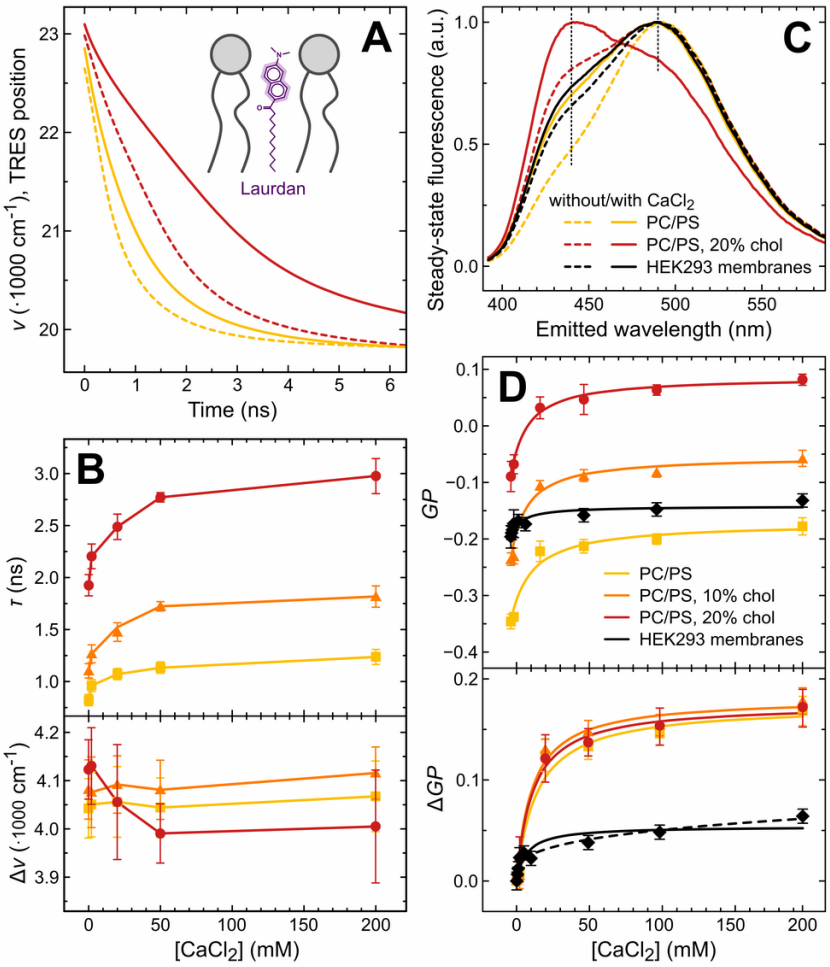

Figure 4.7: Time dependent fluorescence shift (TDFS; A, B) and General polarization (GP; C, D) of Laurdan. Results of experiments performed in POPC/POPS liposomes without (yellow lines) and with 10 or 20 mol% cholesterol (orange and red lines, respectively) at 37 °C, and membranes isolated from HEK293 cells (black lines) at 40 °C in the absence (dashed lines) and presence (solid lines) of $CaCl_2$ are presented. A) Examples of the measured position of the maxima of Time-Resolved Emission Spectra in time after electronic excitation in the TDFS experiment; Laurdan location in the lipid bilayer schematically depicted in the inset. B) integrated relaxation time, τ (upper panel), and total emission shift, $\Delta\nu$ (lower pannel), as a function of bulk $CaCl_2$ concentration. C) Examples of steady-state emission spectra; 440 and 490 nm peaks characteristic for the emission from the solid and liquid disordered phases, respectively, marked by vertical dotted lines. D) GP calculated from the fluorescence intensities emitted at 440 and 490 nm as a function of bulk $CaCl_2$ concentration (upper panel) and the GP difference, ΔGP, upon $CaCl_2$ addition (lower panel). Solid lines represent best fit to Langmuir adsorption model [Langmuir, 1918] and dashed line – to Langmuir-Freundlich model [Sips, 1950] which better describes roughness of highly inhomogenious surface of HEK293 membranes.

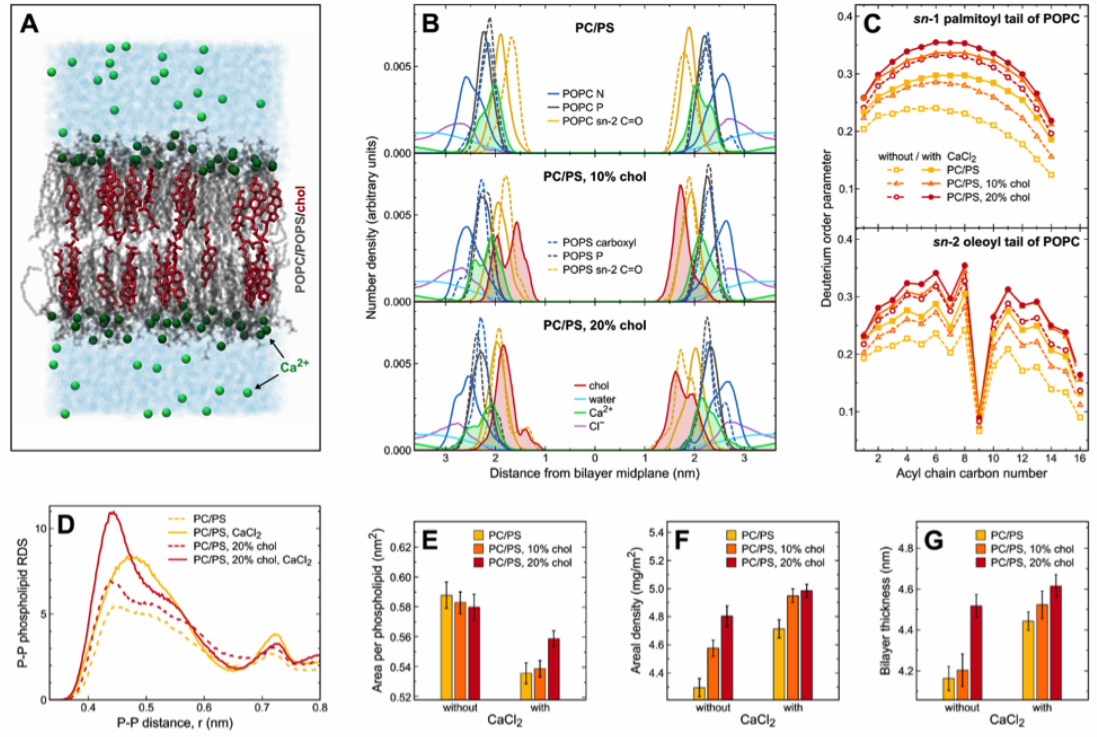

Figure 4.8: Results of MD simulation of POPC/POPS (80/20, mol/mol) bilayers without and with 10 or 20 mol% cholesterol exposed to $CaCl_2$. A) Representative snapshot of the simulation box for POPC/POPS/20mol%chol system (phospholipid molecules in grey, cholesterol in red, adsorbed Ca^{2+} ions in dark green and Ca^{2+} ions in bulk water in light green), B) Number density profiles along the bilayer normal, C) Deuterium order parameters of sn-1 (upper panel) and sn-2 (lower panel) acyl chains of POPC, D) Radial distribution function (RDF) between lipid phosphorus atoms, E) Area per phospholipid, F) Areal density - total mass of phospholipids and cholesterol divided by membrane surface area, G) Membrane thickness measured as phosphate-phosphate distance.

in all PC/PS, POPC/POPS/10%chol, and POPC/POPS/20%chol systems (Figure 4.7 upper panel) showing rigidification of the membranes caused by Ca^{2+} ions. The Ca^{2+} effects are observable already at 2 mM $CaCl_2$ concentration and saturate for larger concentrations. 10 mol% of cholesterol shifts the τ values up comparably to the increase of $CaCl_2$ concentration from 0 to 200 mM. Evidence that these two factors have a comparable rigidifying effect on the membranes can be read also from the Laurdan emission spectra (Figure 4.7C), where the shift of the steady state Laurdan emission spectrum to lower wavelengths reflects the change in the membrane rigidity as the peaks at 440 and 490 nm are characteristic for the emission from the solid and liquid-ordered phase, respectively. The changes in the steady state spectra can be evaluated by Generalized Polarization (GP) values, defined as $GP(\lambda_{EX}) = (I_{440} - I_{490}/(I_{440} + I_{490})$, where I_{440} and I_{490} are the fluorescence intensities at emission wavelengths of 440 nm and 490 nm, respectively, upon excitation at λ_{EX}. Reported GP_{EX} values were averaged over λ_{EX} range of 320-400 nm. Noticebly, the addition of both cholesterol and calcium increase the intensity of fluorescence emitted at 440 nm, however only the simultaneous addition of 20 mol% cholesterol and 200 mM $CaCl_2$ makes the 440 nm peak dominate over the 490 nm one. Since the changes in polarity, depicted by total spectral shift, $\Delta\nu$, are minor (Figure 4.7B, lower panel), the observed changes in GP values upon $CaCl_2$ addition (Figure 4.7D, upper panel) can be interpreted as the hindrance of mobility of lipid carbonyls rather than their dehydration. To better compare the GP results of the studied systems we present GP changes also in the form of $\Delta GP = GP - GP([CaCl_2] = 0)$ (Figure 4.7D, lower panel). The similarity of the ΔGP curves obtained for the three studied model membranes shows that the presence of cholesterol does not influence the GP increase caused by $CaCl_2$. This suggests that the hindrance of local lipid mobility caused by cholesterol and calcium is likely independent from each other. We corroborate this finding with MD simulations. The results are sumarized in Figure 4.8 with a snapshot of the equilibrated POPC/POPS/20%chol lipid bilayer embedded in $CaCl_2$ solution depicted in Figure 4.8A.

The hindrance of lipid mobility evidenced by τ parameter and GP values in TDFS and by steady state experiments, respectively, can be linked to the membrane compression given by area per lipid (APL). Here, we quantify the membrane compression by two different parameters, area per phospholipid (APP) and areal density. APP represents the total area of the membrane divided by the number of phospholipid molecules, disregarding cholesterol molecules, hence giving a measure of distance between phospholipids. Without the action of Ca^{2+}, cholesterol causes only slight decrease of APP (Figure 4.8E), whereas the addition of $CaCl_2$ clearly reduces the distances between the phospholipid moieties as the headgroups are bridged by Ca^{2+} ions. Interestingly, once reduced by calcium, APP can only be increased by the cholesterol addition, which is clearly seen in the increase of APP when going from POPC/POPS system to POPC/POPS/20%chol. Lipids in POPC/POPS bilayer seem to be compressed by Ca^{2+} ions to the point where steric effects of the cholesterol addition dominate over its condensing tendencies (Figure 4.8E). Surprisingly, the distances in between phosphorus atoms of the neighboring lipids are decreased as evidenced in the radial distribution functions (RDF) showing distances between phosphorus atoms of phospholipids (Figure 4.8D). In the presence of $CaCl_2$, the first RDF

maximum for POPC/POPS/20%chol is shifted to lower distances (∼0.45 nm) compared to that of POPC/POPS (∼0.48 nm). A similar trend, however much less pronounced, was observed in the RDF between phospholipid carbonyls **??**. Thus, even though the APP results suggest an increase of the mean area occupied by a phospholipid, the phospholipid headgroups are closer to each other , which can be explained by a directional reorientation of the headgroups to a more favorable manner.

In the absence of $CaCl_2$, cholesterol significantly increases the areal density, i.e., the total mass of phospholipid and cholesterol molecules divided by the total membrane area (Figure 4.8F). Also, the $CaCl_2$ addition increases this parameter in accordance with the bilayer compression evidenced by APP reduction. At high $CaCl_2$ concentrations, we observe saturation of the areal density caused by cholesterol addition. Such results lead us to a conclusion that both Ca^{2+} ions and cholesterol increase the packing of POPC/POPS membranes in an additive manner, but together, in sufficient amounts, they reach the limit of membrane compressibility. Similarly, we see saturation in the increase of thickness induced by calcium and cholesterol (Figure 4.8G).

oOrdering of the lipid acyl chains is closely related to the increased membrane packing and thickness as is depicted in Figure 4.8C, which shows deuterium order parameters calculated for the carbon atoms of sn-1 and sn-2 chains of POPC molecules. Both cholesterol and Ca^{2+} increase the order of the whole acyl chains. The presence of Ca^{2+} thus does not diminish the well known ordering effect [Chong et al., 2009, Róg et al., 2009, Martinez-Seara et al., 2010, Almeida et al., 2011] of cholesterol. Interestingly, although the Ca^{2+} ions are adsorbed in the headgroup region, they indirectly elevate the order of the whole acyl chains. The ordering of acyl chains also reaches its limits in the presence of both cholesterol and calcium.

Despite the MD simulations and fluorescence experiments are in a good agreement, we noticed a different saturation behaviour of the simultaneous effects of calcium and cholesterol in these two methods. While the structural effects observed in MD simulations show clear saturation, the saturation of ΔGP observed at large $CaCl_2$ concentrations is not influenced by cholesterol addition up to 20 mol%. Hence, the effects of cholesterol and calcium on bilayer structure and kinetics are additive within certain limits. When the bilayer cannot be further compacted and ordered, i.e., the changes of structural parameters are saturated, the lipid mobility is still slowing down with the further addition of cholesterol and Ca^{2+}.

The analysis of the binding sites in membranes enriched with cholesterol revealed no direct interaction of Ca^{2+} with cholesterol moieties. The number and character of the binding sites (Chapter 4.1, Figure 4.5) is not altered by the addition of neither 10 nor 20 mol% of cholesterol. The most potent binding sites are PO_4 groups of both POPC and POPS followed by COO^- of POPS and sn-2 carbonyls of all phospholipids. The relative occupancy of PO_4 and C=O regions remains the same reagardless of the cholesterol content, although the average total number of the adsorbed Ca^{2+} ions slightly increases (Table 4.2). A detailed analysis of MD trajectories revealed that cholesterol hydroxyl group resides in the proximity of sn-2 C=O of phospholipids, which is a Ca^{2+} binding moiety. Cholesterol, however, interacts with the carbonyls from the hydrophobic part of

Lipid bilayer	Number of adsorbed Ca^{2+}	Ca^{2+} coordination numbers		
		PO_4	C=O	COO^-
PC/PS (80/20)	0.45 ± 0.01	0.44 ± 0.01	0.20 ± 0.01	—
PC/PS/10%chol (72/18/9)	0.46 ± 0.01	0.43 ± 0.01	0.16 ± 0.01	0.01 ± 0.2
PC/PS/20%chol (67/17/17)	0.49 ± 0.01	0.45 ± 0.01	0.16 ± 0.01	0.01 ± 0.01

Table 4.2: Average number of adsorbed Ca^{2+} ions per phospholipid, and average numbers of the adsorbed Ca^{2+} ions in the first coordination shell of the given groups. Standard deviations are given.

the membrane whereas Ca^{2+} ions bind from the outside. Hence, even though Ca^{2+} and cholesterol share an interaction site they do not compete nor interfere with each other. The minor increase of Ca^{2+} binding upon adding cholesterol (Table 4.2) is thus not caused by any direct interaction between cholesterol and the ions, but rather by a slightly bigger membrane area (as suggested in Chapter 4.2 and paper [Melcrova et al., 2017]).

The effects of calcium on plasma membrane-enriched fractions (PMFs) extracted from HEK293 cells were then investigated. PMFs are far too complex for TDFS experiments and proper MD simulation. Instead, we analyze them using the GP approach. In Figure 4.7C, there is an example of Laurdan emission spectra measured at HEK293 PMFs. We observe a shift towards the peak at 440 nm suggesting the rigidifying effect upon addition of $CaCl_2$. The changes in GP, resp. ΔGP, (Figure 4.7D) show that the influence of calcium on HEK293 membranes is much smaller than on the synthetic model membranes. The results indicate that biological membranes are indeed protected from rigidification by calcium, however cholesterol does not play this role. As the responsible component could be the proteins, we address the influence of transmembrane peptides on calcium-membrane interaction later in Chapter 4.5.

4.4 Influence of monovalent ions on cholesterol-containing membranes

Further, we tested action of other physiologically relevant ions, namely Cs^+, K^+, Na^+ and Li^+, in POPC/POPS and POPC/POPS/cholesterol membranes as well as PMFs from HEK293 cells. The impact of monovalent salts in the concentrations of 0.2, 0.4, and 0.8 M was compared with 0.05, 0.1, and 0.2 M of $CaCl_2$ in systematic GP measurements (results are sumarized in Figure 4.9). The concentrations were chosen to match the ionic strength directly at the membrane where we can exclude the strength of chloride ions which are not adsorbed to the membrane.

All studied cations rigidify the studied model membranes (Figure 4.9A). The effects of the monovalent ions follow reversed Hofmeister series and are much smaller compared to the effects of Ca^{2+} (even at four times higher concentrations). The addition of cholesterol increases the measured GP values independently of the kind of salt present in the solution. Increased salt concentration further rigidifies

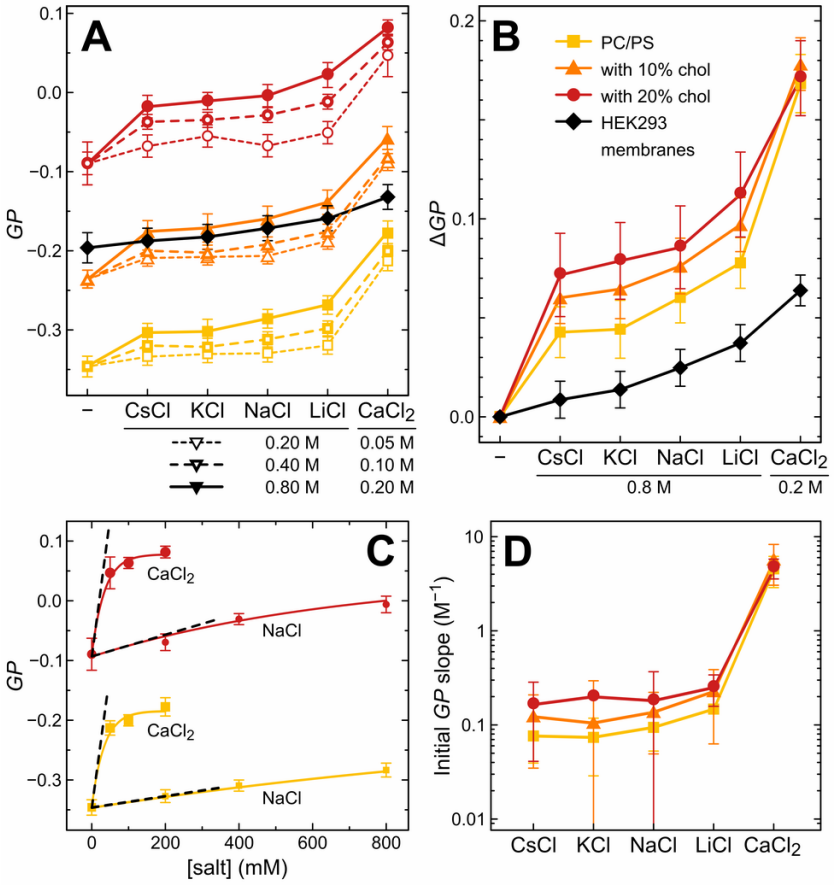

Figure 4.9: Laurdan Generalized Polarization (GP) experiments obtained for the adsorption of Cs^+, K^+, Na^+, Li^+, and Ca^{2+} to POPC/POPS vesicles without (yellow) and with 10 or 20 mol% of cholesterol (orange and red, respectively) at 37 °C, and membranes isolated from HEK293 cells (black) at 40 °C. Data for monovalent ions at HEK293 membranes are obtained from [Vošahlíková et al., 2014]. Standard deviations are presented. A) Absolute GP values measured without any salt, and in the presence of CsCl, KCl, NaCl, and LiCl or $CaCl_2$ at 3 various concentrations (see the legend below the x-axis). B) GP difference, ΔGP, upon the addition of either 0.8 M of monovalent salt solution or 0.2 M of $CaCl_2$. C) Examples of the GP values as a function of salt concentration fitted with Langmuir adsorption model [Langmuir, 1918] (solid lines) and their initial slopes represented by black dashed lines. D) Initial GP slopes obtained for the model systems as shown in panel C.

the membranes. Contrary to $CaCl_2$, adding cholesterol slightly but systematically enhances the effects of monovalent salts as evidenced by the increase of ΔGP values (Figure 4.9B). The magnitudes of the measured differences are, however, mostly within the error of the measurements. Note that in the case of $CaCl_2$, cholesterol presence does not change ΔGP values.

To estimate the ion specifity also at low salt concentrations we fitted the GP data with Langmuir absorption model, and determined initial GP slopes (Figure 4.9C,D). The differences in the initial GP slope between the monovalent ions are minor, even smaller than in ΔGP values.

Interestingly, in the neutral membranes (PC) the number of adsorbed Ca^{2+} ions, but not Na^+ ions, increase with the addition of cholesterol (Chapter 4.2, [Melcrova et al., 2017]). Here we show that in negatively charged POPC/POPS membranes the number of adsorbed monovalent ions increases with the addition of cholesterol as well.

As for PMFs from HEK293 cells, the trends for different ions are qualitatively the same however much smaller when compare to the model systems. Interestingly, Ca^{2+} does not stand out from the monovalent ions which leads us to conclusion that the response of the real plasma membrane in comparison to model membranes is much ßmore diminished for Ca^{2+} than for monovalent ions. This buffering against the influence of ions is however also present for monovalent ions and is not caused by cholesterol presence but rather another plasma membrane component.

4.5 Influence of transmembrane domain of membrane proteins on calcium-membrane interaction

Approximately 50 % of the mass of cellular plasma membrane consists of membrane proteins [Alberts et al., 2002, Nelson and Cox, 2005]. The estimated fraction of the transmembrane domains in the plasma membrane is about 3 mol%. Hence, we took another step in improving our model of the inner leaflet of the plasma membrane by incorporating transmembrane peptides. We designed the peptide as a single transmembrane helix with either zero total charge or with a mild amount of positive charge. The positively charged peptide follows the so called positive-inside rule stating that the excess positive charge of helical TM proteins resides at the cytoplasmic side of the plasma membrane [Pogozheva et al., 2013, Charneski and Hurst, 2013, Ulmschneider et al., 2005]. Hence, in the context of mimicking the inner leaflet of the plasma membrane it is biologically relevant to study peptides with the excessive positive charge. The positive charge is however expected to repel the calcium ions.

The design of the peptides used in this study is depicted in Figure 4.10. The artificial peptides referred as WALP-KD and WALP-KK^{2+} have a $(Leu\text{-}Ala)_n$ sequence forming their hydrophobic core surrounded by two Tyr residues. The crucial difference between the two peptides are the two residues neighbouring the Tyr-Tyr residues. WALP-KD has a zwitterioninc Lys-Asp sequence, while WALP-KK^{2+} has a positively charged Lys-Lys pair resulting in the additional +2 charge at both N and C termini of the peptide. In our symmetric membrane

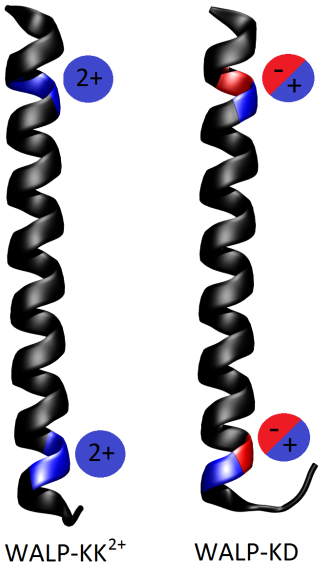

Figure 4.10: Illustration of the secondary structure of the artificial transmembrane peptides WALP-KD and WALP-KK^{2+}.

models, the positive charge is evenly distributed on both sides of the membrane, i.e., in both leaflets of the symmetric lipid bilayers. Full amino-acid sequences of the two peptides are the following:

WALP-KD GTSTS**KD**WW(LA)$_8$LWW**KD**FSTS
WALP-KK^{2+} GTSTS**KK**WW(LA)$_8$LWW.**KK**FSTS

Such a design of the peptides gives us the possibility to reproducibly investigate the influence of a transmembrane α-helix on the Ca^{2+} binding to the membranes, as well as the impact of the positive charge of the peptide on the cations binding.

We measured the influence of Ca^{2+} on zwitterioninc POPC and negatively charged POPC/POPS (80/20, mol/mol) membranes using the TDFS technique (Figure 4.11). The results without action of the Ca^{2+} ions (4.11, light blue and light green for POPC and POPC/POPS respectively) indicate a clear rigidifying effect of both studied peptides on the studied membranes (evidenced by higher relaxation times, τ, upon peptides incorporation, Figure 4.11A). Note that the rigidifying effect of the positively charged peptide, WALP-KK^{2+}, is always higher. The two peptides are not different in their sequence at the carbonyl region probed by Laurdan, however the differences in integrated relaxation time τ are visible at this level. The positive charge of WALP-KK^{2+} is located in a close vicinity of the water-membrane interface, hence we expect the headgroup region of the phospholipids to be affected even more.

The total spectral shift parameter, $\Delta\nu$, (Figure 4.11B) shows no significant change in the hydration of the membranes with and without the peptides.

Ca^{2+} further rigidifies all the studied membranes (Figure 4.11A, darkening color depicts the increasing Ca^{2+} concentration). Interestingly, the percentual increase of τ is the same regardless of the peptide presence or its charge. Hence, Ca^{2+} binding seems to be unaffected by the presence of either of the peptides. From the $\Delta\nu$ parameter (Figure 4.11B), we can observe a slight dehydration effect upon the Ca^{2+} binding for the POPC/POPS systems. Neither this behavior is

affected by the peptides presence.

The amount of bound Ca^{2+} can be indirectly evaluated by zeta potential measurements. This technique gives us the electric potential at the electrical double layer formed around the vesicles. The results are summarized in Figure 4.12. POPC membranes without the peptides do not have any charge nearby their surface. The charge neutrality is maintained upon the addition of the zwitterionic WALP-KD peptide, whereas the charge increases to the positive values with the addition of WALP-KK^{2+} (Figure 4.12, blue bars).

We, however, got different results from POPC/POPS membranes, which are negatively charged with the zeta potential values around -60 mV. Both peptides, WALP-KD and WALP-KK^{2+}, increase the zeta potential to -45 mV (Figure 4.12, green bars). The efect of the WALP-KD peptide is surprising as it does not carry any charge and still increases the zeta potential on the POPC/POPS vesicles. Since the zeta potential technique is sensitive to the electric potential on top of the electrical double layer of ions around the membrane surface, the change introduced by WALP-KD arises from the shielding of the effective charge at this layer. We performed a test experiment with another negatively charged phospholipid exchanging POPS in the LUVs, namely 1-palmitoyl-2-oleoyl-sn-glycero-3-phosphoglycerol (POPG). POPG has the same charge and a similar headgroup size as POPS. The results from zeta potential measurements on POPC/POPG (80/20, mol/mol) vesicles are analogical to those obtained from neutral, pure POPC, vesicles. Hence, the increase of zeta potential with the addition of WALP-KD is likely PS specific. We hypothesize that the peptide induces tilting of the PS headgroups resulting in the effective shielding of their negative charge.

$CaCl_2$ addition in the concentration of 2 mM has a little effect on the vesicles. Increasing of the concentration to 20 mM incereases the zeta potential of all the studied vesicles (Figure 4.12). The absolute increase is the same regardless the presence of the peptide, i.e., ($+15 \pm 3$) mV and ($+51 \pm 3$) mV for POPC and POPC/POPS vesicles, respectively. Hence, the peptides, either zwitterionic or negatively charged, has no influence on Ca^{2+} binding.

In conclusion, we found out that both transmembrane peptides, WALP-KD and WALP-KK^{2+}, indeed rigidify phospholipid bilayers. The positive charge of WALP-KK^{2+} only strenghtens this effect but it has surprisingly no influence on calcium binding to membranes as evidenced by both TDFS and zeta potential measurements. The diminished ionic effects in real biological membranes presented in Chapter 4.4 are thus caused neither by the presence of the transmembrane domains of membrane proteins, nor by the presence of cholesterol. The most probable cause for the smaller Ca^{2+} binding to cellular membranes are interactions with specific calcium binding sites in the cellular plasma membrane proteins, which were not, by design, present in our studies with transmembrane WALP peptides.

4.6 The importance of the two palmitoylations on PAG peptide

Phosphoprotein associated with glycosphingolipid-enriched microdomains in the plasma membrane (PAG) is a transmembrane adaptor protein recruiting the cy-

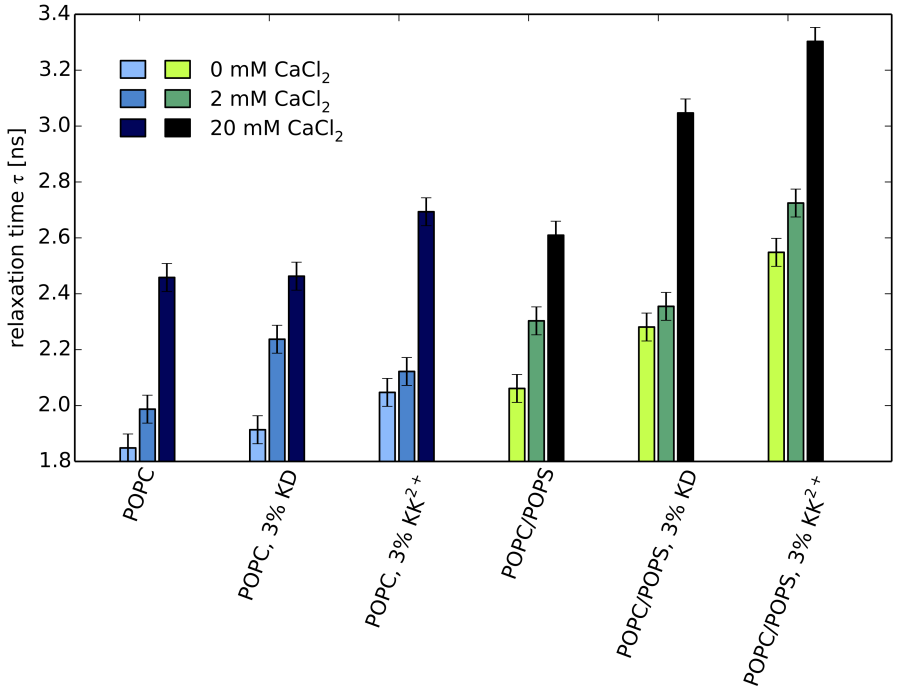

(a) Integrated relaxation time of Laurdan

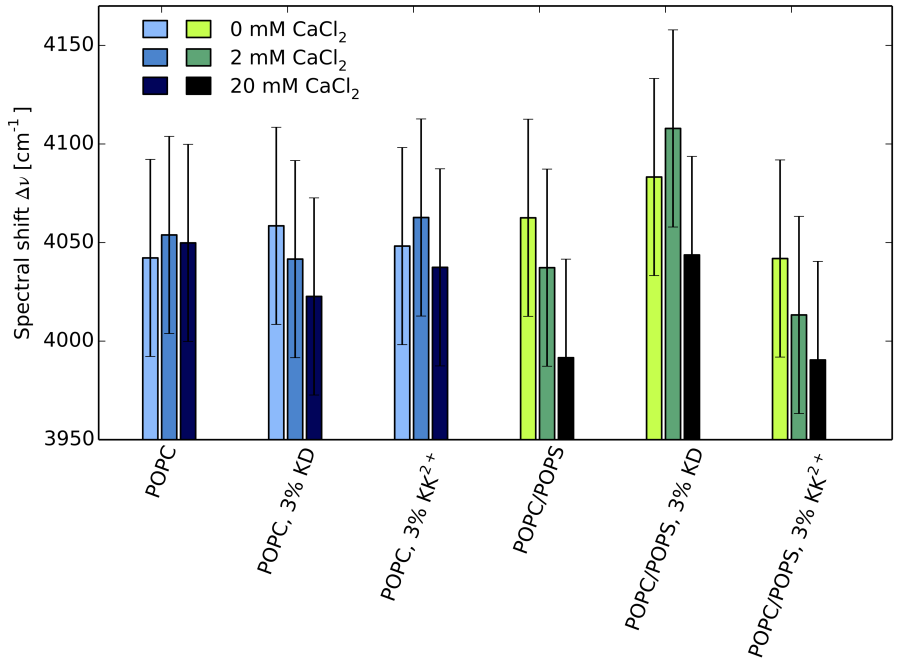

(b) Total stepctral shift of Laurdan

Figure 4.11: Time dependent fluorescence shift (TDFS) of Laurdan. a) Integrated relaxation time, τ, and b) total spectral shift, $\Delta\nu$, measured at large unilamellar vesicles (LUVs) composed of POPC or POPC/POPS (80/20, mol/mol) without peptides, with 3 mol% of WALP-KD, or with 3 mol % of WALP-KK^{2+} peptide. All samples contain 1 mol% of the probe. The LUVs were dispersed in 0.01 mM EDTA. $CaCl_2$ was titrated after the extrusion of the LUVs. After the salt addition, the samples were gently sonicated in a bath for 1 min and left for >10 min to equilibrate. Measured at 293 K. Standard deviations are depicted.

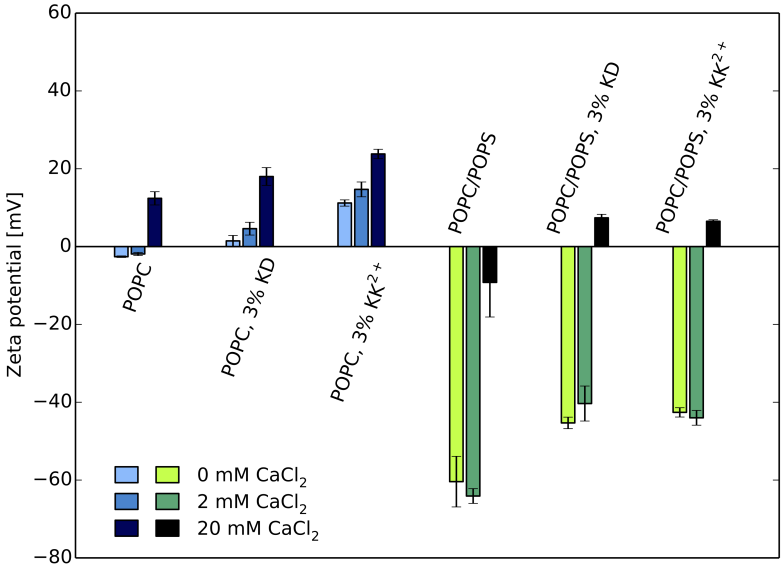

Figure 4.12: Zeta potential measurements at large unilamellar vesicles (LUVs) composed of POPC or POPC/POPS (80/20, mol/mol). The LUVs were dispersed in 0.01 mM EDTA. $CaCl_2$ was titrated after the extrusion of the LUVs. After the salt addition, the samples were gently sonicated in a bath for 1 min and left for >10 min to equilibrate. Measured at 293 K. Standard deviations are depicted.

toplasmic tyrosine kinase Csk to the plasma membrane [Svec, 2008, Hrdinka and Horejsi, 2014]. Csk recruitment is accompanied by the interation of PAG with cortical actin cytoskeleton [Svec, 2008, Hrdinka and Horejsi, 2014]. Such processes form the initial steps of different signaling pathways making PAG an important and strategic molecule for cellular survival. A trigger between an active and passive form of PAG is its lipid modification – palmitoylation. PAG localizes to the plasma membrane independently of its palmitoylation [Chum et al., 2016]. Hence, this reversible post-translational modification likely regulates its accumulation in nanoscopic membrane domains not yet visualized in living cells [Levental et al., 2010].

The full amino-acid sequence of the transmembrane part of the PAG used in our study is the following:

QITLWGSLAAVAIFFVITFLIFL**C**SS**C**DRE.

The palmitoylations are introduced at membrane-proximal Cys residues located near the peptide C-terminal, i.e., residues Cys-24 and Cys-27 (highlighted in bald font in the amino-acid sequence), resulting in palmitoylated residues denoted as CysP-24 and CysP-27, respectively.

We use all-atom MD simulations to study the behavior of the transmembrane domain of PAG and its modified version with two palmitoylations (denoted as PAGpalm) in the POPC lipid bilayer. We focus on changes in the biophysical properties of the surrounding lipid bilayer as well as the peptide upon incorporation of the palmitoyls. Results of this study are currently being prepared for a publication as [Melcrova et al., 2019a]. Both PAG and doubly-palmitoylated

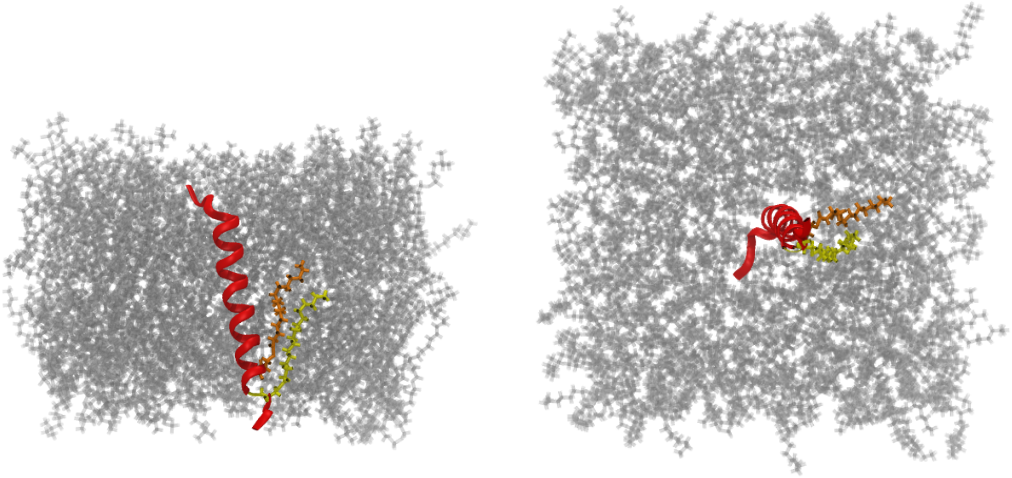

Figure 4.13: Representative snapshots of the doubly-palmitoylated PAG peptide inside of the POPC bilayer. The lipids are depicted in grey, peptide in red, CysP-24 and CysP-27 palmitoyls in orange and yellow, respectively. Side view (left), top view (right).

PAGpalm were stable during the 1 μs long simulations, the two palmitoyls stayed inside of the bilayer for the whole simulation run. Representative snapshots of the PAGpalm in the POPC membrane are depicted in Figure 4.13.

Detailed analysis of the peptide position inside of the lipid bilayer can be read from the density profiles (Figure 4.14). Position of CysP-27 is significantly shifted towards the interior of the bilayer when compared to the non-palmitoylated Cys-27. It is located below the phosphate groups and, hence, enclosed in the hydrophobic part of the membrane. Consequently the hydrophobic part of the PAGpalm is prominently stretched – the distance between the residues 27 and 31 is prolonged from $\sim$0.4 nm in PAG to $\sim$1.1 nm in PAGpalm. The palmitoyl chain of CysP-27 occupies the region down to the bilayer midplane whereas palmitoyl of CysP-24 is partially able to cross the midplane and reach the other bilayer leaflet. Note, that the crossing of the midplane by CysP-24 can lead to disruption of orderring of POPC molecules also at the opposite leaflet of the bilayer.

Incorporation of the two palmitoyls prolongs the α-helical structure of the peptide by 2-3 residues at the side where the palmitoylations are introduced as evidenced by the significantly increased helicity of PAGpalm between residues 22 and 26 (Figure 4.15, left panel). This suggests that palmitoylations of transmembrane helical segments do not deform their structure, but stabilize it instead. Such stabilization of the membrane-embedded α-helix by acylation was previously reported [Poschner and Langosch, 2009], however without any knowledge on the mechanism. The region between residues 22 and 26 is exposed to the aquaeous phase in the case of PAG, whereas after palmitoylations it is burried inside of the hydrophobic core of the bilayer (Figure 4.14), where the α-helical structure is energetically favorable.

Minor differences in the peptide hydration (Figure 4.15, right panel) can be spotted at the palmitoylation site Cys-27, where the hydration slightly increases,

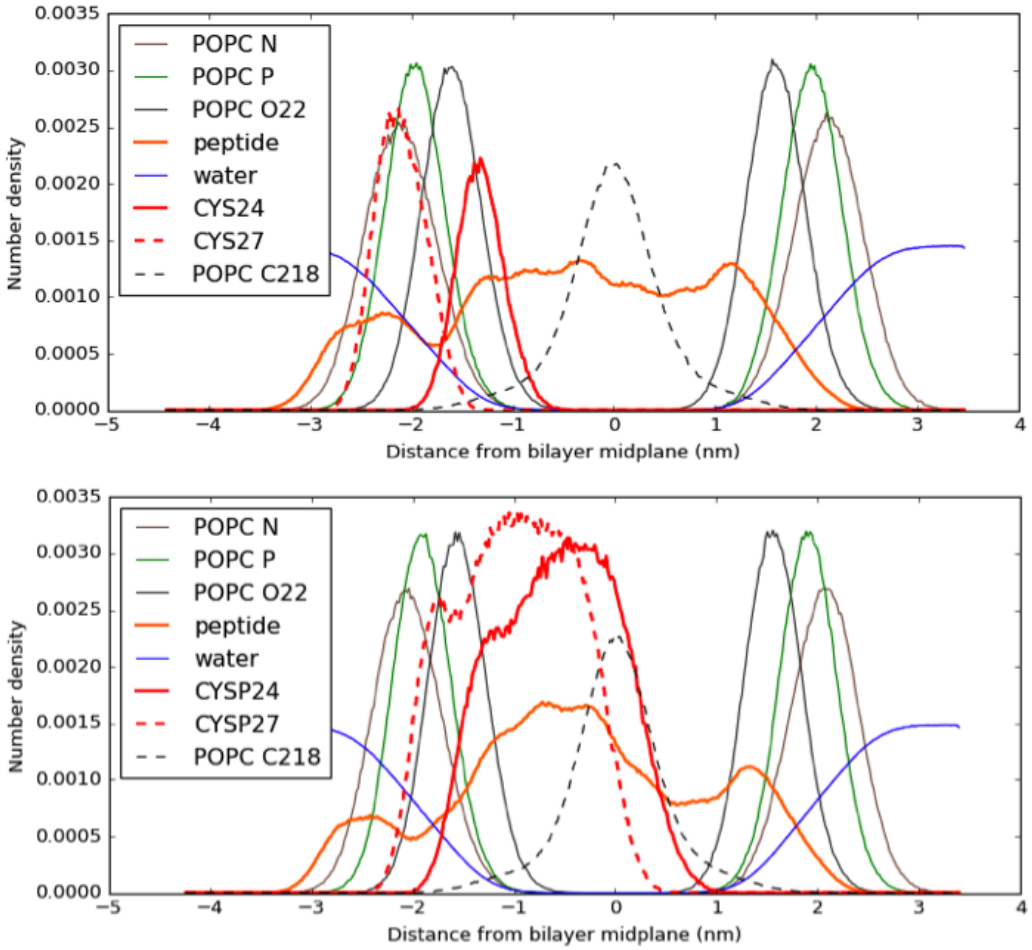

Figure 4.14: Density profiles of POPC nitrogen (grey, solid line), phosphorus (green, solid line), carbonyl oxygens at sn-1 (grey, dashed lined) and sn-2 (green, dashed line) chains, non-palmitoylated and palmitoylated peptide (orange, solid line), water (blue, solid line), end carbons of sn-1 (light grey, dashed line) and sn-2 (dark grey, dashed line) acyl chains, palmitoyls CysP-24 (red, solid line) and CysP-27 (red, dashed line). Density profiles in POPC bilayer with PAG (top), and doubly-palmitoylated PAGpalm (bottom) are depicted.

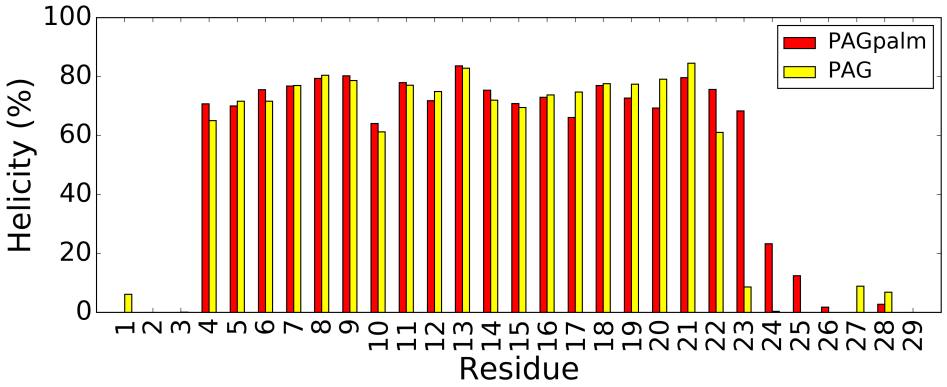

(a) Helicity of PAG and PAGpalm

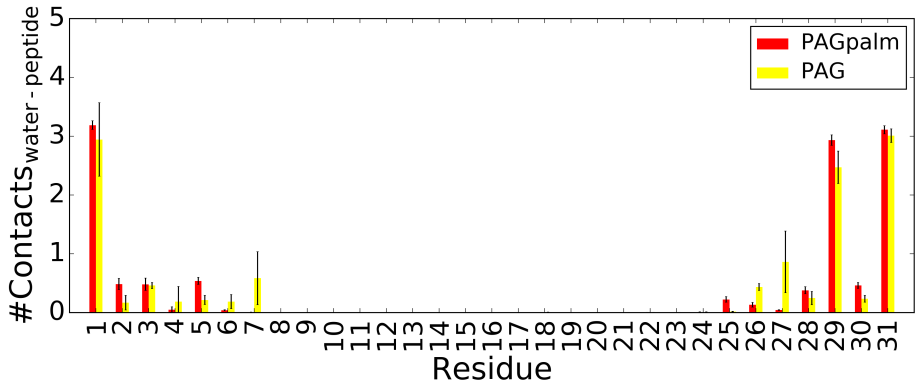

(b) Hydration of PAG and PAGpalm

Figure 4.15: a) Helicity, and b) hydration of the PAG peptide and its doubly-palmitoylated variant PAGpalm. Hydration is given as the number of near contacts between water oxygens and the respective peptide residue. Pamitoylations in PAGpalm are at Cys-24 and Cys-27.

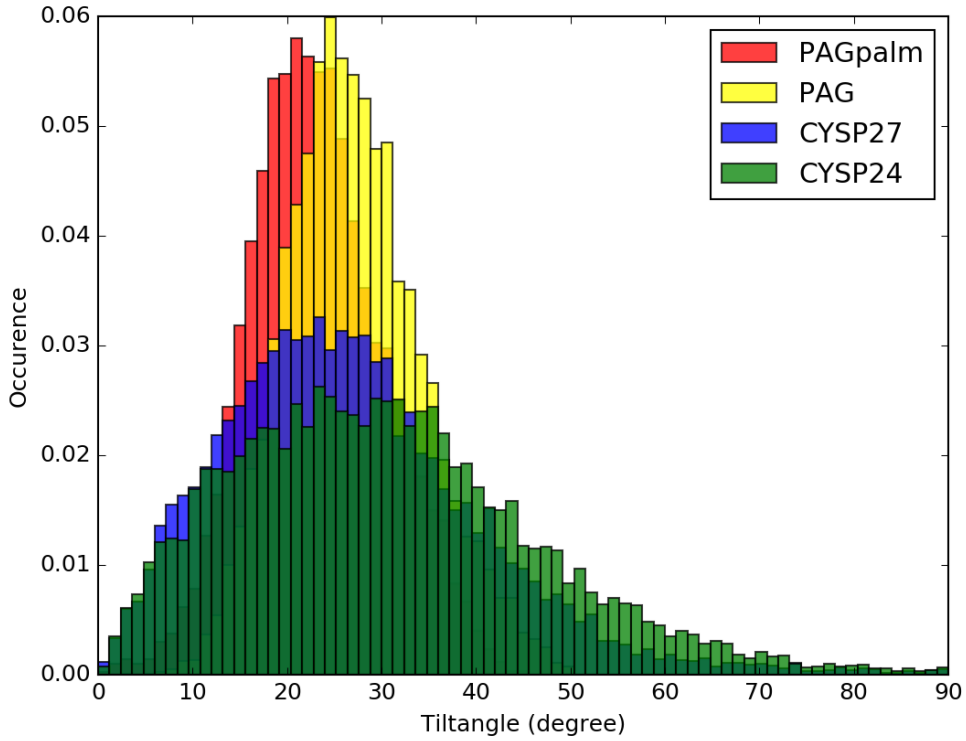

Figure 4.16: Tilt angle distribution of α-helix of PAG and its doubly-palmitoylated variant PAGpalm, and that of palmitoyls CysP-24 and CysP-27. Tilt angles are calculated with respect to the POPC bilayer normal.

and surprisingly, at the membrane-water interface opposite to the site of the palmitoylations, where we also see an increased hydration. It can be surprising that the palmitoylations lead to the increased hydration despite being hydrophobic. The changes are most likely caused by the disruption of the lipids ordering in the close vicinity of the peptide in both bilayer leaflets making the membrane more permeable for polar water molecules (discussed bellow).

Tilt angle distributions (Figure 4.16) of both CysP-24 and CysP-27 chains showed their predominant orientation towards the membrane interior, i.e., parallel to the α-helix of the peptide. The distributions of CysP-24 and CysP-27, however, show long tails at higher angle values meaning that both these palmitoyls are highly flexible and can attain also orientations nearly parallel to the membrane. A closer look at the dynamics of their movement, however, shows quite different behavior of the two palmitoyls. but the chain terminal can freely wobble back and forth in the membrane and thus bent towards the headgroups of phospholipids. The palmitoyl of CysP-27, located near the aquaeous phase, has less contacts with the α-helix in its initial and middle segments, and have comparable contacts in the tail terminus to CysP-24. Overall, CysP-27 has looser connection with the peptide than CysP-24, however, it is less flexible as CysP-27 acyl chain does not bent towards the lipid headgroups.

Having addressed the different behaviour of the two palmitoyls and their effect on the peptide, we took a look on their influence on the surrounding lipid membrane. The membrane thickness was analyzed employing two-dimensional

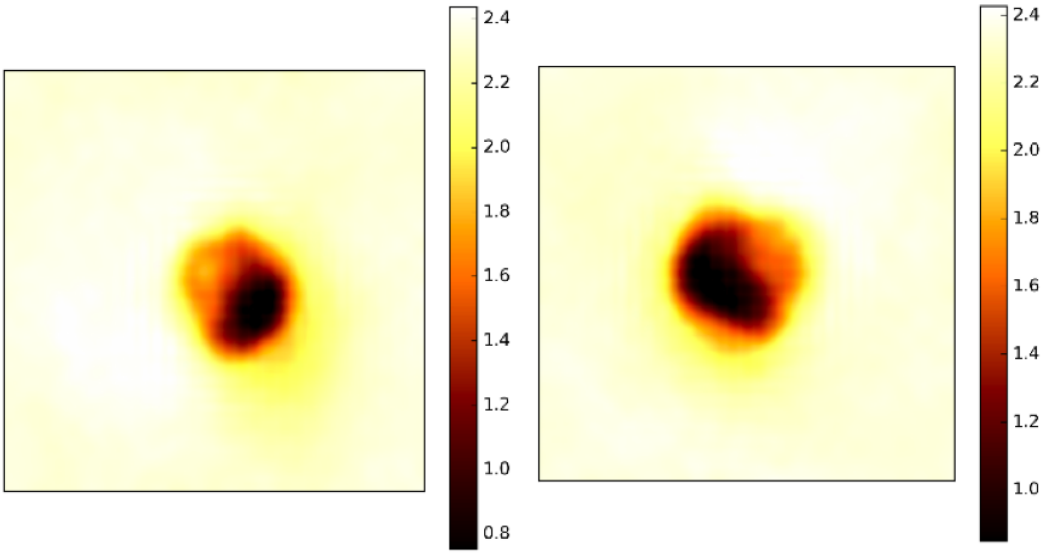

(a) PAG (b) PAGpalm

Figure 4.17: 2D map of POPC membrane thickness with a) PAG, and b) its doubly-palmitoylated variant PAGpalm. Peptide α-helix is in the center of the box, position of Cα-S vector of Cys-24, reps. CysP-24, is fixed to the top edge of the map fixing the rotation of the peptide. The box size is 6.43 nm.

top-view maps (Figure 4.17). The maps depict the average membrane thickness throughout the simulation run. To fully evaluate for the directional influence of the palmitoylations, we analyzed the trajectories with a fixed rotation of the peptide. In practice, we aligned the simulation trajectories over Cα-S vector of Cys-24 (resp. CysP-24) pointing to the top edge of the 2D maps in Figure 4.17. Note, that the non-observed axiosymmetry of the map around PAG is a direct consequence of the fixed rotation. The bilayer thickness is reduced in the close vicinity of both peptides due to the formation of a pore in the lipid bilayer for the peptide accomodation. The thickness then gradually increases. The peptide influences the membrane thickness up to the distance of $\sim$2 nm. Even though we observe a local stretching of the membrane around the CysP-27 palmitoyl in the density profiles (Figure 4.14), this change is not reflected in the average membrane thickness. The palmitoyls presence just slightly decreases the thinning of the bilayer at the closest proximity of the peptide. Although the local changes are mild, they may affect the preferential positioning of the palmitoylated peptides at the border between liquid-ordered and liquid-disordered phases in the phase separated systems as was recently reported [de Jong et al., 2013, Lin et al., 2018]. The observed changes are however minor, at least in model POPC membranes, and are unlikely the driving force for the translocation of the peptide.

Similarly to the membrane thickness we analyzed the order parameters of the surrounding POPC lipids using two-dimensional maps. The order parameters of POPC acyl chains and glycerol regions are not affected by the palmitoylations. It was previously shown that palmitoylations can influence lipid headgroups, and change the order parameters of the atoms in their glycerol and headgroup regions [Botan et al., 2015]. In the case of PAG and PAGpalm, glycerol region is not

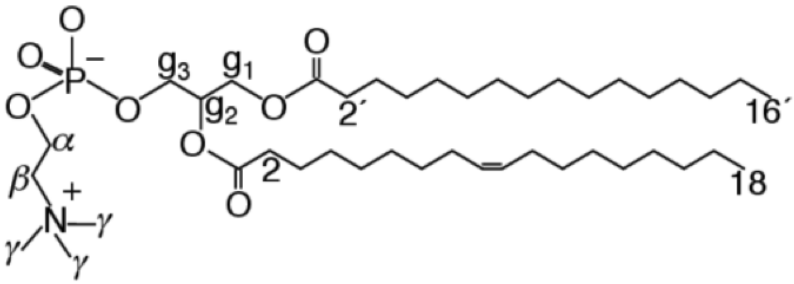

(a) Chemical structure of POPC

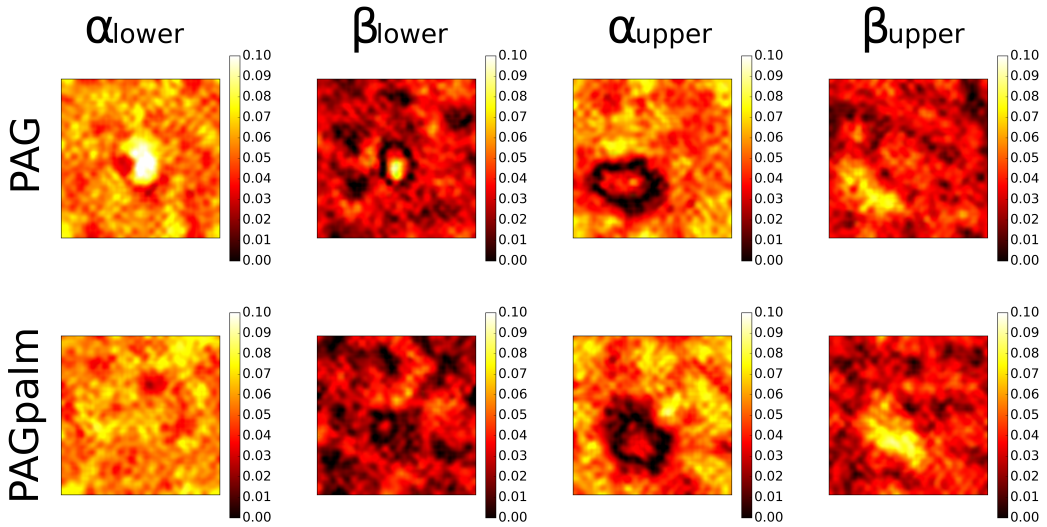

(b) Order parameters in the POPC headgroup region.

Figure 4.18: a) Chemical structure of 1-palmitoyl-2-oleoylphosphatidylcholine (POPC). Figure taken from [Botan et al., 2015], b) Order parameters in POPC headgroups around PAG (upper panel) and its doubly-palmitoylated variant PAGpalm (lower panel) peptide. Order parameters of α and β segments in the lower and upper leaflet of the POPC bilayer are depicted. 2D maps were calculated from the trajectories with the fixed peptide center of mass in the center of the simulation box and fixed position of the Cα-S vector in Cys-24 (for PAG) and CysP-24 residue (for PAGpalm). The palmitoyls CysP-24 and CysP-27 are located in the lower leaflet of the POPC bilayer.

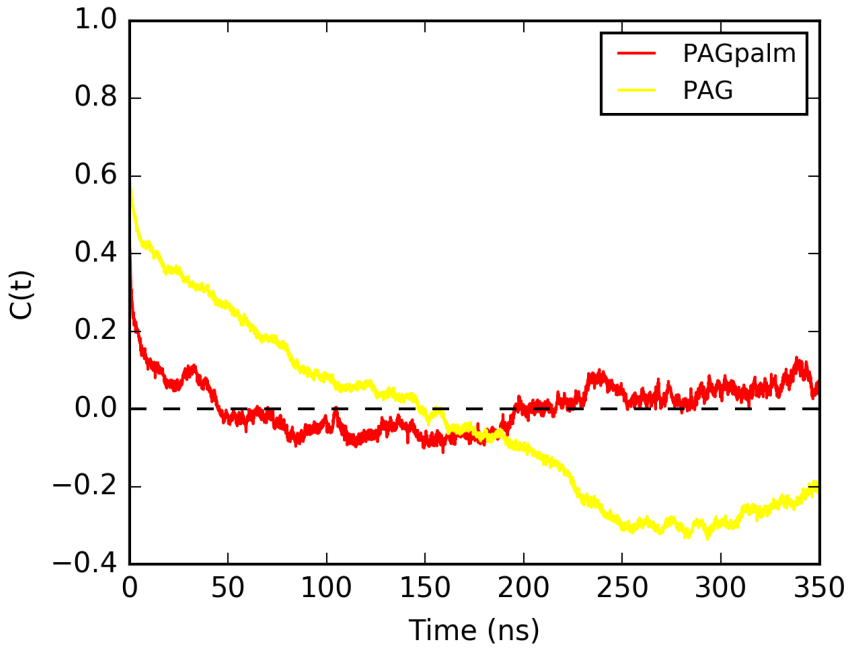

Figure 4.19: Time autocorrelation function of close contacts between the lipid headgroups and the PAG and its doubly-palmitoylated variant PAGpalm.

affected, whereas headgroup order parameteres (see structure of POPC in Figure 4.18a) are influenced (Figure 4.18). In PAG, we see a local increase of the order parameters of both α and β segments (the bright spot in the center of the maps). The observed reduction of lipid mobility is a result of direct interactions between the headgroups and the peptide. Interestingly, this effect is not present in the case of PAGpalm, as the relatively mobile palmitoyl chains of PAGpalm prevent direct contacts between lipid headgroups and the peptide α-helix. This explanation is further supported by the fact that this effect is stronger for the α carbons, which are closer to the membrane interior and, hence, affected more strongly by the palmitoyls. Noteworthy, slight influence is also visible at the opposite leaflet to the placement of the palmitoyls.

Next, we analyze the time autocorrelation functions of the close contacts between the lipid headgroups and the peptide (Figure 4.19). In PAG, such autocorrelation is kept above the zero value for ∼200 ns revealing a long memory of headgroups-peptide contacts. Such memory arises from the sticking of the phospholipid molecules to PAG. The correlation time is shortened to ∼50 ns in the case of PAGpalm suggesting strong affection of the mobility of the lipids closely surrounding the peptide.

Put together, we see lower organization in the headgroup region of phospholipids evidenced by the changes in the order parameters, easier accessibility of the PAGpalm for the water molecules, and much shorter memory of lipid headgroups-peptide contacts upon the attachment of the two palmitoyls to PAG. All these findings prove that palmitoyls disrupt the lipid organization in the vicinity of the peptide resulting in their increased mobility. The increased lipid mobility together with the local changes in the membrane thickness might ease the translocation of the palmitoylated PAG protein to thicker lipid domains, the place of PAG

signaling [Hrdinka and Horejsi, 2014].

5. Break up of the tear film of the human eye

After each blink of the eye, the tear film (TF) undergoes a complex structural evolution [Braun, 2012] and in final stages of this develoment the TF ruptures apart which is so called tear film break up [J. P. Craig and A. Tomlinson, 1997, Ewen King-Smith et al., 2013, Willcox et al., 2017]. In dry eye disease (DED) the stability of the TF is reduced as the time of the break up is shortened and consequently the evaporation of tears from the ocular surface is increased [J. P. Craig and A. Tomlinson, 1997, Isreb et al., 2003, Ewen King-Smith et al., 2013, Millar and Schuett, 2015, Willcox et al., 2017]. As described in section 1.2, the aqueous tear layer at the corneal surface is stabilized by the presence of a thin layer of lipids at the water-air interface – tear film lipid layer (TFLL) [McCulley and Shine, 1997, Olson et al., 2003, Foulks, 2007, Willcox et al., 2017]. One of the hypothesis claims that people suffering from DED have their TFLL composition altered in the way that they lack some part of the polar lipids in the TFLL [J. P. Craig and A. Tomlinson, 1997, Foulks, 2007, Millar and Schuett, 2015].

Some relatively simple surfactant molecules are able to stabilize the TF in mice and humans suffering from DED [Amrane et al., 2014, Quentric et al., 2016]. Some other surfactant molecules which are being used to preserve eye drops on contrary destabilize the TF. My study on the TF investigates the interaction of these molecules with other surfactant molecules in the TF. The focus of the study is thus on the molecular mechanism of their stabilizing or destabilizing effect.

We use coarse grain MD simulations to model a large area of the TF employing the coarse grain MARTINI force field [Marrink et al., 2007]. Our TF model is composed of a layer of water surrounded by two lipid films, which are exposed to the gas phase. Such an approach allows us to realistically model the TF and investigate the molecular interactions between stabilizing molecules and their impact on overall behavior of the TF. The results of our studies were published in [Cwiklik et al., 2018, Riedlova et al., 2018].

The lipid composition of the TFLL in our studies was approximated by using dominant lipid classes found in human tears in lipidomic studies [Rantamäki et al., 2011]. The polar layer is formed by 1-palmitoyl-2-oleoyl-phosphatidylcholine (POPC), 1-palmitoyl-2-oleoyl-phosphatidylethanolamine (POPE), N-palmitoyl-d-erythrosphingosine (PPCE), and N-palmitoyl-d-erythro-sphingosylphosphorylcholine (PPCS). Non-polar lipids are represented by an equimolar mixture of glycerine trioleate (TO) and cholesteryl oleate (CO).

5.1 A proposed mechanism for the tear film break up: a molecular level view by employing in silico approach

Cetalkonium chloride (CKC) stabilizes the TF in both mice and humans [Amrane et al., 2014, Quentric et al., 2016]. In the presented study, published in [Cwiklik et al., 2018], we investigate the role of natural lipids in the TFLL as well as the

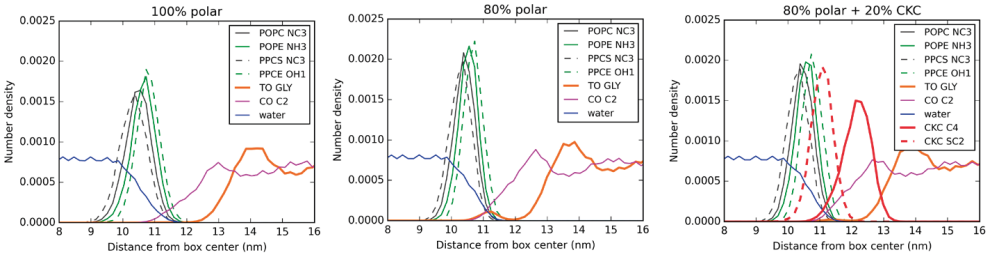

Figure 5.1: Density profiles of the system with full content of polar lipids (left), the system with 80% of polar lipids (middle), and the system with 80% of polar lipids supplemented with CKC (right). The area under each number density is normalized to unity. The density of the choline (POPC, PPCS), amine (POPE), and hydroxyl groups (PPCE) is shown. In TO, the glycerol group is depicted, and the terminus of C20-C27 side chain is shown for CO. In CKC, the terminus of the non-polar chain (C4), as well as the charged headgroup (SC2), are presented. Figure taken from [Cwiklik et al., 2018].

specific interactions between CKC and TF lipids. To mimic a DED tear film we model the TFLL with deficiency in individual lipid components. Additionally, cations of CKC were incorporated in the lipid film in some of the simulated systems.

First, we evaluated the "non-deficient" TFLL. with such an amount of polar and non-polar lipids that a full film was formed at the water-air interface. A monolayer of polar lipids was formed on the surface of the the water layer, while non-polar lipids formed a multilayer on top of the polar layer. After that, we prepared a lipid-deficient system with only 80% of the polar lipids in comparison to the previous model of the relaxed TF. This polar lipid-deficient TF was then enriched with 20% of CKC molecules. Hence, we prepared a model of polar lipid-deficient TF (like in DED patients) supplemented with CKC-contatining emulsion as a treatment for DED.

The density profiles of the simulated systems are depicted in Figure 5.1. In all three models, polar lipids have a monolayer-like arrangement at the air-water interface with their polar groups being in contact with water. The arrangement of non-polar lipids on top of this monolayer varies depending on the composition of the polar monolayer. In the non-deficient system (Figure 5.1, left) the molecules of TO do not have any direct contact with polar lipids in the monolayer. Molecules of CO are much closer to polar lipids, as evidenced by a partial overlap of the corresponding density profiles. In the polar lipids-deficient system (Figure 5.1, middle), a minor peak at the density profile of TO is formed in the region occupied by polar lipids. The deficiency of polar lipids thus promotes porous defects in the monolayer, which allows TO molecules to come into a direct contact with the lipids and, also, water molecules. Treatment with CKC molecules leads to healing of such porous defects diminishing of these TO-polar lipids contacts, as the small peak in TO density profile disappears when CKC is incorporated in-between polar lipids (5.1 right).

In the non-deficient TFLL, part of the interface is covered by a lens-like multilayer structure made by non-polar lipids (Figure 5.2, left). There is enough polar lipids to cover the rest of the water surface with a continuous monolayer.

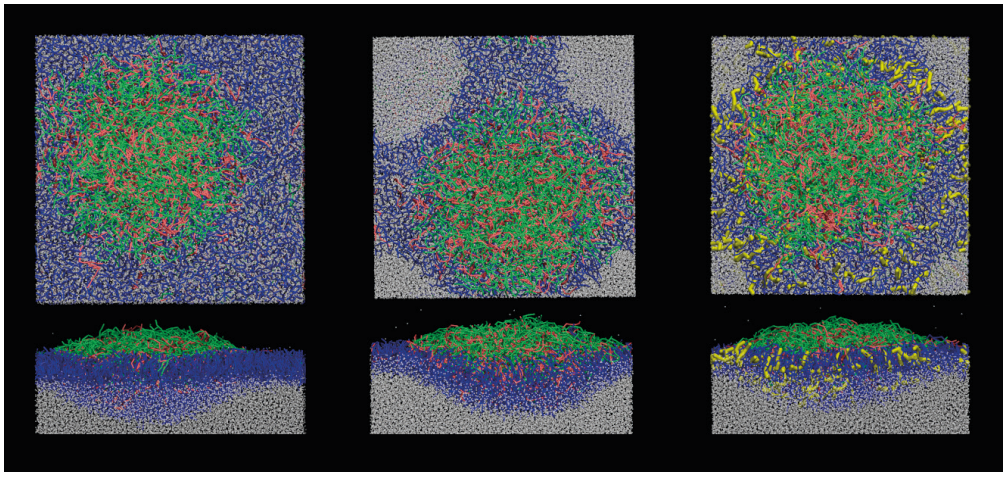

Figure 5.2: Representative snapshots of the simulated systems. The system with full content of polar lipids (left), the system with 80% of polar lipids (middle), and the system with 80% of polar lipids supplemented with CKC (right) are shown. The first and second rows show a top and side views respectively. Water is shown in gray, polar lipids in blue, TO in green, CO in brown, CKC in yellow. Figure taken from [Cwiklik et al., 2018].

The reduced amount of polar lipids in the polar lipids-deficient system leads to poration of the monolayer around the lens-like structure (Figure 5.2, middle). In the system supplemented with CKC, the effective surface area of the monolayer increases decreasing the exposed water surface (Figure 5.2, right), so that CKC effectively promotes spreading of polar lipids in otherwise polar lipid-deficient TFLL.

In summary, a polar lipid-deficient TFLL has a reduced capability of covering the TF. As a consequence, the water phase of the TF is more exposed to the air increasing its evaporation. CKC increases the effective surface of the TFLL preventing also the unfavorable water-TO contacts, which decreases the effects of the dry eye syndrome in DED patients.

5.2 Influence of benzalkonium chloride on tear film lipid layer stability: molecular level view by employing in silico modeling

Bezalkonium chlorides (BAK), short-chain analogues of CKC, are a mixture of aliphatic C12 and C14 quaternary ammonia, traditionally used to preserve eye drops thanks to their bactericidal and bacteriostatic properties [Kurup et al., 1992, Campanac et al., 2002]. However, BAK was proved to decrease the TF breakup time in patients, and hence, it destabilizes the TFLL despite its analogy with CKC, in contrast improves the TFLL stability (5.1, [Cwiklik et al., 2018]). We investigate the interactions between individual components of a model TFLL and BAK molecules (both C12 and C14) and analyze their influence on the TFLL organization and stability.

In order to address the issue of BAK interactions with polar lipid-deficient

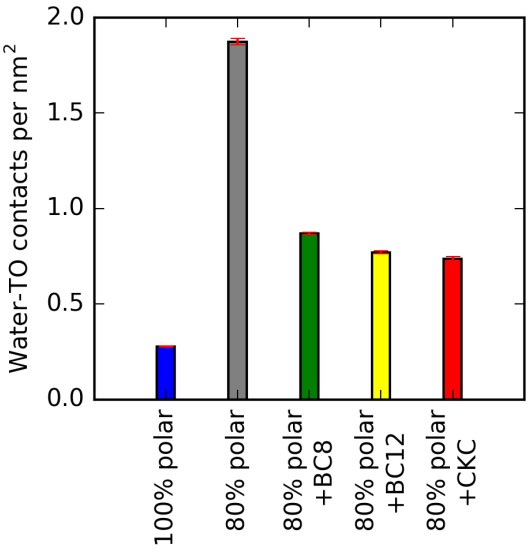

Figure 5.3: Number of water-TO close contacts (<0.8 nm) per interfacial unit area in the non-deficient system, the system with 80% of polar lipids and the polar lipids-deficient systems supplemented with BC8, BC12 and CKC. Figure taken from [Riedlova et al., 2018].

TFLL, we used our previous TFLL in silico model with 20% of polar lipids removed. Benzalkonium cations with either C8 or C12 lipid chains (designated as BC8 and BC12) were added to the polar lipids-deficient TFLL model as well as to the non-deficient TFLL model. Additionally, we compared the action of these molecules with C16 BAK analogue, i.e., CKC.

Previously, we identified reduction of polar lipids in the TFLL model as a major factor leading to lipid film destabilization (Chapter 5.1, [Cwiklik et al., 2018]). In polar lipid-deficient system, the number of water-TO lipid contacts is increased. All the three supplements, BC8, BC12 and CKC, significantly reduce this unfavorable contacts (Figure 5.3). All three surfactant molecules thus directly interact with the TFLL model.

Density profiles (Figure 5.4) show the details of molecular-level interactions between the system components. All three surfactant molecules incorporate by their headgroups into the polar lipids monolayer. Their headgroups are however closer to the nonpolar layer than the headgroups of the phospholipids in the monolayer. The tail terminals penetrate into the nonpolar layer. Such a position in between the polar and nonpolar layers is in accordance with reduced contacts between water layer and TO molecules. Such a feature is often accompanied by an enhanced stability of the TF.

Further insight into localization of BAK and CKC in the polar layer, however, revealed their different orientation with respect to the other TFLL lipids (schematic representation in Figure 5.5). The sn-2 acyl chains of phospholipids attain orientations parallel (i.e., tilt angle $\sim 180^o$) to the water-air interface regardless of the presence and type of the supplement molecule. All three suplements (BC8, BC12, and CKC) have smaller values of tilt angles ($\sim 100^o$, $\sim 125^o$, and $\sim 150^o$, respectively) compared with sn-2 tails of POPC, hence not fully

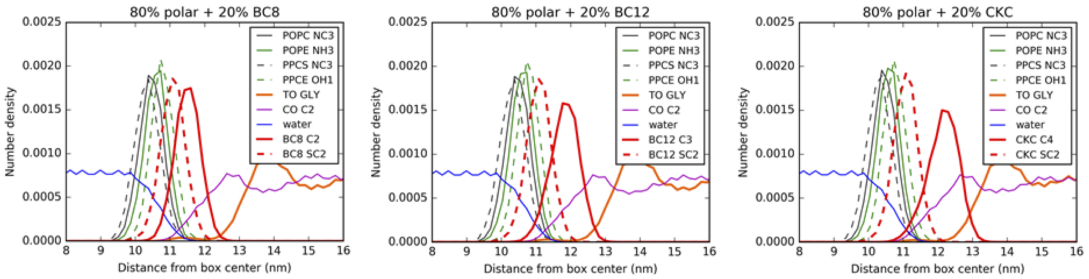

Figure 5.4: Density profiles of the non-deficient system, the system with 80% of polar lipids and the polar lipids-deficient systems supplemented with BC8, BC12 and CKC. The area under each number density is normalized to unity. The density of the choline (POPC, PPCS), amine (POPE), and hydroxyl groups (PPCE) is shown. In TO, the glycerol backbone is depicted, and the C2 carbon is shown for CO. Profiles of polar headgroup (SC2) and nonpolar chain terminals of the supplementing surfactants (BC8 C2, BC12 C3 and CKC C4) are also depicted. Figure taken from [Riedlova et al., 2018].

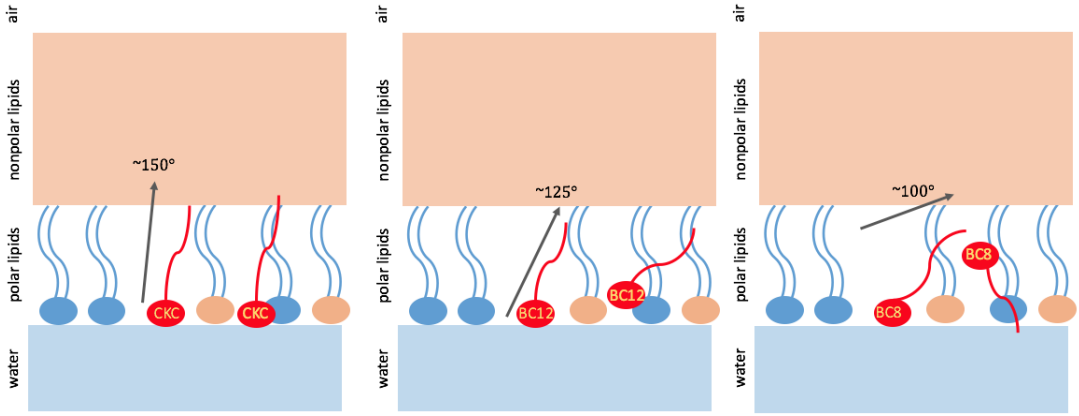

Figure 5.5: A cartoon representation of tilt angles and orientaion of Density profiles of CKC, BC12 and BC8 molecules in the model of the TFLL. Estimates of the most populated tilt angles are given. Figure taken from [Riedlova et al., 2018].

matching the orientations of the phospholipids in the TFLL model. CKC has the orientation close to that of the TFLL phospholipids. In contrast, the overall orientation of the BC8 and BC12 chains is less ordered with their average orientations more tilted. Both BC8 and BC12 have non-negligible populations of the reversed orientation with their nonpolar tail oriented towards the water phase, and BC8 in particular, is able to significantly reorient while being in the polar sublayer forming defects in the polar lipids structure.

In summary, all the investigated surfactant molecules, BC8, BC12 and CKC, incorporate into the polar sublayer of the TFLL model, and reduce the unfavorable water-TO interactions in polar lipids-deficient TFLL model. Their orientation in the polar monolayer, however, differs. CKC, having comparable length with the TFLL phospholipids, behaves similarly to the native phospholipids forming the polar monolayer of the TFLL. Both BC8 and BC12 attain more flexible orientations, which is particularly significant for the shortest BC8 which can

even point its tail toward the aquaeous phase. Hence, we conclude that the CKC molecule stabilizes the TFLL, while the shorter BAK molecules, and especially the shortest BC8, destabilize the TFLL by the reduction of the order in acyl chains of the monolayer of polar lipids.

Summary

Within the first part of the presented thesis we investigate in detail the interactions of a variety of monovalent cations and divalent Ca^{2+} with model membranes mimicking the inner leaflet of the plasma membrane [Melcrova et al., 2016, 2017, 2019b]. First, we identified the binding sites for Ca^{2+} ions and characterized their effects on the biophysical properties in phospholipid membranes, both zwitterionic (PC) and negatively charged (PC/PS, 80/20 mol/mol) [Melcrova et al., 2016]. In PC/PS bilayers, we distinguish three possible binding sites: phosphate groups of PC and PS, carbonyl groups of PC and PS, and carboxylic acid groups of PS. From our MD simulations we have observed that Ca^{2+} often binds simulataneously to multiple binding sites, both within a single lipid molecule and between multiple lipids bridging them together. In POPC bilayers, Ca^{2+} interacts the most with the phosphate groups, and slightly less with the sn-2 carbonyl groups. Ca^{2+} affinity to distinct binding sites in the PC/PS system depends on the salt concentration. In a low concentration regime, the binding occurs predominantly to carboxylic acid groups of PS closely followed by phosphate and sn-2 carbonyl groups. At high concentration of $CaCl_2$, the binding to phosphates is more favoured. Such characteristics, obtained from MD simulations, agree well with our experimental findings, which showed that both phosphate and carbonyl regions are affected by Ca^{2+} binding in both PC and PC/PS systems. Moreover, Ca^{2+} rigidifies the membranes, but does not decrease its hydration significantly, which is consistently obtained from both simulations and experiments. Noteworthy, we observe a reversible aggregation of vesicles at 5-50 mM $CaCl_2$ concentrations arising from the bridging of the opposing vesicles by Ca^{2+} ions. Our results, hence, suggest that bridging of the vesicles can be the role of Ca^{2+} in membrane fusion as was previously hypothesized [Potoff et al., 2008, Tarafdar et al., 2012].

The interaction of Na^+ with zwitterionic (POPC and POPC/20mol%chol) membranes is dramatically different from that of Ca^{2+} [Melcrova et al., 2017, Binder and Zschörnig, 2002, Porasso et al., 2009, Catte et al., 2016, Melcr et al., 2018]. In contrast to strong calcium binding, the interaction of Na^+ with phospholipid bilayers is weaker and adopts faster kinetics. The number of bound Na^+ ions is determined solely by the number of the available binding sites, i.e., PC headgroups. Ca^{2+} ions on the other hand occupy all the available surface area [Melcrova et al., 2017], hence, their binding increases with a larger membrane surface area.

Our study on detailed interactions between various ions and membrane components in cholesterol-containing systems (POPC/POPS without and with 10 mol% and 20 mol% of cholesterol, and membranes extracts from HEK293 cells) further revealed the nature of the ionic binding to more complex membrane systems [Melcrova et al., 2019b]. Both cholesterol and calcium hinder the mobility of the phospholipids, condense the membranes, inrease the membrane thickness, and increase the order of the acyl chains [Melcrova et al., 2019b]. The effects of calcium and cholesterol on structural characteristics are additive and independent within certain limits. When the membrane is already compressed by a large amount of Ca^{2+} ions, no further compression by cholesterol addition can be achieved. Interestingly, after the saturation of the structural characteristics,

the lipid mobility is still slowing down. Ca^{2+} and cholesterol do not directly interact in the bilayer, even though they share an interaction site at the sn-2 carbonyls of the phospholipids. Cholesterol interacts with the carbonyls from the hydrophobic core of the membrane, whereas Ca^{2+} binds from the water phase. Hence, they do not compete nor interfere with each other. The small increase in Ca^{2+} binding to cholesterol-containing membranes observed in our simulations is likely caused by an increase in the membrane area as suggested in [Melcrova et al., 2017].

The monovalent ions (Cs^+, K^+, Na^+, and Li^+) also rigidify the POPC/POPS membranes, both without and with cholesterol. Contrarily to Ca^{2+}, the addition of cholesterol slightly enhances their effects on the lipid mobility. Interestingly enough, such an effect is not present in neutral memrbanes [Melcrova et al., 2017]. The negative charge of PS, hence, changes the nature of Na^+ binding. Biological membranes are to some extent protected from the rigidification induced by the ions, Ca^{2+} effects being buffered more than those of monovalent ions. We prove, that such buffering is not caused by cholesterol presence but rather by some other plasma membrane components [Melcrova et al., 2019b].

We added a transmembrane peptide to our model of the plasma membrane. The peptide was designed as a single transmembrane α-helix with either zero (WALP-KD) or a mild positive charge (WALP-KK^{2+}). Both studied peptides rigidify both POPC and POPC/POPS membranes, with the rigidifying effect of WALP-KK^{2+} being always higher. Positively charged WALP-KK^{2+} increase the zeta potential at zwitterionic, as well as negatively charged vesicles. Surprisingly, non-charged WALP-KD increases the zeta potential at POPC/POPS vesicles as well, sugesting that the peptide presence shields the effective charge of POPS headgroups. Interestingly enough, neither of the studied peptides has any influence on Ca^{2+} binding to the model membranes. Hence, the diminished effects of Ca^{2+} on biological membranes are not caused by transmembrane domains of membrane proteins.

Phosphoprotein associated with glycosphingolipid-enriched microdomains in the plasma membrane (PAG) is switched to its active form by the incorporation of two palmitoyls to its cytoplasmic membrane-proximal Cys residues [Svec, 2008, Hrdinka and Horejsi, 2014]. In our simulations, we observe that both palmitoylations are stable and fully incorporated into the hydrophobic core of the POPC bilayer [Melcrova et al., 2019a]. The α-helix of the palmitoylated PAGpalm is longer by 2-5 residues as a consequence of the enclosure of both palmitoyls into the hydrophobic part of the bilayer. This is, however, only a local effect, which does not affect the overall membrane thickness. Both palmitoyls are quite flexible and can attain also orientations parallel to the membrane. Acyl chain of CysP-24 can even bend toward the headgroups of the surrounding POPC molecules. Such a behavior together with the stretching of the CysP-24 tail across the midplane of the POPC bilayer leads to the disruption of the order of the POPC molecules in the close vicinity of PAGpalm in both leaflets of the bilayer. We report a significantly lower autocorrelation time of the close contacts between POPC headgroups and the peptide, lower headgroup order parameters, and easier permeation of water molecules to the peptide surroundings resulting in an increased hydration despite the hydrophobic nature of the added palmitoyls. We hypothesize that the disruption of the phospholipid organization resulting in the increased mobility of

the lipids can ease the translocation [Hrdinka and Horejsi, 2014] of PAG protein to signaling domains after its palmitoylations. The local changes in membrane thickness might lead to preferential positioning of the palmitoylated proteins at the edge of such domains with their palmitoyls facing the more ordered phase as was recently suggested [de Jong et al., 2013, Lin et al., 2018].

Our research on the tear film lipid layer (TFLL) is focused on the molecular mechanism of the healing effect of cetalkonium chloride (CKC) and bezalkonium chloride (BAK) on polar lipids-deficient TFLL, mimicking the conditions of dry eye disease (DED) [Cwiklik et al., 2018, Riedlova et al., 2018]. The deficiency of polar lipids leads to non-favorable contacts between non-polar lipids, specifically glycerine trioleate (TO), and water molecules. The polar lipid-deficient TFLL also has a reduced capability to cover water-air interface leading to the evaporation of water from the corneal surface. Treatment with CKC diminishes the unfavorable TO-water contacts and helps to spread TFLL on the water surface to prevent the evaporation. We compared the obtained results on CKC (chain length of 16 carbons) with BAK cations with either 8 or 12 carbons in their lipid chains (BC8 and BC12, respectively). All three supplements significantly reduce the unfavorable TO-water interactions, CKC performing the best. All of them are incorporated by their headgroup into the polar lipids monolayer, however, they obtain a different orientation within the TFLL layer. The orientation of CKC is close to the TFLL phospholipids while the BC8 and BC12 molecules are less ordered. Especially BC8 is able to significantly reorient even to parallel or reversed orientations with its nonpolar tail oriented towards the water phase. CKC, having its length comparable to the TFLL natural lipids, behavest similarly to them and stabilizes the monolayer, whereas BAK molecules, especially BC8, form defects in the structure of the TFLL and, hence, destabilize the TFLL by the reduction of the order in the acyl chains of the polar lipids. This has important consequences for the production of eye drops, which usually contain a mixture of BAK molecules as a preservant for their bactericidal and bacteriostatic properties [Kurup et al., 1992, Campanac et al., 2002]. Avoiding the BAK molecules in the eye drops composition may yield improved effects of the eye drops in DED patients.

Bibliography

Bruce Alberts, Dennis Bray, Alexander Johnson, Julian Lewis, Martin Raff, Keith Roberts, and Peter Walter. *Základy buněčné biologie - Úvod do molekulární biologie buňky*. Espero, Praha, 2002.

Michael P. Allen and Domonic J. Tildesley. *Computer Simulation of Liquids*. Oxfor University Press, New York, 1987. ISBN 978-0-19-855645-9.

Paulo F Almeida, Alexis Best, and Anne Hinderliter. Monte Carlo simulation of protein-induced lipid demixing in a membrane with interactions derived from experiment. *Biophysical journal*, 101(8): 1930–7, oct 2011. ISSN 1542-0086. doi: 10.1016/j.bpj.2011.09.015. URL `http://www.pubmedcentral.nih.gov/articlerender.fcgi?artid=3192976&tool=pmcentrez&rendertype=abstract`.

M. Amrane, C. Creuzot-Garcher, P. Y. Robert, D. Ismail, J. S. Garrigue, P. J. Pisella, and C. Baudouin. Ocular tolerability and efficacy of a cationic emulsion in patients with mild to moderate dry eye disease - A randomised comparative study. *Journal Francais d'Ophtalmologie*, 37(8):589–598, 2014. ISSN 01815512. doi: 10.1016/j.jfo.2014.05.001.

S. Arzhantsev, N. Ito, M. Heitz, and M. Maroncelli. Solvation dynamics of coumarin 153 in several classes of ionic liquids: Cation dependence of the ultrafast component. *Chemical Physics Letters*, 381(3-4):278–286, 2003. ISSN 00092614. doi: 10.1016/j.cplett.2003.09.131.

Kia Balali-Mood, Peter J. Bond, and Mark S.P. Sansom. Interaction of monotopic membrane enzymes with a lipid bilayer: A coarse-grained MD simulation study. *Biochemistry*, 48(10):2135–2145, 2009. ISSN 00062960. doi: 10.1021/bi8017398.

W. F.Drew Bennett, Justin L. MacCallum, Marlon J. Hinner, Siewert J. Marrink, and D. Peter Tieleman. Molecular view of cholesterol flip-flop and chemical potential in different membrane environments. *Journal of the American Chemical Society*, 131(35):12714–12720, 2009. ISSN 00027863. doi: 10.1021/ja903529f.

W. F.Drew Bennett, Chun Kit Hong, Yi Wang, and D. Peter Tieleman. Antimicrobial Peptide Simulations and the Influence of Force Field on the Free Energy for Pore Formation in Lipid Bilayers. *Journal of Chemical Theory and Computation*, 12(9):4524–4533, 2016. ISSN 15499626. doi: 10.1021/acs.jctc.6b00265.

Oliver Berger, Olle Edholm, and Fritz Jahnig. Molecular Dynamics Simulations of a Fluid Bilayer of Dipalmitoylphosphatidylcholine at Full Hydration, Constant Pressure, and Constant Temperature. *Biophysical Journal*, 72(5):2002–2013, 1997. ISSN 00063495. doi: 10.1016/S0006-3495(97)78845-3.

Michael J. Berridge, Martin D. Bootman, and H. Llewelyn Roderick. Calcium signalling: Dynamics, homeostasis and remodelling. *Nature Reviews Molecular Cell Biology*, 4(7):517–529, 2003. ISSN 14710072. doi: 10.1038/nrm1155.

Hans Binder and Olaf Zschörnig. The effect of metal cations on the phase behavior and hydration characteristics of phospholipid membranes. *Chemistry and physics of lipids*, 115(1-2):39–61, may 2002. ISSN 0009-3084. URL http://www.ncbi.nlm.nih.gov/pubmed/12047897.

Rainer A. Böckmann and Helmut Grubmüller. Multistep binding of divalent cations to phospholipid bilayers: a molecular dynamics study. *Angewandte Chemie (International ed. in English)*, 43(8):1021–4, feb 2004a. ISSN 1433-7851. doi: 10.1002/anie.200352784. URL http://www.ncbi.nlm.nih.gov/pubmed/14966897.

Rainer A Böckmann and Helmut Grubmüller. Multistep Binding of Divalent Cations to Phospholipid Bilayers: A Molecular Dynamics Study. *Angewandte Chemie International Edition*, 43(8):1021–1024, 2004b.

M. Bockstedte, A. Kley, J. Neugebauer, and M. Scheffler. Density-functional theory calculations for poly-atomic systems: electronic structure, static and elastic properties and ab initio molecular dynamics. *Comput. Phys. Commun.*, 107:187, 1997. ISSN 00104655. doi: 10.1016/S0010-4655(97)00117-3.

Alexandru Botan, Fernando Favela-Rosales, Patrick F J Fuchs, Matti Javanainen, Matej Kanduč, Waldemar Kulig, Antti Lamberg, Claire Loison, Alexander Lyubartsev, Markus S. Miettinen, Luca Monticelli, Jukka Määttä, O. H Samuli Ollila, Marius Retegan, Tomasz Róg, Hubert Santuz, and Joona Tynkkynen. Toward Atomistic Resolution Structure of Phosphatidylcholine Headgroup and Glycerol Backbone at Different Ambient Conditions. *Journal of Physical Chemistry B*, 119(49):15075–15088, 2015. ISSN 15205207. doi: 10.1021/acs.jpcb.5b04878.

Richard J Braun. Dynamics of the Tear Film. *Annual Review of Fluid Mechanics*, 44:267–297, 2012.

Tomas Brdicka, Dagmar Pavlistova, Albrecht Leo, Eddy Bruyns, Vladimir Korinek, Pavla Angelisova, Jeanette Scherer, Andrej Shevchenko, Anna Shevchenko, Ivan Hilgert, Jan Cerny, Karel Drbal, Yasuhiro Kuramitsu, Birgit Kornacker, Vaclav Horejsi, and Burkhart Schraven. Phosphoprotein associated with glycosphingolipid-enriched microdomains (PAG), a novel ubiquitously expressed transmembrane adaptor protein, binds the protein tyrosine kinase csk and is involved in regulation of T cell activation. *The Journal of experimental medicine*, 191(9):1591–1604, 2000. ISSN 00221007. doi: 10.1084/jem.191.9.1591. URL http://www.pubmedcentral.nih.gov/articlerender.fcgi?artid=2213442{&}tool=pmcentrez{&}rendertype=abstract.

Simon H Brown, Carolina M E Kunnen, Eric B Papas, Percy L de la Jara, Mark D P Willcox, Stephen J Blanksby, and Todd W Mitchell. Intersubject and interday variability in human tear and meibum lipidomes : a pilot study. *The Ocular Surface*, 14(1):43–48, 2016.

Igor A Butovich. The Meibomian Puzzle: Combining Pieces Together Igor. *Progress in Retinal and Eye Research*, 28(6):483–498, 2009. doi: 10.1016/j.preteyeres.2009.07.002.The.

C. Campanac, L. Pineau, A. Payard, G. Baziard-Mouysset, and C. Roques. Interactions between biocide cationic agents and bacterial biofilms. *Antimicrobial Agents and Chemotherapy*, 46(5):1469–1474, 2002. ISSN 00664804. doi: 10.1128/AAC.46.5.1469-1474.2002.

R Car and M Parrinello. Unified Approach for Molecular Dynamics and Density-Functional Theory. *Physical review letters*, 55(22):2471–2474, 1985. ISSN 0031-9007. doi: 10.1103/physrevlett.55.2471.

Andrea Catte, James C. Patterson, Denys Bashtovyy, Martin K. Jones, Feifei Gu, Ng Li, Aldo Rampioni, Durba Sengupta, Timo Vuorela, Perttu Niemela, Mikko Karttunen, Siewert Jan Marrink, Ilpo Vattulainen, and Jere P. Segrest. Structure of spheroidal HDL particles revealed by combined atomistic and coarse-grained simulations. *Biophysical Journal*, 94(6):2306–2319, 2008. ISSN 15420086. doi: 10.1529/biophysj.107.115857.

Andrea Catte, Mykhailo Girych, Matti Javanainen, Claire Loison, Josef Melcr, Markus S. Miettinen, Luca Monticelli, Jukka Määttä, Vasily S. Oganesyan, O. H. Samuli Ollila, Joona Tynkkynen, and Sergey Vilov. Molecular electrometer and binding of cations to phospholipid bilayers. *Phys. Chem. Chem. Phys.*, 18(47):32560–32569, 2016. ISSN 1463-9076. doi: 10.1039/C6CP04883H. URL `http://xlink.rsc.org/?DOI=C6CP04883H`.

Marek Cebecauer, Mariana Amaro, Piotr Jurkiewicz, Maria Joao Sarmento, Radek Šachl, Lukasz Cwiklik, and Martin Hof. Membrane Lipid Nanodomains. *Chemical Reviews*, 2018. ISSN 15206890. doi: 10.1021/acs.chemrev.8b00322.

Catherine A Charneski and Laurence D Hurst. Positive Charge Loading at Protein Termini Is Due to Membrane Protein Topology , Not a Translational Ramp. *Molecular Biology and Evolution*, 31(1):70–84, 2013. doi: 10.1093/molbev/mst169.

Feng Chen and Paul E. Smith. Simulated surface tensions of common water models. *Journal of Chemical Physics*, 126(22):2005–2008, 2007. ISSN 00219606. doi: 10.1063/1.2745718.

S.W. Chiu, Eric Jakobsson, R. Jay Mashl, and H. Larry Scott. Cholesterol-Induced Modifications in Lipid Bilayers: A Simulation Study. *Biophysical Journal*, 83(4):1842–1853, 2002. ISSN 00063495. doi: 10.1016/S0006-3495(02)73949-0. URL `http://linkinghub.elsevier.com/retrieve/pii/S0006349502739490`.

Parkson Lee-Gau Chong, Weiwei Zhu, and Berenice Venegas. On the lateral structure of model membranes containing cholesterol. *Biochimica et biophysica acta*, 1788(1):2–11, jan 2009. ISSN 0006-3002. doi: 10.1016/j.bbamem.2008.10.010. URL `http://www.ncbi.nlm.nih.gov/pubmed/19010302`.

Tomáš Chum, Daniela Glatzová, Zuzana Kvíčalová, Jan Malínský, Tomáš Brdička, and Marek Cebecauer. The role of palmitoylation and transmembrane domain in sorting of transmembrane adaptor proteins. *Journal of cell science*, 129:95–107, 2016. ISSN 1477-9137. doi: 10.1242/jcs.175190. URL `http://www.ncbi.nlm.nih.gov/pubmed/26585312`.

C. W. Cotman, M. L. Blank, A. Moehl, and F. Snyder. Lipid composition of synaptic plasma membranes isolated from rat brain by zonal centrifugation. *Biochemistry*, 8(11):4606–4612, 1969. doi: 10.1021/bi00839a056.

Lukasz Cwiklik. Biochimica et Biophysica Acta Tear fi lm lipid layer : A molecular level view. *BBA - Biomembranes*, 1858(10):2421–2430, 2016. ISSN 0005-2736. doi: 10.1016/j.bbamem.2016.02.020. URL `http://dx.doi.org/10.1016/j.bbamem.2016.02.020`.

Lukasz Cwiklik, Adela Melcrova, Philippe Daull, and Jean-sebastien Garrigue. A proposed mechanism for tear film breakup : a molecular level view by employing in-silico approach. *Journal for Modeling in Ophthalmology*, 1:19–23, 2018.

Djurre H. de Jong, Cesar a. Lopez, and Siewert J. Marrink. Molecular view on protein sorting into liquid-ordered membrane domains mediated by gangliosides and lipid anchors. *Faraday Discussions*, 161:347–363, 2013. ISSN 1359-6640. doi: 10.1039/c2fd20086d.

David Deamer. The Role of Lipid Membranes in Life's Origin. *Life*, 7(1):5, 2017. ISSN 2075-1729. doi: 10.3390/life7010005. URL `http://www.mdpi.com/2075-1729/7/1/5`.

Callum J. Dickson, Benjamin D. Madej, Åge A. Skjevik, Robin M. Betz, Knut Teigen, Ian R. Gould, and Ross C. Walker. Lipid14: The amber lipid force field. *Journal of Chemical Theory and Computation*, 10(2):865–879, 2014. ISSN 15499626. doi: 10.1021/ct4010307.

Giray Enkavi, Heikki Mikkolainen, Burçin Güngör, Elina Ikonen, and Ilpo Vattulainen. Concerted regulation of npc2 binding to endosomal/lysosomal membranes by bis(monoacylglycero)phosphate and sphingomyelin. *PLoS Computational Biology*, 13(10):1–21, 2017. ISSN 15537358. doi: 10.1371/journal.pcbi.1005831.

Santi Esteban-Martín, H. Jelger Risselada, Jesús Salgado, and Siewert J. Marrink. Stability of asymmetric lipid bilayers assessed by molecular dynamics simulations. *Journal of the American Chemical Society*, 131(42):15194–15202, 2009. ISSN 00027863. doi: 10.1021/ja904450t.

P. Ewen King-Smith, Kathleen S. Reuter, Richard J. Braun, Jason J. Nichols, and Kelly K. Nichols. Tear film breakup and structure studied by simultaneous video recording of fluorescence and tear film lipid layer images. *Investigative Ophthalmology and Visual Science*, 54(7):4900–4909, 2013. ISSN 01460404. doi: 10.1167/iovs.13-11878.

Gerald W Feigenson. Phase behavior of lipid mixtures. *Nature Chemical Biology*, 2(11):560–563, 2006. ISSN 15524469. doi: 10.1038/nchembio1106-560. URL `http://www.nature.com/doifinder/10.1038/nchembio1106-560`.

Gerald W Feigenson. Phase Boundaries and Biological Membranes. *Annual Rreview of Biophysics and Biomolecular Structure*, 36:63–77, 2007. ISSN 1056-8700. doi: 10.1146/annurev.biophys.36.040306.132721.Phase.

Tiago Mendes Ferreira, Filipe Coreta-Gomes, O. H. Samuli Ollila, Maria João Moreno, Winchil L.C. Vaz, and Daniel Topgaard. Cholesterol and POPC segmental order parameters in lipid membranes: Solid state1H-13C NMR and MD simulation studies. *Physical Chemistry Chemical Physics*, 15(6):1976–1989, 2013. ISSN 14639076. doi: 10.1039/c2cp42738a.

Nicolas Foloppe and Alexander D Jr MacKerell. All-atom empirical force field for nucleic acids : I. Parameter optimization based on small molecule and condensed phase macromolecular target data. *Journal of Computational Chemistry*, 21(2):2–3, 2000. ISSN 1096-987X. doi: 10.1002/(SICI)1096-987X(20000130)21:2⟨86::AID-JCC2⟩3.0.CO;2-G.

Gary N. Foulks. The Correlation Between the Tear Film Lipid Layer and Dry Eye Disease. *Survey of Ophthalmology*, 52(4):369–374, 2007. ISSN 00396257. doi: 10.1016/j.survophthal.2007.04.009.

Pim W.J.M. Frederix, Rein V. Ulijn, Neil T. Hunt, and Tell Tuttle. Virtual screening for dipeptide aggregation: Toward predictive tools for peptide self-Assembly. *Journal of Physical Chemistry Letters*, 2(19):2380–2384, 2011. ISSN 19487185. doi: 10.1021/jz2010573.

Ran Friedman, Syma Khalid, Camilo Aponte-Santamaría, Elena Arutyunova, Marlon Becker, Kevin J. Boyd, Mikkel Christensen, João T.S. Coimbra, Simona Concilio, Csaba Daday, Floris J. van Eerden, Pedro A. Fernandes, Frauke Gräter, Davit Hakobyan, Andreas Heuer, Konstantina Karathanou, Fabian Keller, M. Joanne Lemieux, Siewert J. Marrink, Eric R. May, Antara Mazumdar, Richard Naftalin, Mónica Pickholz, Stefano Piotto, Peter Pohl, Peter Quinn, Maria J. Ramos, Birgit Schiøtt, Durba Sengupta, Lucia Sessa, Stefano Vanni, Talia Zeppelin, Valeria Zoni, Ana Nicoleta Bondar, and Carmen Domene. Understanding Conformational Dynamics of Complex Lipid Mixtures Relevant to Biology. *Journal of Membrane Biology*, 251(5-6):609–631, 2018. ISSN 14321424. doi: 10.1007/s00232-018-0050-y. URL `http://dx.doi.org/10.1007/s00232-018-0050-y`.

Samuel Genheden and Jonathan W. Essex. A Simple and Transferable All-Atom/Coarse-Grained Hybrid Model to Study Membrane Processes. *Journal of Chemical Theory and Computation*, 11(10):4749–4759, 2015. ISSN 15499626. doi: 10.1021/acs.jctc.5b00469.

Davit Hakobyan and Andreas Heuer. Phase separation in a lipid/cholesterol system: Comparison of coarse-grained and united-atom simulations. *Journal of Physical Chemistry B*, 117(14):3841–3851, 2013. ISSN 15205207. doi: 10.1021/jp312245y.

Xianlin Han and W. Gross, Richard. Electrospray ionization mass spectroscopic analysis of human erythrocyte plasma membrane phospholipids. *Proceedings of the National Academy of Sciences of the United States of America*, 91:10635–10639, 1994. URL `http://www.transnational-dispute-management.com/article.asp?key=511`.

L Herbette, C A Napolitano, and R V McDaniel. Direct determination of the calcium profile structure for dipalmitoyllecithin multilayers using neutron diffraction. *Biophysical journal*, 46(6):677, 1984.

M L Horng, J A Gardecki, A Papazyan, and M Maroncelli. Subpicosecond Measurements of Polar Solvation Dynamics: Coumarin 153 Revisited. *J Phys Chem*, 99(48):17311–17337, 1995. doi: 10.1021/j100048a004. URL http://pubs.acs.org/doi/pdfplus/10.1021/j100048a004.

M. Hrdinka and V. Horejsi. PAG - a multipurpose transmembrane adaptor protein. *Oncogene*, 33:4881–4892, 2014. ISSN 0950-9232. doi: 10.1038/onc.2013.485. URL http://dx.doi.org/10.1038/onc.2013.485.

Jochen S. Hub and Neha Awasthi. Probing a Continuous Polar Defect: A Reaction Coordinate for Pore Formation in Lipid Membranes. *Journal of Chemical Theory and Computation*, 13(5):2352–2366, 2017. ISSN 15499626. doi: 10.1021/acs.jctc.7b00106.

D Huster, K Arnold, and K Gawrisch. Strength of Ca(2+) binding to retinal lipid membranes: consequences for lipid organization. *Biophysical journal*, 78 (6):3011–8, jun 2000. ISSN 0006-3495. doi: 10.1016/S0006-3495(00)76839-1. URL http://www.pubmedcentral.nih.gov/articlerender.fcgi?artid=1300884&tool=pmcentrez&rendertype=abstracthttp://www.ncbi.nlm.nih.gov/pubmed/10827979.

J A Ingram, R S Moog, N Ito, R Biswas, and M Maroncelli. Solute Rotation and Solvation Dynamics in a Room-Temperature Ionic Liquid. *J. Phys. Chem. B*, 107(24):5926–5932, 2003. ISSN 1520-6106. doi: 10.1021/jp034231e. URL http://pubs3.acs.org/acs/journals/doilookup?in{_}doi=10.1021/jp034231e.

Jacob N. Israelachvili. *Intermolecular and Surface Forces (3rd ed.)*. Academic Press, 2011. ISBN 978-0-12-391927-4.

M. A. Isreb, J. V. Greiner, D. R. Korb, T. Glonek, S. S. Mody, V. M. Finnemore, and C. V. Reddy. Correlation of lipid layer thickness measurements with fluorescein tear film break-up time and Schirmer's test. *Eye*, 17(1):79–83, 2003. ISSN 0950222X. doi: 10.1038/sj.eye.6700224.

N. Ito, S. Arzhantsev, M. Heitz, and M. Maroncelli. Solvation Dynamics and Rotation of Coumarin 153 in Alkylphosphonium Ionic Liquids. *The Journal of Physical Chemistry B*, 108(18):5771–5777, 2004. ISSN 1520-6106. doi: 10.1021/jp0499575. URL http://pubs.acs.org/doi/abs/10.1021/jp0499575.

J. P. Craig and A. Tomlinson. Importance of the Lipid Layer in Human Tear Film Stability and Evaporation. *Optometry and vision science*, 74(1):8–13, 1997.

Joakim P.M. Jämbeck and Alexander P. Lyubartsev. Another piece of the membrane puzzle: Extending slipids further. *Journal of Chemical Theory and Computation*, 9(1):774–784, 2013. ISSN 15499618. doi: 10.1021/ct300777p.

Joakim P.M. M Jämbeck and Alexander P. Lyubartsev. An Extension and Further Validation of an All-Atomistic Force Field for Biological Membranes. *Journal of Chemical Theory and Computation*, 8(8):2938–2948, 2012a. ISSN 15499618. doi: 10.1021/ct300342n.

Joakim P.M. M Jämbeck and Alexander P. Lyubartsev. Derivation and Systematic Validation of a Refined All-Atom Force Field for Phosphatidylcholine Lipids. *Journal of Physical Chemistry B*, 116(10):3164–3179, 2012b. ISSN 15205207. doi: 10.1021/jp212503e.

Thomas J Jentsch. VRACs and other ion channels and transporters in the regulation of cell volume and beyond. *Nature Reviews Molecular Cell Biology*, 17(5):293–307, may 2016. ISSN 1471-0072. doi: 10.1038/nrm.2016.29. URL `http://www.nature.com/articles/nrm.2016.29`.

Piotr Jurkiewicz, Jan Sýkora, Agnieszka Olżyńska, Jana Humpolícková, and Martin Hof. Solvent Relaxation in Phospholipid Bilayers: Principles and Recent Applications - Springer. *Journal of fluorescence*, 15(6):883–894, dec 2005. ISSN 1053-0509. doi: 10.1007/s10895-005-0013-4. URL `http://dx.doi.org/10.1007/s10895-005-0013-4`.

Piotr Jurkiewicz, Lukasz Cwiklik, Alžběta Vojtíšková, Pavel Jungwirth, and Martin Hof. Structure, dynamics, and hydration of POPC/POPS bilayers suspended in NaCl, KCl, and CsCl solutions. *Biochimica et biophysica acta*, 1818 (3):609–16, mar 2012. ISSN 0006-3002. doi: 10.1016/j.bbamem.2011.11.033. URL `http://www.ncbi.nlm.nih.gov/pubmed/22155683`.

Parimal Kar and Michael Feig. Hybrid All-Atom/Coarse-Grained Simulations of Proteins by Direct Coupling of CHARMM and PRIMO Force Fields. *Journal of Chemical Theory and Computation*, 13(11):5753–5765, 2017. doi: 10.1021/acs.jctc.7b00840.

P. M. Kasson, N. W. Kelley, N. Singhal, M. Vrljic, A. T. Brunger, and V. S. Pande. Ensemble molecular dynamics yields submillisecond kinetics and intermediates of membrane fusion. *Proceedings of the National Academy of Sciences*, 103 (32):11916–11921, 2006. ISSN 0027-8424. doi: 10.1073/pnas.0601597103. URL `http://www.pnas.org/cgi/doi/10.1073/pnas.0601597103`.

Peter M. Kasson and Vijay S. Pande. Control of membrane fusion mechanism by lipid composition: Predictions from ensemble molecular dynamics. *PLoS Computational Biology*, 3(11):2228–2238, 2007. ISSN 1553734X. doi: 10.1371/journal.pcbi.0030220.

Jochen W. Klingelhoefer, Timothy Carpenter, and Mark S.P. Sansom. Peptide nanopores and lipid bilayers: Interactions by coarse-grained molecular-dynamics simulations. *Biophysical Journal*, 96(9):3519–3528, 2009. ISSN 15420086. doi: 10.1016/j.bpj.2009.01.046. URL `http://dx.doi.org/10.1016/j.bpj.2009.01.046`.

Miriam Kohagen, Philip E. Mason, and Pavel Jungwirth. Accurate description of calcium solvation in concentrated aqueous solutions. *The Journal*

of Physical Chemistry B, 118(28):7902–7909, 2014. ISSN 15205207. doi: 10.1021/jp5005693.

Miriam Kohagen, Philip E. Mason, and Pavel Jungwirth. Accounting for Electronic Polarization Effects in Aqueous Sodium Chloride via Molecular Dynamics Aided by Neutron Scattering. *Journal of Physical Chemistry B*, 120(8): 1454–1460, 2016. ISSN 15205207. doi: 10.1021/acs.jpcb.5b05221.

Alexander B. Kuhn, Srinivasa M. Gopal, and Lars V. Schäfer. On Using Atomistic Solvent Layers in Hybrid All-Atom/Coarse-Grained Molecular Dynamics Simulations. *Journal of Chemical Theory and Computation*, 11(9):4460–4472, 2015. ISSN 15499626. doi: 10.1021/acs.jctc.5b00499.

T.R.R. Kurup, Wan L.S.C., and L.W. Chan. Preservative requirements in emulsions. *Pharmaceutica Acta Helvetiae*, 67:204–208, 1992. ISSN 00316865.

Joseph R. Lakowicz. *Principles of fluorescence spectroscopy (2nd ed.)*. Kluwer Academic/Plenum, New York, 1999. ISBN 0-306-46093-9.

I. Langmuir. Adsorption of gases on plain surfaces of glass mica platinum. *J. Am. Chem. Soc.*, 40(1914):1361–1403, 1918. ISSN 0361476X. doi: 10.1006/ceps.2001.1094.

Igor Leontyev and Alexei Stuchebrukhov. Accounting for electronic polarization in non-polarizable force fields. *Physical Chemistry Chemical Physics*, 13(7): 2613, 2011. ISSN 1463-9076. doi: 10.1039/c0cp01971b. URL `http://xlink.rsc.org/?DOI=c0cp01971b`.

Cheuk Yui Leung, Liam C. Palmer, Bao Fu Qiao, Sumit Kewalramani, Rastko Sknepnek, Christina J. Newcomb, Megan A. Greenfield, Graziano Vernizzi, Samuel I. Stupp, Michael J. Bedzyk, and Monica Olvera De La Cruz. Molecular crystallization controlled by pH regulates mesoscopic membrane morphology. *ACS Nano*, 6(12):10901–10909, 2012. ISSN 19360851. doi: 10.1021/nn304321w.

Ilya Levental, Daniel Lingwood, Michal Grzybek, Ünal Coskun, and Kai Simons. Palmitoylation regulates raft affinity for the majority of integral raft proteins. *Proceedings of the National Academy of Sciences of the United States of America*, 107(51):22050–22054, 2010. ISSN 0027-8424. doi: 10.1073/pnas.1016184107.

Xubo Lin, Alemayehu A Gorfe, and Ilya Levental. Protein Partitioning into Ordered Membrane Domains: Insights from Simulations. *Biophysj*, 114(8): 1936–1944, 2018. ISSN 0006-3495. doi: 10.1016/j.bpj.2018.03.020. URL `http://www.cell.com/biophysj/pdf/S0006-3495(18)30387-4.pdf`.

Craig N. Lumb and Mark S.P. Sansom. Defining the membrane-associated state of the PTEN tumor suppressor protein. *Biophysical Journal*, 104(3):613–621, 2013. ISSN 00063495. doi: 10.1016/j.bpj.2012.12.002. URL `http://dx.doi.org/10.1016/j.bpj.2012.12.002`.

Alexander D. Mackerell, Michael Feig, and Charles L. Brooks. Extending the treatment of backbone energetics in protein force fields: Limitations of gas-phase quantum mechanics in reproducing protein conformational distributions in molecular dynamics simulation. *Journal of Computational Chemistry*, 25 (11):1400–1415, 2004. ISSN 01928651. doi: 10.1002/jcc.20065.

Negin Maftouni, Mehriar Amininasab, Mansour Vali, Mohammadreza Ejtehadi, and Farshad Kowsari. A molecular dynamics simulation study of nanomechanical properties of asymmetric lipid bilayer. *Journal of Membrane Biology*, 246 (1):67–73, 2013. ISSN 00222631. doi: 10.1007/s00232-012-9505-8.

Aniket Magarkar, Piotr Jurkiewicz, Christoph Allolio, Martin Hof, and Pavel Jungwirth. Increased Binding of Calcium Ions at Positively Curved Phospholipid Membranes. *Journal of Physical Chemistry Letters*, 8(2):518–523, 2017. ISSN 19487185. doi: 10.1021/acs.jpclett.6b02818.

Siewert J Marrink and Alan E Mark. The Mechanism of Vesicle Fusion as Revealed by Molecular Dynamics Simulations. *Journal of the American Chemical Society*, pages 1–5, 2003a. doi: 10.1021/ja036138.

Siewert J. Marrink and Alan E. Mark. Molecular Dynamics Simulation of the Formation, Structure, and Dynamics of Small Phospholipid Vesicles. *Journal of the American Chemical Society*, 125(49):15233–15242, 2003b. ISSN 00027863. doi: 10.1021/ja0352092.

Siewert J. Marrink and D. Peter Tieleman. Perspective on the Martini model. *Chemical Society Reviews*, 42(16):6801–6822, 2013. ISSN 14604744. doi: 10.1039/c3cs60093a.

Siewert J. Marrink, Alex H. de Vries, and Alan E. Mark. Coarse Grained Model for Semiquantitative Lipid Simulations. *The Journal of Physical Chemistry B*, 108(2):750–760, jan 2004. ISSN 1520-6106. doi: 10.1021/jp036508g. URL `http://pubs.acs.org/doi/abs/10.1021/jp036508g`.

Siewert J Marrink, H Jelger Risselada, Serge Yefimov, D Peter Tieleman, and Alex H de Vries. The MARTINI force field: coarse grained model for biomolecular simulations. *The journal of physical chemistry. B*, 111(27):7812–24, 2007. ISSN 1520-6106. doi: 10.1021/jp071097f. URL `http://www.ncbi.nlm.nih.gov/pubmed/17569554`.

Siewert Jan Marrink and Alan E. Mark. Molecular view of hexagonal phase formation in phospholipid membranes. *Biophysical Journal*, 87(6):3894–3900, 2004. ISSN 00063495. doi: 10.1529/biophysj.104.048710. URL `http://dx.doi.org/10.1529/biophysj.104.048710`.

Alberto Martín-Molina, César Rodríguez-Beas, and Jordi Faraudo. Effect of calcium and magnesium on phosphatidylserine membranes: experiments and all-atomic simulations. *Biophysical journal*, 102(9): 2095–103, may 2012. ISSN 1542-0086. doi: 10.1016/j.bpj.2012.03.009. URL `http://www.pubmedcentral.nih.gov/articlerender.fcgi?artid=3341548&tool=pmcentrez&rendertype=abstract`.

Hector Martinez-Seara, Tomasz Róg, Marta Pasenkiewicz-Gierula, Ilpo Vattulainen, Mikko Karttunen, and Ramon Reigada. Interplay of unsaturated phospholipids and cholesterol in membranes: effect of the double-bond position. *Biophysical journal*, 95(7):3295–3305, 2008. ISSN 00063495. doi: 10.1529/biophysj.108.138123.

Hector Martinez-Seara, Tomasz Róg, Mikko Karttunen, Ilpo Vattulainen, and Ramon Reigada. Why is the sn-2 chain of monounsaturated glycerophospholipids usually unsaturated whereas the sn-1 chain is saturated? Studies of 1-stearoyl-2-oleoyl-sn-glycero-3-phosphatidylcholine (SOPC) and 1-oleoyl-2-stearoyl-sn-glycero-3-phosphatidylcholine (OSPC). *Journal of Physical Chemistry B*, 113(24):8347–8356, 2009. ISSN 15206106. doi: 10.1021/jp902131b.

Hector Martinez-Seara, Tomasz Róg, Mikko Karttunen, Ilpo Vattulainen, and Ramon Reigada. Cholesterol induces specific spatial and orientational order in cholesterol/phospholipid membranes. *PLoS ONE*, 5(6), 2010. ISSN 19326203. doi: 10.1371/journal.pone.0011162.

James P. McCulley and Ward Shine. A compositional based model for the tear film lipid layer. *Trans Am Ophthalmol Soc*, 95:79–88, 1997.

Josef Melcr, Daniel Bonhenry, Štěpán Timr, and Pavel Jungwirth. Transmembrane Potential Modeling: Comparison between Methods of Constant Electric Field and Ion Imbalance. *Journal of Chemical Theory and Computation*, 12 (5):2418–2425, 2016. ISSN 15499626. doi: 10.1021/acs.jctc.5b01202. URL `http://dx.doi.org/10.1021/acs.jctc.5b01202`.

Josef Melcr, Hector Martinez-Seara, Ricky Nencini, Jiri Kolafa, Pavel Jungwirth, and O.H. Samuli Ollila. Accurate Binding of Sodium and Calcium to a POPC Bilayer by Effective Inclusion of Electronic Polarization. *The Journal of Physical Chemistry B*, page acs.jpcb.7b12510, 2018. ISSN 1520-6106. doi: 10.1021/acs.jpcb.7b12510. URL `https://doi.org/10.1021/acs.jpcb.7b12510%0Ahttp://pubs.acs.org/doi/10.1021/acs.jpcb.7b12510`.

Adela Melcrova, Sarka Pokorna, Saranya Pullanchery, Miriam Kohagen, Piotr Jurkiewicz, Martin Hof, Pavel Jungwirth, Paul S. Cremer, and Lukasz Cwiklik. The complex nature of calcium cation interactions with phospholipid bilayers. *Scientific Reports*, 6(38035), dec 2016. ISSN 2045-2322. doi: 10.1038/srep38035. URL `http://www.nature.com/articles/srep38035`.

Adela Melcrova, Matti Javanainen, Aniket Magarkar, Piotr Jurkiewicz, Martin Hof, Pavel Jungwirth, and Hector Martinez-Seara. Two cations, two mechanisms: interactions of sodium and calcium with zwitterionic lipid membranes. *Chem. Commun.*, 53(39):5380–5383, 2017. ISSN 1359-7345. doi: 10.1039/C7CC02208E. URL `http://xlink.rsc.org/?DOI=C7CC02208E`.

Adela Melcrova, Marek Cebecauer, and Lukasz Cwiklik. The importance of the two palmitoylations on PAG peptide – all-atom MD study. *Biophysical journal*, Submitted, 2019a.

Adela Melcrova, Sarka Pokorna, Miroslava Vosahlikova, Jan Sykora, Petr Svoboda, Martin Hof, Lukasz Cwiklik, and Piotr Jurkiewicz. Simultaneous compression of lipid membranes by calcium and cholesterol. *Langmuir*, Submitted, 2019b.

Thomas J. Millar and Burkhardt S. Schuett. The real reason for having a meibomian lipid layer covering the outer surface of the tear film - A review. *Experimental Eye Research*, 137:125–138, 2015. ISSN 10960007. doi: 10.1016/j.exer.2015.05.002.

Ole G. Mouritsen. Model answers to lipid membrane questions. *Cold Spring Harbor Perspectives in Biology*, 3(9):1–15, 2011. ISSN 19430264. doi: 10.1101/cshperspect.a004622.

Poonam Mudgil. Antimicrobial Role of Human Meibomian Lipids at the Ocular Surface. *Investigative Ophthalmology and Visual Science*, 55(11):7272–7277, 2014. doi: 10.1167/iovs.14-15512.

Teemu Murtola, Timo A. Vuorela, Marja T. Hyvönen, Siewert Jan Marrink, Mikko Karttunen, and Ilpo Vattulainen. Low density lipoprotein: Structure, dynamics, and interactions of apoB-100 with lipids. *Soft Matter*, 7(18):8135–8141, 2011. ISSN 1744683X. doi: 10.1039/c1sm05367a.

D. Nelson and M. Cox. *Lehninger principles of biochemistry (4th ed.)*. W.H. Freeman and Company, New York, 2005.

S Nir, J Bentz, J Wilschut, and N Duzgunes. Aggregation and Fusion of Phospholipid-Vesicles. *Progress in Surface Science*, 13(1):1–124, 1983. doi: Doi10.1016/0079-6816(83)90010-2.

Rebecca Notman, Massimo G Noro, and Jamshed Anwar. Molecular simulation of the mechanism of action of oleic acid as a drug penetration enhancer Interaction of Oleic Acid with Dipalmitoylphosphatidylcholine (DPPC) Bilayers Simulated by Molecular Dynamics. *Journal of Physical Chemistry B*, 111:12748–12755, 2007.

Fumiko Ogushi, Reiko Ishitsuka, Toshihide Kobayashi, and Yuji Sugita. Rapid flip-flop motions of diacylglycerol and ceramide in phospholipid bilayers. *Chemical Physics Letters*, 522:96–102, 2012. ISSN 00092614. doi: 10.1016/j.cplett.2011.11.057. URL `http://dx.doi.org/10.1016/j.cplett.2011.11.057`.

Mary Catherine Olson, Donald R. Korb, and Jack V. Greiner. Increase in tear film lipid layer thickness following treatment with warm compresses in patients with meibomian gland dysfunction. *Eye and Contact Lens*, 29(2):96–99, 2003. ISSN 15422321. doi: 10.1097/01.ICL.0000060998.20142.8D.

Sten Orrenius, Boris Zhivotovsky, and Pierluigi Nicotera. Regulation of cell death: the calcium-apoptosis link. *Nature reviews. Molecular cell biology*, 4(7):552–65, 2003. ISSN 1471-0072. doi: 10.1038/nrm1150. URL `http://www.ncbi.nlm.nih.gov/pubmed/12838338`.

Biswaranjan Pani and Brij B Singh. Lipid rafts/caveolae as microdomains of calcium signaling. *Cell calcium*, 45(6):625–33, jun 2009. ISSN 1532-1991. doi: 10.1016/j.ceca.2009.02.009. URL http://www.pubmedcentral.nih.gov/articlerender.fcgi?artid=2695836&tool=pmcentrez&rendertype=abstract.

U R Pedersen, C Leidy, P Westh, and G H Peters. The effect of calcium on the properties of charged phospholipid bilayers. *Biochimica Et Biophysica Acta-Biomembranes*, 1758(5):573–582, 2006. doi: DOI10.1016/j.bbamem.2006.03.035.

Xavier Periole, Thomas Huber, Siewert Jan Marrink, and Thomas P. Sakmar. G protein-coupled receptors self-assemble in dynamics simulations of model bilayers. *Journal of the American Chemical Society*, 129(33):10126–10132, 2007. ISSN 00027863. doi: 10.1021/ja0706246.

Mónica Pickholz and Giovanni Giupponi. Coarse grained simulations of local anesthetics encapsulated into a liposome. *Journal of Physical Chemistry B*, 114(20):7009–7015, 2010. ISSN 15205207. doi: 10.1021/jp909148n.

Irina D Pogozheva, Stephanie Tristram-Nagle, Henry I Mosberg, and Andrei L Lomize. Structural adaptations of proteins to different biological membranes. *BBA - Biomembranes*, 1828(11):2592–2608, 2013. ISSN 0005-2736. doi: 10.1016/j.bbamem.2013.06.023. URL http://dx.doi.org/10.1016/j.bbamem.2013.06.023.

Rodolfo D Porasso, J J L Cascales, and J J López Cascales. Study of the effect of Na+ and Ca2+ ion concentration on the structure of an asymmetric DPPC/DPPC + DPPS lipid bilayer by molecular dynamics simulation. *Colloids and surfaces. B, Biointerfaces*, 73(1):42–50, oct 2009. ISSN 1873-4367. doi: 10.1016/j.colsurfb.2009.04.028. URL http://www.ncbi.nlm.nih.gov/pubmed/19487110.

Bernhard C. Poschner and Dieter Langosch. Stabilization of conformationally dynamic helices by covalently attached acyl chains. *Protein Science*, 18(8):1801–1805, 2009. ISSN 09618368. doi: 10.1002/pro.155.

Jeffrey J Potoff, Zeena Issa, Charles W Manke, and Bhanu P Jena. Ca2+-dimethylphosphate complex formation: providing insight into Ca2+-mediated local dehydration and membrane fusion in cells. *Cell biology international*, 32(4):361–6, apr 2008. ISSN 1065-6995. doi: 10.1016/j.cellbi.2008.03.002. URL http://www.ncbi.nlm.nih.gov/pubmed/18452809.

Shan Shan Qin, Yang Xin Yu, Qi Kai Li, and Zhi Wu Yu. Interaction of human synovial phospholipase A2 with mixed lipid bilayers: A coarse-grain and all-atom molecular dynamics simulation study. *Biochemistry*, 52(8):1477–1489, 2013. ISSN 00062960. doi: 10.1021/bi3012687.

Yann Quentric, Philippe Daull, Laurence Feraille, Pierre-paul Elena, and Jean-Sebastien Garrigue. Efficacy of a preservative-free cationic emulsion vehicle eye drop in a mouse model of dry eye. 2016. doi: 10.5301/ejo.5000779.

Antti H. Rantamäki, Tuulikki Seppänen-Laakso, Matej Oresic, Matti Jauhiainen, and Juha M. Holopainen. Human tear fluid lipidome: From composition to function. *PLoS ONE*, 6(5):1–7, 2011. ISSN 19326203. doi: 10.1371/journal.pone.0019553.

W Rawicz, B a Smith, T J McIntosh, S a Simon, and E Evans. Elasticity, strength, and water permeability of bilayers that contain raft microdomain-forming lipids. *Biophysical journal*, 94(12): 4725–36, jun 2008. ISSN 1542-0086. doi: 10.1529/biophysj.107.121731. URL `http://www.pubmedcentral.nih.gov/articlerender.fcgi?artid=2397373&tool=pmcentrez&rendertype=abstract`.

Kamila Riedlova, Adela Melcrova, Agnieszka Olzynska, Philippe Daull, Jean-Sebastien Garrigue, and Lukasz Cwiklik. Influence of benzalkonium chloride on Tear Film Lipid Layer stability: a molecular level view by employing in silico modeling. *Journal for Modeling in Ophthalmology*, Accepted for publication, 2018.

H. J. Risselada and S. J. Marrink. The molecular face of lipid rafts in model membranes. *Proceedings of the National Academy of Sciences*, 105(45):17367–17372, 2008. ISSN 0027-8424. doi: 10.1073/pnas.0807527105. URL `http://www.pnas.org/cgi/doi/10.1073/pnas.0807527105`.

H. Jelger Risselada and Siewert J. Marrink. The freezing process of small lipid vesicles at molecular resolution. *Soft Matter*, 5(22):4531–4541, 2009a. ISSN 1744683X. doi: 10.1039/b913210d.

H. Jelger Risselada and Siewert J. Marrink. Curvature effects on lipid packing and dynamics in liposomes revealed by coarse grained molecular dynamics simulations. *Phys. Chem. Chem. Phys.*, 11:2056–2067, 2009b. doi: 10.1039/b818782g.

H. Jelger Risselada, Alan E. Mark, and Siewert J. Marrink. Application of mean field boundary potentials in simulations of lipid vesicles. *Journal of Physical Chemistry B*, 112(25):7438–7447, 2008. ISSN 15206106. doi: 10.1021/jp0758519.

Yoel Rodríguez, Mihaly Mezei, and Roman Osman. Association free energy of dipalmitoylphosphatidylserines in a mixed dipalmitoylphosphatidylcholine membrane. *Biophysical journal*, 92(9):3071–80, may 2007. ISSN 0006-3495. doi: 10.1529/biophysj.106.089078. URL `http://www.pubmedcentral.nih.gov/articlerender.fcgi?artid=1852338&tool=pmcentrez&rendertype=abstract`.

Tomasz Róg, Marta Pasenkiewicz-Gierula, Ilpo Vattulainen, and Mikko Karttunen. Ordering effects of cholesterol and its analogues. *Biochimica et biophysica acta*, 1788(1):97–121, jan 2009. ISSN 0006-3002. doi: 10.1016/j.bbamem.2008.08.022. URL `http://www.ncbi.nlm.nih.gov/pubmed/18823938`.

Michael J Russell, Roy M Daniel, Allan Hall, Michael Russell, R O Y M Daniel, and Allan J Hall. On the emergence of life via catalytic iron-sulphide membranes. *Terra Nova*, 5:343–347, 1993.

Amy Y. Shih, Peter L. Freddolino, Anton Arkhipov, and Klaus Schulten. Assembly of lipoprotein particles revealed by coarse-grained molecular dynamics simulations. *Journal of Structural Biology*, 157(3):579–592, 2007. ISSN 10478477. doi: 10.1016/j.jsb.2006.08.006.

S. J. Singer and Garth L. Nicolson. The fluid mosaic model of the structure of cell membranes. *Hydrobiological Journal*, 175(4023):720–731, 1972. ISSN 00188166.

R. Sips. On the Structure of a Catalyst Surface. II. *J. Chem. Phys.*, 18(8): 1024–1026, 1950.

Shirley W.I. Siu, Robert Vácha, Pavel Jungwirth, and Rainer A. Böckmann. Biomolecular simulations of membranes: Physical properties from different force fields. *Journal of Chemical Physics*, 128(12):1–12, 2008. ISSN 00219606. doi: 10.1063/1.2897760.

Jesper Sørensen, Xavier Periole, Katrine K. Skeby, Siewert-J. Marrink, and Birgit Schiøtt. Protofibrillar Assembly Toward the Formation of Amyloid Fibrils. *The Journal of Physical Chemistry Letters*, 2(19):2385–2390, 2011. ISSN 1948-7185. doi: 10.1021/jz2010094. URL `http://pubs.acs.org/doi/abs/10.1021/jz2010094`.

Michiel Sprik, Jürg Hutter, and Michele Parrinello. Ab initio molecular dynamics simulation of liquid water: Comparison of three gradient-corrected density functionals. *Journal of Chemical Physics*, 105(3):1142–1152, 1996. ISSN 00219606. doi: 10.1063/1.471957.

Ove Sten-Knudsen. *Biological membranes: Theory of transport, potentials and electric impulses*. Cambridge University Press, New York, 2002.

Alexandr Svec. Phosphoprotein associated with glycosphingolipid-enriched microdomains / Csk-binding protein : A protein that matters. *Pathology - Research and Practice*, 204:785–792, 2008. doi: 10.1016/j.prp.2008.06.006.

Pradip K Tarafdar, Hirak Chakraborty, S Moses Dennison, and Barry R Lentz. Phosphatidylserine inhibits and calcium promotes model membrane fusion. *Biophysical journal*, 103(9):1880–9, nov 2012. ISSN 1542-0086. doi: 10.1016/j.bpj.2012.09.030. URL `http://www.pubmedcentral.nih.gov/articlerender.fcgi?artid=3491704&tool=pmcentrez&rendertype=abstract`.

D. Peter Tieleman, Justin L. MacCallum, Walter L. Ash, Christian Kandt, Zhitao Xu, and Luca Monticelli. Membrane protein simulations with a united-atom lipid and all-atom protein model: Lipid-protein interactions, side chain transfer free energies and model proteins. *Journal of Physics Condensed Matter*, 18(28), 2006. ISSN 09538984. doi: 10.1088/0953-8984/18/28/S07.

Richard Tjörnhammar and Olle Edholm. The shape and free energy of a lipid bilayer surrounding a membrane inclusion. *Chemistry and Physics of Lipids*, 169:2–8, 2013. ISSN 00093084. doi: 10.1016/j.chemphyslip.2012.12.005. URL `http://dx.doi.org/10.1016/j.chemphyslip.2012.12.005`.

Hui-Hsu Gavin Tsai, Wei-Xiang Lai, Hong-Da Lin, Jian-Bin Lee, Wei-Fu Juang, and Wen-Hsin Tseng. Molecular dynamics simulation of cation-phospholipid clustering in phospholipid bilayers: possible role in stalk formation during membrane fusion. *Biochimica et biophysica acta*, 1818(11):2742–55, nov 2012. ISSN 0006-3002. doi: 10.1016/j.bbamem.2012.05.029. URL `http://www.ncbi.nlm.nih.gov/pubmed/22683599`.

Mark E. Tuckerman. Efficient and general algorithms for path integral Car-Parrinello molecular dynamics. *Journal of Chemical Physics*, 104(14):5579–5588, 1996. ISSN 00219606. doi: 10.1063/1.471771.

Daniela Uhríková, Norbert Kucerka, José Teixeira, Valentin Gordeliy, and Pavol Balgavý. Structural changes in dipalmitoylphosphatidylcholine bilayer promoted by Ca2+ ions: a small-angle neutron scattering study. *Chemistry and physics of lipids*, 155(2):80–9, oct 2008. ISSN 0009-3084. doi: 10.1016/j.chemphyslip.2008.07.010. URL `http://www.ncbi.nlm.nih.gov/pubmed/18721799`.

Martin B Ulmschneider, Mark S P Sansom, and Alfredo Di Nola. Properties of Integral Membrane Protein Structures : Derivation of an Implicit Membrane Potential. *PROTEINS: Structure, Function, and Bioinformatics*, 59:252–265, 2005. doi: 10.1002/prot.20334.

Robert Vácha, Max L. Berkowitz, and Pavel Jungwirth. Molecular model of a cell plasma membrane with an asymmetric multicomponent composition: Water permeation and ion effects. *Biophysical Journal*, 96(11):4493–4501, 2009. ISSN 00063495. doi: 10.1016/j.bpj.2009.03.010. URL `http://dx.doi.org/10.1016/j.bpj.2009.03.010`.

Gerrit van Meer, Dennis R. Voelker, and Gerald W Feigenson. Membrane lipids: where they are and how they behave. *Nature Reviews Molecular Cell Biology*, 9(2):112–124, 2008. ISSN 0270-6474. doi: 10.1038/nrm2330.Membrane. URL `http://www.ncbi.nlm.nih.gov/pubmed/10575041`.

G. Vereb, J. Szollosi, J. Matko, P. Nagy, T. Farkas, L. Vigh, L. Matyus, T. A. Waldmann, and S. Damjanovich. Dynamic, yet structured: The cell membrane three decades after the Singer-Nicolson model. *Proceedings of the National Academy of Sciences*, 100(14):8053–8058, 2003. ISSN 0027-8424. doi: 10.1073/pnas.1332550100. URL `http://www.pnas.org/cgi/doi/10.1073/pnas.1332550100`.

Miroslava Vošahlíková, Piotr Jurkiewicz, Lenka Roubalová, Martin Hof, and Petr Svoboda. High- and low-affinity sites for sodium in δ-OR-Gi1α (Cys351-Ile351) fusion protein stably expressed in HEK293 cells; functional significance and correlation with biophysical state of plasma membrane. *Naunyn-Schmiedeberg's Archives of Pharmacology*, 387(5):487–502, may 2014. ISSN 0028-1298. doi: 10.1007/s00210-014-0962-8. URL `http://link.springer.com/10.1007/s00210-014-0962-8`.

Timo Vuorela, Andrea Catte, Perttu S. Niemelä, Anette Hall, Marja T. Hyvönen, Siewert Jan Marrink, Mikko Karttunen, and Ilpo Vattulainen. Role of Lipids

in Spheroidal High Density Lipoproteins. *PLoS Computational Biology*, 6(10), 2010. ISSN 1553734X. doi: 10.1371/journal.pcbi.1000964.

Tsjerk A. Wassenaar, Kristyna Pluhackova, Rainer A. Böckmann, Siewert J. Marrink, and D. Peter Tieleman. Going backward: A flexible geometric approach to reverse transformation from coarse grained to atomistic models. *Journal of Chemical Theory and Computation*, 10(2):676–690, 2014. ISSN 15499618. doi: 10.1021/ct400617g.

Mark D P Willcox, Pablo Argüeso, Georgi A Georgiev, Juha M Holopainen, Gordon W Laurie, Tom J Millar, Eric B Papas, Jannick P Rolland, Tannin A Schmidt, Ulrike Stahl, Tatiana Suarez, Lakshman N Subbaraman, B S Optom, and O Omür. The Ocular Surface TFOS DEWS II Tear Film Report. *Ocular Surface*, 15(3):366–403, 2017. ISSN 1542-0124. doi: 10.1016/j.jtos.2017.03.006. URL `http://dx.doi.org/10.1016/j.jtos.2017.03.006`.

J Wilschut, N Duzgunes, and D Papahadjopoulos. Calcium-Magnesium Specificity in Membrane-Fusion - Kinetics of Aggregation and Fusion of Phosphatidylserine Vesicles and the Role of Bilayer Curvature. *Biochemistry*, 20 (11):3126–3133, 1981. doi: DOI10.1021/bi00514a022.

Semen O. Yesylevskyy and Alexander P. Demchenko. How cholesterol is distributed between monolayers in asymmetric lipid membranes. *European Biophysics Journal*, 41(12):1043–1054, 2012. ISSN 01757571. doi: 10.1007/s00249-012-0863-z.

Jejoong Yoo and Qiang Cui. Curvature generation and pressure profile modulation in membrane by lysolipids: Insights from coarse-grained simulations. *Biophysical Journal*, 97(8):2267–2276, 2009. ISSN 15420086. doi: 10.1016/j.bpj.2009.07.051. URL `http://dx.doi.org/10.1016/j.bpj.2009.07.051`.

List of Figures

List of Tables

List of Abbreviations

APL	area per lipid
APP	area per phospholipid
C=O	carbonyl group of phospholipids
CKC	cetalkonium chloride
CO	cholesteryl oleate
COO^-	carboxylate group of phospholipids
DED	dry eye disease
DLPC	1,2-diauroyl-sn-glycero-3-phospocholine
DLS	dynamic light scattering
DMPC	1,2-dimyristoyl-sn-glycero-3-phosphocholine
DOPC	1,2-dioleoyl-sn-glycero-3-phosphocholine
DOPS	1,2-dioleoyl-sn-glycero-3-phosphoserine
DPPC	1,2-dipalmitoyl-sn-glycero-3-phospcholine
Dtmac	4-[(n-dodecylthio)methyl]-7-(N,N-dimethylamino)-coumarin
EDTA	ethylenediaminetetraacetic acid
ECC	electronic continuum correction
GP	generalized polarization
Laurdan	6-Dodecanoyl-2-Dimethylaminonaphthalene
LUV	large unilamellar vesicle
MD	molecular dynamics
NMR	nuclear magnetic resonance
PA	phosphatidic acid
PC	phosphatidylcholine
PE	phosphatidylethanolamine
PG	phosphatidylglycerol
PI	phosphatidylinositol
PMF	plasma membrane-enriched fraction
PO_4	phosphate group of phospholipids
POPC	1-palmitoyl-2-oleoyl-sn-glycero-3-phosphocholine
POPG	1-palmitoyl-2-oleoyl-sn-glycero-3-phosphoglycerol
POPS	1-palmitoyl-2-oleoyl-sn-glycero-3-phosphoserine
PS	phosphatidylserine
SM	sphingomyelin
TCSPC	time correlated single photon counting
TDFS	time-dependent fluorescence shift
TF	tear film
TFLL	tear film lipid layer
TO	glycerine trioleate
VSFS	vibrational sum frequency spectroscopy

List of publications

The thesis is based on the following papers.
Papers I - V are attached to the end of the thesis.

I Melcrova, A., Pokorna, S., Pullanchery, S., Kohagen, M., Jurkiewicz, P., Hof, M., Jungwirth, P., Cremer, P. S., Cwiklik, L. The complex nature of calcium cation interactions with phospholipid bilayers. Scientific Reports, 2016, 6, doi: 10.1038/srep38035

II Melcrova, A., Javanainen, M., Magarkar, A., Jurkiewicz, P., Hof, M., Jungwirth, P., Martinez-Seara, H. Two cations, two mechanisms: interactions of sodium and calcium with zwitterionic lipid membranes. Chemical Communications, 2017, 53, 5380-5383, doi: 10.1039/C7CC02208E

III Cwiklik, L., Melcrova, A., Daull, P., Garrigue, J.S. A proposed mechanism for tear film breakup: a molecular level view by employing in-silico approach. Journal for Modeling in Ophtalmology, 2018, 2(1), 19-23

IV Riedlova, K., Melcrova., A., Olzynska, A., Daull, P., Garrigue, J.S., Cwiklik, L. Influence of benzalkonium chloride on Tear Film Lipid Layer stability: a molecular level view by employing in silico modeling. Journal for Modeling in Ophtalmology. Accepted for publication in August 2018.

V Melcrova, A., Pokorna, S., Vosahlikova, M., Sykora, J., Svoboda, P., Hof, M., Cwiklik, L., and Jurkiewicz., P. Simultaneous compression of lipid membranes by calcium and cholesterol. Submitted in 2019.

VI Melcrova, A., Cebecauer, M., and Cwiklik, L. The importance of the two palmitoylations on PAG peptide - all-atom MD study. In preparation for submission in 2019.

Other papers which are not included in the thesis:

I Kocisova, E., Vodakova, A., Prochazka, M. DCDR spectroscopy as efficient tool for liposome studies: Aspect of preparation procedure parameters. Spectroscopy: An International Journal, 2012, 27(5-6), 349-353, doi: 10.1155/2012/182720

II Plasek, J., Melcrova, A., Gaskova, D. Enhanced sensitivity of pHluorin-based monitoring of intracellular pH changes achieved through synchronously scanned fluorescence spectra. Analytical Chemistry, 2015, 87(19), 9600-9604, doi: 10.1021/acs.analchem.5b02779

III Melcrova, A., Kessler, J., Bour, P., Kaminsky, J. Relation of the glucose and mannose structure to their Raman optical activity. Phys. Chem. Chem. Phys., 2016, 18(3), 213-2142, doi: 10.1039/c5cp04111b